Development of a Computational Framework for Aeroelasticity of Geometrically Nonlinear Structures: A Partitioned Coupling Approach

Srikanth Vasudevan

Aerospace Structures & Materials
Faculty of Aerospace Engineering

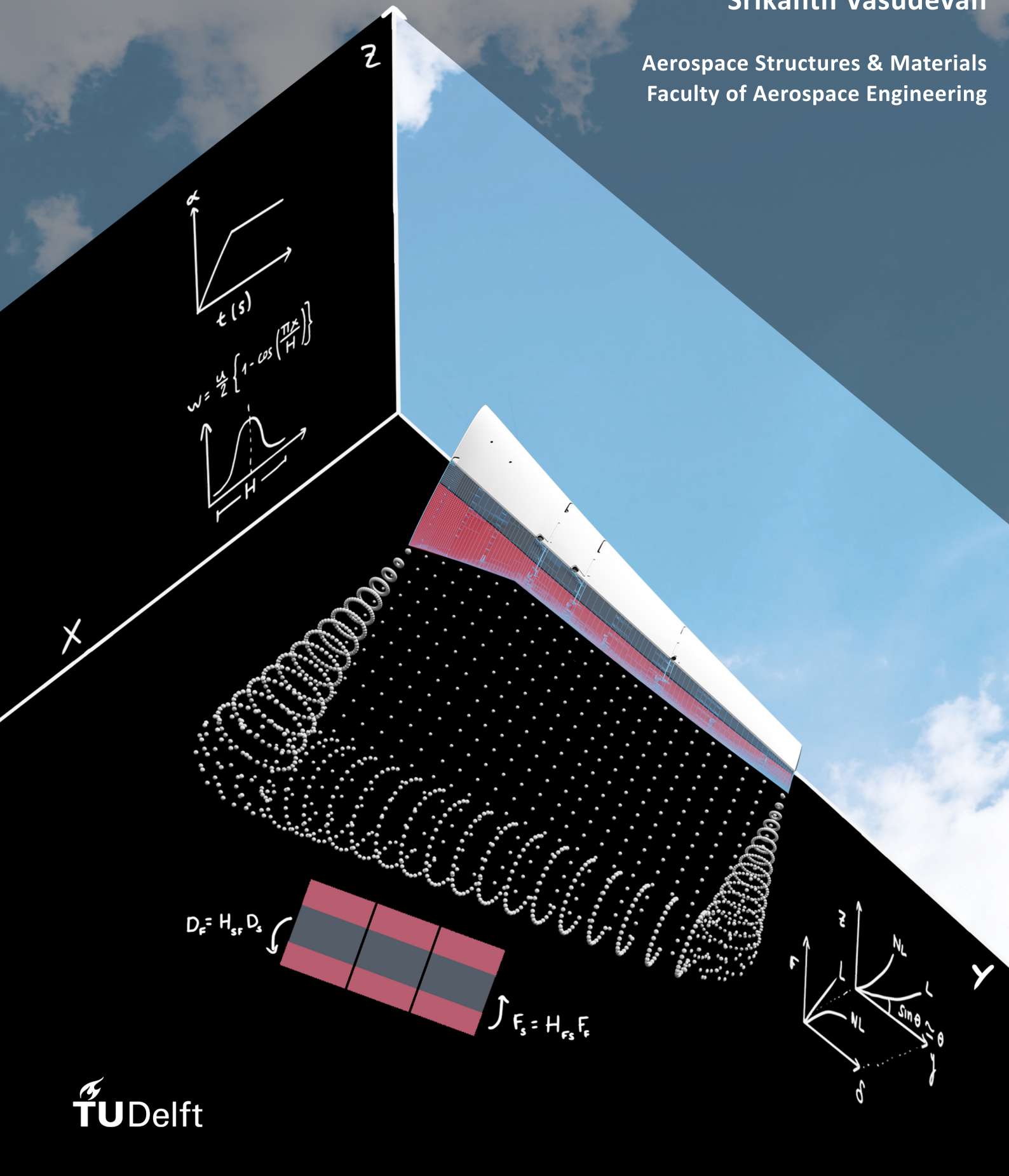

TU Delft

Development of a Computational Framework for Aeroelasticity of Geometrically Nonlinear Structures: A Partitioned Coupling Approach

by

Srikanth Vasudevan

in partial fulfilment of the requirements for the degree of

Master of Science
in Aerospace Engineering
Aerospace Structures and Materials

at the Delft University of Technology,
to be defended publicly on Tuesday, June 15th, 2021 at 09:00 AM.

Student number:	4893832	
Project duration:	August 1, 2020 – June 15th, 2021	
Thesis Committee:	Dr. Ir. R. De Breuker,	TU Delft (ASM), Chair / Supervisor
	Dr. J. Sodja,	TU Delft (ASM)
	Dr. Ing. S. G. P. Castro	TU Delft (ASM)
	Dr. A. H. van Zuijlen	TU Delft (AWEP)

An electronic version of this report is available at http://repository.tudelft.nl/.

TU Delft Delft University of Technology

ACKNOWLEDGEMENTS

The last two and a half years have easily been the most challenging times in my life with a lot of ups and downs. It all started with a decision to come to TU Delft a couple of years ago, without a confirmed accommodation in a new country. Little did I know that this was just the start of a mountaineering expedition. Looking back, I have learnt, evolved and grown, both personally and professionally. Along the way, I have met some of the smartest and sweetest people, without whom I would not have come this far. Here is a formal note to all those who have supported and helped me transform from a *"Stressed-Engineer"* into a *"Stress Engineer"* .

I would like to express my sincere gratitude to my thesis guides, Professor Roeland and Paul Lancelot. Professor Roeland, one of the coolest supervisors I've worked with. A computational master thesis amidst a pandemic means that one has to hone their introversion skills for some lonely, indefinite screen time confined to a $10m^2$ space. I remember eagerly waiting for the monthly meetings where Professor would so generously fill me up with motivation. Jokes and casual discussions about *Friends* and *Tintin* (among other things) have been of great help during stressful times. The immense autonomy I have had with this thesis, although challenging, has been quite liberating. Autonomy also means some unnecessary / wrong turns and we often need some guidance on a regular basis. "Brother from another mother" is the most suitable description for Paul. For without Paul, I could not have done half of what I have done in this thesis. His expertise in Nastran cannot be matched. Our biweekly meetings, some of which lasted almost two hours discussing about everything possible will always be remembered. Your positive words during some stressful times amidst the pandemic has helped me keep a level head.

Jurij is one of the most amazing people I've met. Without his help at the most important time of my life in Delft, I wouldn't be writing this now. The internship at DLR Gottingen was a dream come true and I believe that it has significantly contributed to my academic trajectory. I had the opportunity to meet and work with some of the smartest people. A big thanks to Yves Govers (DLR) and Keith Soal (DLR) for an amazing time in Göttingen and the confidence they have given me and to Jurij and Prof. Roeland for a great opportunity to prove myself. The 6 months I spent in Göttingen was also the most stress-free period in the last two and a half years, thanks to Jurij. Saullo is beyond just another professor or supervisor and is a true wellwisher. He has managed to say such kind words everytime we have met in the last 2 years. I will constantly aim to be as good as he thinks I am and will always cherish our meetings. I am eagerly looking forward to the basketball game that we have scheduled. All of the above are mentors of life and not just supervisors. They believed in me more than I believe in myself and in that process, brought out the best in me. Most importantly, their humble and down-to-earth nature is truly inspirational.

With such high stress levels, I was fortunate to have a personal circle of friends in The Netherlands who are also equally responsible for the successful completion of this endeavour. I am highly indebted to Vikram, who was kind enough to accommodate me at his place during my initial days in The Netherlands. It is because of people like Vikram that I still have faith in humanity. I was lucky to find a good mix of competitive friends who have supported each other during tough times. Thanks to Harsha and Arvind for sharing the pandemic thesis hardships. Thanks to Siddharth for all the basketball sessions and the food at necessary times.Shout-out to Deacon for all the mountain rides, basketball games, drinks (icecreams for me, haha) and technical discussions. I wish for more such moments in the future. Srivathsan Anna and Sindhuja Akka have been of immense support during the whole time. Our road trip to Germany, hitting 215kmph on the Autobahn, their sumptuous Indian dishes, all those "kalaaichifying" and movie sessions are all fond memories of life. Their place has been a home away from home. And I have loved every minute with them. A special thanks to my roomie Iñaki Jiménez, for bringing the idea of this thesis cover to a beautiful reality. Chico, esto es genial!

The most important people without whom none of this would have happened. My parents Vasu and Rev, and Prema Paati. A huge thanks for bearing the financial burden of this journey. The situation at home has been very challenging in the last two years with each of us at different places going through our courses of life. The only reason we could pull this off is because of my sister, Anusooya. She's made sure to keep us all connected amidst her own stressful life experiences. Her exceptional insights in the field of mathematics has been of great help in completing my thesis. For after all, she possesses a Gold Medal in Mathematics. If she can't help, I'm not sure who can. A big thanks to all their sacrifices to help me get through this. I have deeply missed our family times that were mostly filled with laughter and joy. I am eagerly looking forward to our family reunion that's round the corner.

Finally, Swathi, my girlfriend. Inspite of a very long distance between us, she has been beside me through some of the most testing times and rough patches. I truly appreciate her cool-headed support, without which I would have buckled under stress. Having a mental support during a Delft-Pandemic thesis was crucial to have reached this finish line. Thanks for her support through high and some deeply low moments in the last two and a half years. I would not have made it without her.

Srikanth Vasudevan
Delft, June 2021

ABSTRACT

High Altitude Long Endurance (HALE) configurations have gained much popularity in the recent past. Although, HALE aircraft enable efficient and environmental-friendly flying, they necessitate a large Aspect-Ratio wing. These slender structures are prone to large, nonlinear deformations which further increase the unsteady nature of aerodynamic flow that can detrimentally impact the structure. In the light of this trend towards an efficient aviation industry of tomorrow, Airbus Innovations UK has ventured into the development of a folding wing tip concept whose benefits are two-fold. First, the ability to increase span during flight, thereby reducing the induced drag. The folding capability also ensures entry gate requirements at airports. Secondly, the folding mechanism presents load alleviation capabilities with appropriate hinge setup. Alleviation of loads on lifting surfaces directly translates to reduction of the Wing Root Bending Moment (WRBM), which means a reduction of weight. Thus, a further improvement in efficiency of flight.

In this work, a nonlinear aeroelastic solver is developed. The proposed partitioned framework couples the industry standard commercial software package MSC Nastran, a structural solver to the Unsteady Vortex Lattice Method (UVLM), an aerodynamic solver. The UVLM module developed, exhibits both static and dynamic capabilities. Three wake models are incorporated. Horse-shoe wake is employed for static simulations and convective wake procedures are available for transient dynamic simulations. The independent modular solvers are coupled using Radial Basis Functions (RBFs) and Nearest Neighbour (NN) approaches. This framework enables the solver to capture the combined effects of structural nonlinearities and unsteady flows. The proposed solver is then verified and validated for two different test cases: NASA CRM Wing and Pazy Wing. Experimental validation is carried out using existing results from related work. The solver is then used to evaluate the "AlbatrossOne", a hinged wingtips concept by Airbus Innovations UK. Both static and dynamic responses are analysed for load alleviation capabilities.

Keywords: Nonlinear Aeroelasticity, Unsteady Vortex Lattice Method, Fluid-Structure Interaction, Radial Basis Function, Hinged Wingtips, Maneuver Load Alleviation, Gust Load Alleviation.

CONTENTS

LIST OF FIGURES

LIST OF TABLES

NOMENCLATURE

LIST OF ABBREVIATIONS

AIC	Aerodynamic Influence Coefficient
BMD	Bending Moment Diagram
CFD	Computational Fluid Dynamics
CRM	Common Research Model
CSM	Computational Structural Mechanics
CSS	Conventional Serial Staggered
DLM	Doublet Lattice Method
FEM	Finite Element Method
GLA	Gust Load Alleviation
HALE	High Altitude Long Endurance
MLA	Maneuver Load Alleviation
MRM	Modal Reduction Method
NN	Nearest Neighbour
OOP	Object Oriented Programming
PAT	Passive Aeroelastic Tailoring
RBF	Radial Basis Function
UVLM	Unsteady Vortex Lattice Method
WRBM	Wing Root Bending Moment

1

INTRODUCTION

Aviation industry is at the forefront of technological advancements and is considered to have the fastest growth in the transport sector [20]. The global aviation passenger number is predicted to double by the year 2037 [21]. This directly translates to the steep increase in air traffic and hence higher pollution rates. Figure 1.1 shows the forecasts of the CO_2 and NO_x. The latter is the key driving parameter for development of more efficient and sustainable engines.

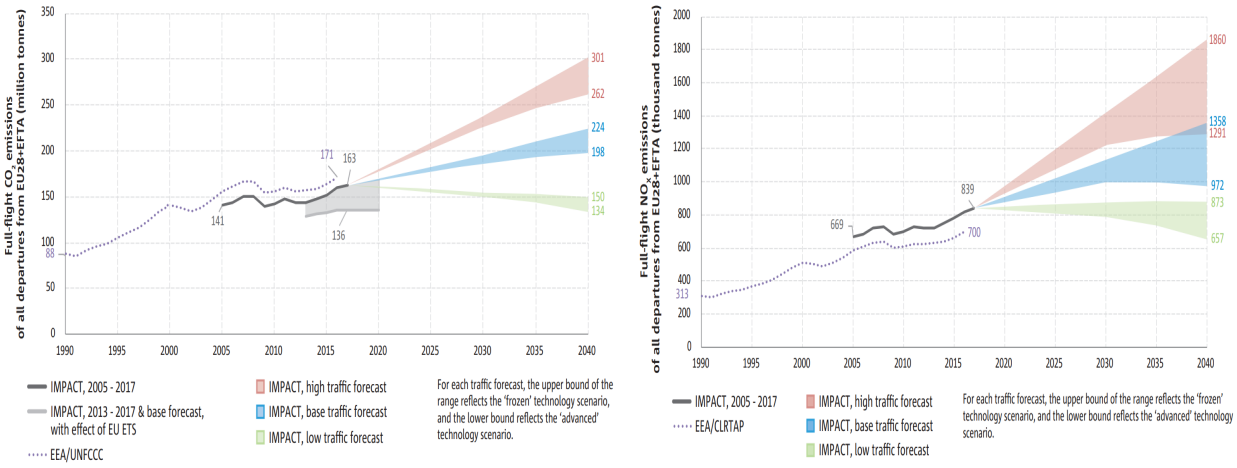

(a) CO_2 emission forecast

(b) NO_x emission forecast

Figure 1.1: Full flight emission forecast upto year 2040 [1].

Analysing the well-known Breguet equation (given in equation 1.1) exposes three main areas where in-flight efficiency improvements can be realised [20]. The propulsion system designers focus on the aforementioned NO_x emissions through efficient engine design, maintenance, repair and operation. The other two domains, namely the aerodynamics (aircraft design) and the structural design are usually interdependent and are the primary focus in the field of aeroelasticity. The subject matter of this field consists of the design of efficient flexible structures and their interactions with the fluid domain and is defined by the well-known Collar's triangle [2].

$$\text{Range} = V t_f = V \times \underbrace{\left(\frac{L}{D}\right)}_{\text{aircraft designer}} \times \underbrace{I_{sp}}_{\text{Propulsion system designer}} \times \underbrace{\ln\left(\frac{W_i}{W_f}\right)}_{\text{Structural designer}} \tag{1.1}$$

In the light of this trend towards an efficient aviation industry of tomorrow, Airbus Innovations UK has ventured into the development of a folding wing tip concept whose benefits are two fold. First, is the ability to increase span during flight. The induced drag accounts for about 30 percent of the total drag of an aircraft [22]. This induced drag is inversely proportional to the span squared and thus increase in span results in reduction of the total drag. The folding capability also ensures entry gate requirements at airports. Secondly, the folding mechanism presents loads alleviation capabilities with appropriate hinge setup. Alleviation of loads on lifting surfaces directly translates to reduction of the Wing Root Bending Moment (WRBM), which translates into a reduction of weight and thus a further improvement in efficiency can be achieved. The nomenclature "Albatross" takes inspiration from the bird species that possess the largest wingspan in the avian kingdom measuring upto 11 feet [23].

This chapter presents an in-depth review of literature in the field of research. A research funnel view is portrayed by the author where the sequence of the presented literature begins from an exploratory phase about the general topics in aeroelasticity and gust load alleviation techniques. From here the focus is shifted towards research gaps that eventually lead to the state-of-the-art. Within each section, a chronological review is presented to observe the trends of major research pathways at specific timelines. The chapter begins with a brief introduction to the interdisciplinary field of aeroelasticity in section 1.1. Section 1.2 presents an overview of the general topics related to load alleviation in aeroelasticity. Section 1.3 illustrates the evolution of computational techniques in the field. Section 1.4 presents the work done at Airbus UK specific to the AlbatrossONE project. The chapter is then concluded with the research objectives of the current work in section1.5.

1.1. Background Knowledge

This section presents some background to the topics involved in this thesis with the aim of setting a stage to the reader. Section 1.1.1 first introduces the subdomains of aeroelasticity. Section 1.1.2 introduces aeroelastic loads and section 1.1.3 illustrates the common numerical modelling techniques used in aeroelastic studies.

1.1.1. What is Aeroelasticity?

Aeroelasticity is defined as the science of mutual interaction between the structural elasticity and aerodynamic forces and the effect of this interaction on the design of aircraft. Although, originally this field was introduced by aeronautical engineers, aeroelastic phenomena is observed in related fields of automotive and civil engineering as well. For aeroelastic phenomenon to be significant, it is imperative to have an elastic structure, an airflow over this structure and a sufficient level of interaction between these domains. Most modern aircraft possess highly flexible structures and hence this field plays a crucial role. The figure 1.2 below, represents the well-known Collar's Triangle that depicts the context of aeroelasticity.

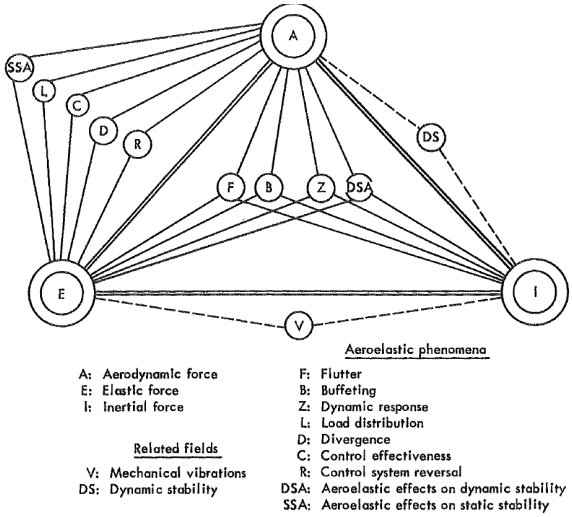

Figure 1.2: Collar's triangle depicting the context of Aeroelasticity [2]

From this classical definition, it is imperative to understand the physics of the basic components that make up the interdisciplinary field. This includes the behaviour of structures and their responses to external forces, the effect of fluid flow over these structures, which are responsible for the aforementioned external forces, and lastly, the effect of these structures back on the fluid around them. These are introduced in the following subsections.

Structural Dynamics

Structural dynamics is the field in which responses of complex structures to dynamic, time dependent loading are studied. The fundamental mathematical background lies in representing the given structure in terms of a combination of spring-mass-damper systems that determine it's degrees of freedom. This thesis assumes a basic background in this field and begins with the discussion of direct, numerical time integration schemes of generalised systems. For a quick recap of journey through free and forced vibrations, the effects of damping, convolution and Fourier analysis to numerical integration, popular books such as *Engineering Vibrations* [24] and *The Finite element method* [25] can be referred.

Aerodynamics

As the structure deforms during it's motion through a fluid, the fluid forces change according the laws of fluid physics. Aerodynamics involves the study of nature of fluid flow around bluff bodies and the resulting forces acting them. The scope of current thesis is limited to the potential flow theory that assumes incompressible and irrotational flow. The crux of this theory lies in spatial distribution of singularity elements in specific orientations that are solutions to the Laplace Equation. Mathematically, the airfoil /wing is discretised into a number of panels. Each of these panels are modelled as a specific type of singularity of unknown strength. A system of linear equations can be solved for the unknown strengths through which pressures and loads are determined. For a more detailed course on panel aerodynamics, readers are referred to the Open Course Ware by Lorena Barba [26].

FSI Coupling

Aeroelasticity is an interdisciplinary field involving aerodynamics and structures as discussed above. It is clear that information must then be transferred between these domains as the aerodynamic loads change with structural configurations which in turn alters these configurations. In most practical applications, mathematical modelling of these domains involve varying mesh sizes that do not match. Thus, interpolation techniques fluid-structure interactions are necessary. A general mathematical description of the fluid-structure interface is given by,

$$\mathbf{U}_f = H_{sf}\mathbf{U}_s$$
$$\mathbf{P}_s = H_{fs}\mathbf{P}_f$$

where U_s and U_f, P_s and P_f are the displacements and the pressures on the structural and the fluid side respectively, coupled using the interpolation matrices H_{sf} and H_{fs}

The coupling between the fluid and the structure is broadly classified into two categories, namely, the consistent and the conservative approach. Consistent approach dictates that the row sum of the interpolation matrix be equal to 1. Whereas, the conservative approach is based on the conservation of virtual work at the interface both at the structural side and at the aerodynamic side. For the conservative approach, one interpolation matrix (F to S/ S to F) depends on the other (S to F/ F to S) and can be shown that,

$$H_{fs} = \left[M_{ff} H_{sf} M_{ss}^{-1}\right]^T$$

Where M_{ff} and M_{ss} are matrices that depend on the discretization of the fluid and the solid domains respectively [27]. The main interpolation techniques are Nearest Neighbour (NN), Radial Basis Function (RBF) approach and the projection methods.

1.1.2. Loads in Aeroelasticity

Aircraft loads are broadly classified into deterministic and non-deterministic (random) loads. Deterministic loads could be either static and dynamic loads. Static loads are manoeuvre loads which are typically, pull-up, push-down and Roll. Figure 1.3a is a typical V-n diagram used for loads analysis. These graphs usually contain information on load factor at various critical speeds. With the help of gust and manoeuvre lines that show their criticality at a given speed, structural sizing can be performed using optimization. Dynamic loads are discrete "1-cos" gusts. These gusts are so named due to their shape. Figure 1.3b shows general "1-cos" gust lengths prescribed by FAA/EASA for analysis and certification purposes. The non-deterministic (random) loads are often analysed using the Power Spectral Density (PSD) techniques. Typical examples are continuous gusts and ground loads. These are defined in the frequency domain and the most common examples of continuous gusts are Von Karman and Dryden Spectrum.

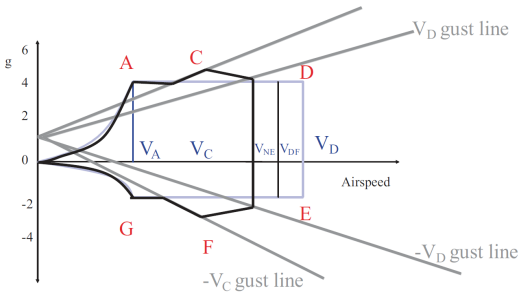

(a) Typical V-n diagram of a transport aircraft showing maneuver and gust limit load factor according to Pratt's Equation[3]

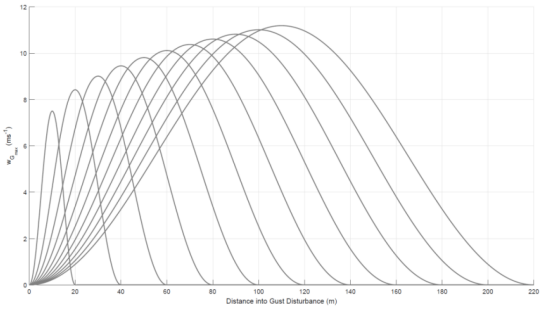

(b) Vertical gust profiles in time domain as prescribed by FAA/EASA [4]

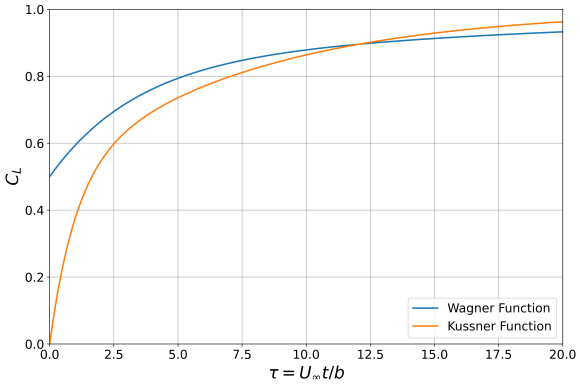

(c) Küssner function (Gusts) and Wagner function (Steady acceleration)

Figure 1.3: Common aeroelastic loads: (a) V-n diagram [3] (b) Gust profiles [4] (c) Transient build up of loads

Among these, Static manoeuvre loads and dynamic discrete "1-cos" gusts are often considered in the aeroelastic studies. Figure 1.3c shows the lag in the development of lift over a wing surface due to unsteady effects. The Küssner and Wagner functions define this build up over time for steady acceleration and a sharp gust encounter respectively. This portrays the importance of wake modelling for accurate prediction of lift build-up in time, over a surface.

1.1.3. Numerical Modelling of Aeroelastic Phenomenon

In Structures, Finite Element (FE) techniques are employed wherein the continuum is discretized into a number of elements through which global mass and stiffness matrices are assembled. Commonly, fidelity of the model is chosen based on the complexity of a given problem. In aeroelasticity, often low fidelity stick models (beam elements) are used to define the structure. The reason for this is two-fold. First, aeroelasticity often is used in the preliminary design stage that does not require detailed modelling. Secondly, due to the extensive load cases that need to be analysed for a given aircraft, computational efficiency dictates the use of simple, but geometrically exact models. However, detailed FE models are also used when coupled with high fidelity aerodynamic modelling such as computational fluid dynamics (CFD). Figures 1.4 and 1.5 show the commonly used numerical models for the structural and the aerodynamic domains for aeroelasticity.

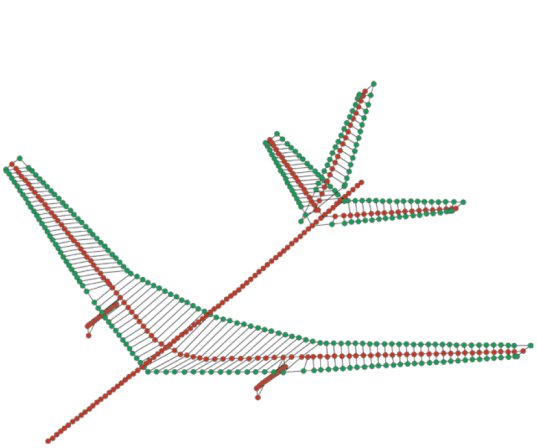

(a) Stick (beam) model with reduced degrees of freedom [5]

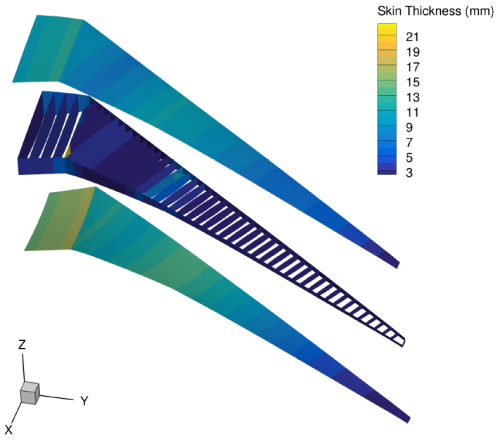

(b) High fidelity structural model of aircraft wingbox [6]

Figure 1.4: Traditionally used structural (finite element) models in aeroelasticity [5, 6].

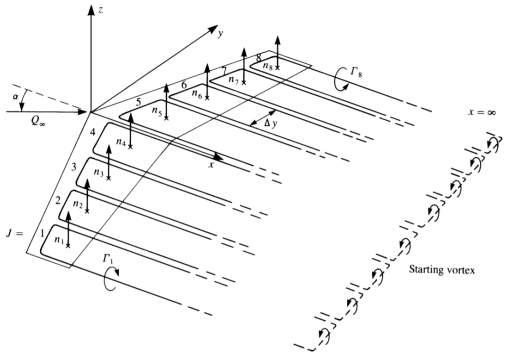

(a) Potential flow based panel methods like DLM,VLM [7].

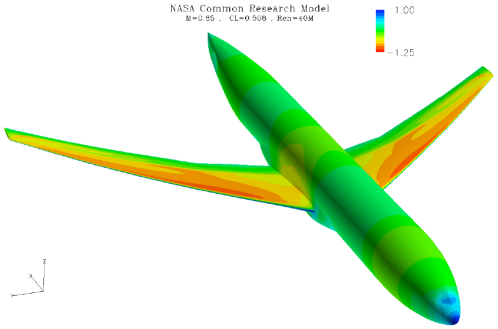

(b) Computational Fluid Dynamics [8]

Figure 1.5: Aerodynamic numerical models [7, 8].

1.2. Active and Passive Gust Load Alleviation

The phenomenon of loads in aeroelasticity was briefly summarized in section **??**. The build-up of loads with time, over a lifting surface varies as given by Kussner or Wagner function. In slender, high Aspect-Ratio wings, these loads not only vary over time, but also due to the elastic deflection of the lifting surfaces. These are often called "follower forces" as they follow the deformation of the structural surfaces. Due to this, load redistribution occurs often and must be accounted for. The simplest way to analyse the criticality of these time-varying loads is to measure the Wing Root Bending Moment (WRBM). From Statics, we know that maximum bending moment due to shear loads in a cantilever beam occurs at the clamped end i.e root of the wing. Thus, the obvious next step is to look for opportunities to reduce these loads over the wing surface, which directly translates to reduction of bending moment at the root. This is referred to as "Loads Alleviation". Gust loads not only have detrimental impact on structural dynamics, but they also affect the aerodynamic loads on lifting sur-

faces, stability and handling characteristics of aircraft. Wu *et al* [28] provide a complete description and an in-depth review of these effects of gust loads.

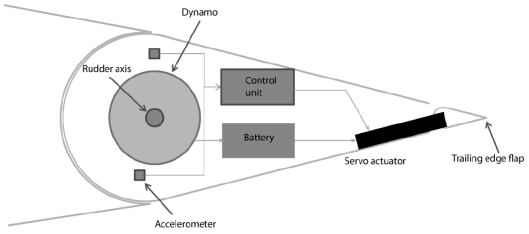

(a) Active load alleviation concept with electronics on wing flaps[10].

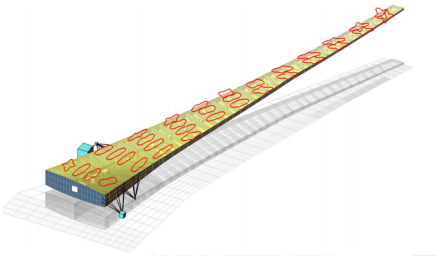

(b) Passive GLA techniques using permanent structural modifications [11].

Figure 1.6: Examples of passive and active gust load alleviation techniques [9–11].

Techniques for alleviation are divided into two main categories. First, active load alleviation where in control surfaces are actuated temporarily in specific ways that bring about reduction in wing loads (fig 1.6a). Second, the structural response is modified passively by incorporating permanent changes in their build. This is often referred to as Passive Aeroelastic tailoring (PAT) and involves structural sizing using precise optimization techniques applied to composite lay-up sequences at various locations of the wing box (fig 1.6b). The effect of such active and passive devices in redistributing the forces on lifting surfaces is illustrated in figure 1.7

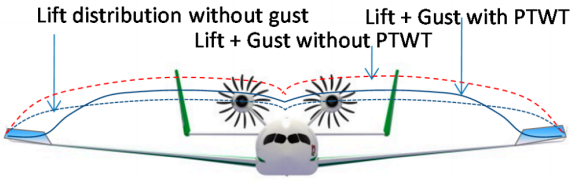

Figure 1.7: Passive wing tip twist concept (PWTW) [9]

Efficiency of the aircraft can be improved through active and passive structural modifications, some sensitivity analysis and optimization techniques that aid in successful load alleviations [20]. Guo *et al* [9] provide a preliminary case study of wingtip design with a passive twist (PWTW). Analysis of PWTW performed in Nastran for gust response, roll damping and manoeuvre show load alleviation in terms of lower wing tip deflection and lower root bending moments. Thus, passive load alleviation was attainable through such permanent structural modifications. Other popular passive techniques that were explored around this time were aeroelastic tailoring of wings using fibre steering [29]. The more recent studies are observed to be extensively on active alleviation techniques using PID controllers and piezo patches [30]. Numerical simulations and experimental validations are successfully achieved in this work. Another active technique is the use of a feed-forward sensor for gust [31] whose control action is the famous symmetric actuation of ailerons whose effectiveness is widely proven in literature. Bussemaker *et al* [32] provide a framework for integration of Gust Load

Alleviation (GLA) and Manoeuvre Load Control (MLC) with structural optimization of the wing. Bi *et al* [33] have successfully developed a servo control mechanism where numerical analysis is carried out using nonlinear FEM and UVLM. Nguyen *et al* [34] present a multi-objective control system on distributed control surfaces on NASA's VCCTEF concept. The research community has noticed the advantages that both active and passive techniques have to offer. The trend in most recent literature is towards combination of the two fields [10]. Techniques to include active and passive methods in the optimization framework using Nastran and Matlab have also been proposed [35]. Readers are also referred to an extensive overview on most recent developments on gust loads [28]. The following table 1.1 presents a chronological review of literature highlighting a major trend towards active control for load alleviation.

Year	**Author**	**Title**	**Summary**
2014	[20] J.E Cooper	From blue skies to green skies: how structural dynamics and uncertainty quantification can benefit future aircraft designs	Review paper on importance of GLA
2014	[36] L Bernhammer *et al*	Design of an autonomous flap for load alleviation	Active Load alleviation.
2015	[9] Shijun Guo et al	Gust Alleviation of a Large Aircraft with a Passive Twist Wingtip	Passive (Permananent structural twist of wingtips)
2016	[30] Ying Bi *et al*	Gust load alleviation wind tunnel tests of a large-aspect-ratio flexible wing with piezoelectric control	Active Load Alleviation
2016	[31] Yonghui Zhao et al	Gust Load Alleviation on a Large Transport Airplane	Active load alleviation through adaptive feedback control
2017	[37] Rajpal, Darwin; De Breuker, Roeland	Preliminary aeroelastic design framework for composite wings subjected to gust loads	Optimization framework for gust analysis
2018	[32] J Bussemaker	Wing Optimization with Active Load Control	Optimization of MLC and GLA controls for gust.
2018	[33] An Chao *et al*	Wind tunnel test and gust load alleviation of flexible wing including geometric nonlinearities with servo control	PID controllers for Active Load Alleviation
2018	[38] Seung Jae Lee *et al*	Robust Gust Load Alleviation Control using Disturbance Observer for Generic Flexible Wing Aircraft in Cruising Condition	Continuous/ Distributed flap control - VCCTEF concept
2018	[34] Nhan Nguyen *et al*	Multi-Objective Adaptive Control for Load Alleviation and Drag Minimization of Flexible Aircraft	Numerical optimization, simulation of ASE control system.
2018	[35] Vega Handojo *et al*	Implementation of Active and Passive Loads Alleviation Methods on a Generic Mid-Range Aircraft Configuration	Study of influence of alleviation systems on structural mass
2018	[10] Roeland de Breuker *et al*	Combined Active and Passive Loads Alleviation through Aeroelastic Tailoring and Control Surface/Control System Optimization	Comparison of passive with active alleviation and proposes an improved combined system
2018	[39] Federico Fonte *et al*	Design of a wing tip device for active maneuver and gust load alleviation	Active wingtip extension for loads alleviation
2019	[40] Versiani *et al*	Gust load alleviation in a flexible smart idealized wing	structural modes attenuation throuhg piezo-actuation
2019	[41] Haojie Liu, Xiao Wang	Aeroservoelastic design of piezo-composite wings for gust load alleviation	Numerical gust load alleviation through ASE control laws
2019	[28] Wu, Z,Cao, Y.,Ismail, M.	Gust loads on aircraft	Review paper on gusts

Table 1.1: Chronological representation of some literature to illustrate major trends in focus areas of gust load alleviation.

1.3. Computational Framework for Aeroelastic Simulations

In this era of rapidly growing computational power, numerical modelling and virtual simulations provide an efficient, cost effective pathway for engineering problems. With the rise of computers, wind tunnel testing is now merely seen as means for validation of the numerical codes [42].

Section 1.3.1 presents a review of literature in the field of computational modelling of aeroelastic phenomenon. Section 1.3.2 discusses the capabilities and limitations of the industry standard software such as MSC Nastran. Section 1.3.3 presents the manner in which panel codes are employed for computational aeroelasticity. Finally, Section 1.3.4 discusses some of common procedures for multi-physics coupling prescribed in literature.

1.3.1. Trends in Computational Aeroelastic Modelling

In general, a complete aeroelastic study involves the solution to trim equations which serve as initial conditions for the dynamic simulations that follow. Discrete "1- cos" gust analysis and the response parameters like wing tip displacements, accelerations, shear force and bending moment distributions along span are observed. Three common aerodynamic modelling approaches are, Strip theory, Panel Codes (DLM, VLM and UVLM) and Computational Fluid Dynamics (CFD). Strip theory possesses the fastest computational capabilities [43]. Willis et al [44] present a method to drastically reduce the computational time which involves conjunction of the typical 3D panel codes with a pFFT algorithm. This uses an agglomeration strategy like the ones generally used in CFD. The agglomeration is based on the number of elements present within the root cell which are then identified as leaf and children cells. This ensures that the required accuracy is achieved at critical regions whereas the non-critical regions are grouped together and hence promises an improvement in computational efficiency. The shift in research focus towards panel codes such as UVLM from the popular CFD techniques is due to the fact that, although accurate, CFD is computationally expensive [45] while the accuracy in results from panels codes are comparable to CFD data.

As mentioned earlier in the previous section, the research focus in the last decade has been in towards HALE aircraft and hence structural nonlinearities that they introduce [46]. It was observed that inclusion of the nonlinear response proved beneficial for the prediction of gust load alleviation. This method had a crucial pitfall as it was based on direct modal approach. Therefore the response of wing deformations that can have a direct modal superposition only would be accurately predicted. Although high fidelity modelling ensures accurate response prediction, it is often not desired due to the extremely high computation times [47]. As a result, panel codes occupied the central stage. Nastran uses Doublet Lattice Method (DLM) for subsonic flow [48]. Although DLM predicts flight mechanics with great accuracy, it's accuracy reduces for unsteady flow behaviour caused due to large nonlinear deflections in the structure. Thus, VLM, in particular UVLM technique began gaining popularity [49]. With the increase in computational capabilities of latest computing systems, effects on unsteady flow into panel codes could be included [50]. In this work, a 3D state

space model based on potential flow theory for unsteady aerodynamics is proposed and verification is made with idealized 2D and 3D cases using prescribed time stepping methods as mentioned by Katz and Plotkin. A prescribed wake is modelled with an initial procedure to determine the wake truncation length. No validation of the method is presented due to the unavailability of similar work in literature. On the structural modelling aspects, recent studies include the combination of flight mechanics with structural dynamics in the same analysis [51]. Nature is often a potential resource for engineering innovations in the aviation industry. To understand the phenomenon of flight physics, engineers often analyse birds and insects [52]. A CFD framework is built to study the effects of flexibilities of flapping wing insects and it is found that nonlinearities reduce flow separation and hence reduce the vortex generation in the wake, thereby proving to be beneficial for in-flight loads. [53].

1.3.2. NASTRAN CAPABILITIES AND LIMITATIONS

MSC Nastran is the standard and commonly commercial software package used for aeroelastic simulations in the industry today. The three main aeroelastic solvers are SOL144 - Linear static steady aeroelasticity, SOL145 - Aeroelastic modes , SOL146 - Dynamic aeroelasticity for gust simulations. Nastran uses standard finite element techniques for the structural domain. Two aerodynamic theories are employed - DLM (for subsonic) and ZONA51 (for supersonic flows). The coupling between the structure and the fluid is obtained using spline theory where interpolation is obtained using SPLINE cards that employ thin plate splines (TPS) and infinite plate splines(IPS) [18, 48]. In spite of Nastran being capable of detailed structural analysis in both linear and nonlinear regimes, the major limitation arises due to non availability of wake information in the aerodynamic models used. While this is not relevant for a steady linear aeroelastic analysis, when unsteady and nonlinear effects are to be studied, the difference is vital.

1.3.3. AERODYNAMIC PANEL CODES

Panel codes are fast and efficient flow simulation techniques which are based on potential flow theory. This brings in an approximation as viscosity is not considered. However, for most subsonic and transonic flows these methods have proved beneficial. In these, a given singularity is distributed across the wing geometry that are used to calculate the lift generated by solving for the strength of the singularity. These codes are classified based on the type of singularities that are used in simulation - i.e a lattice of doublet distribution (DLM), a lattice of vortex ring distribution (VLM). Ideally for a steady case, both DLM and VLM must predict the same lift distribution for a given configuration. In order to incorporate unsteady effects, one must model wake effects wherein the influence of the wake is determined for each time step. This is then termed as Unsteady Vortex Lattice Method (UVLM).

In DLM, a lattice of acceleration - potential doublet elements are arranged to form the wing planform [13]. Due to motion, surface deformation and external flow, at each of these element locations, a velocity is calculated. Flow tangency boundary condition is ensured at control points of these elements. This then reduces to a set of linear equations that relates pressure to the induced downwash. The pressure coefficients can then be computed as,

$$\mathbf{C}_p = \mathbf{A}\mathbf{w}$$

where A is the Aerodynamic Influence Coefficient (AIC) matrix and w is the downwash vector. These coefficients can then be integrated over surfaces to obtain forces and moments. The readers are referred to Katz and Plotkin [7] and Nastran theory manuals [48] for further information.

Unsteady Vortex Lattice Method (UVLM)

Singularity distribution

The wing is divided into M chordwise and N spanwise panels. The vortex rings are then placed such that their leading segments coincide with panels' quarter chord line. This means, the collocation point must be at the center of each vortex ring where non-penetration boundary condition shall be satisfied. Such a positioning also satisfies Kutta condition at the trailing edge automatically. Next, for a time domain simulation, wake is shed at each time-step that satisfies Kelvin condition,

$$\frac{d\Gamma}{dt} = 0 \tag{1.2}$$

where Γ is the complete circulation in the domain. Since this consists of both bound Γ_b and wake Γ_w, change in one automatically means change in the other [12]. This is computed for every time step where a new row of wake panels are shed. Figure 1.8 shows two commonly used wake modelling techniques. i.e. Prescribed wake and a force-free wake. It is evident that the free wake shown in figure 1.8b is computationally expensive. For static simulations, often a "Horse-shoe" wake is modelled which is fast and fairly accurate [7].

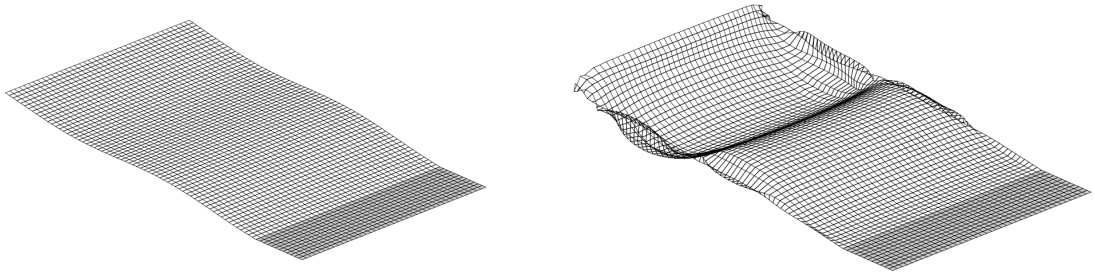

(a) Prescribed wake

(b) Force Free wake

Figure 1.8: Unsteady wake modelling types as incorporated in SHARPy [12].

Time Stepping Algorithm

Figure 1.9 illustrates the time-stepping algorithm of UVLM codes in literature. A simple backward difference approach can be employed for marching in time. At each timestep, a row of wake panels are shed behind the TE at the local velocity.

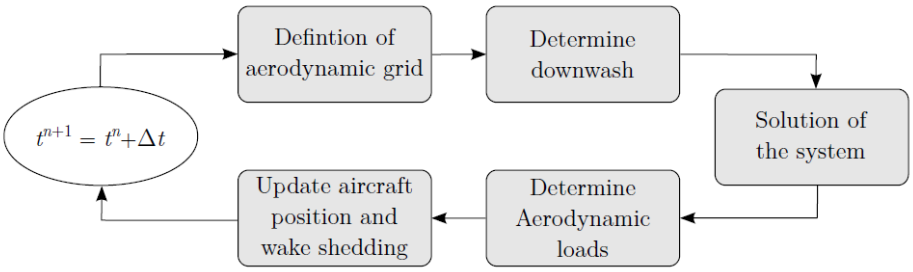

Figure 1.9: Algorithm for time stepping realising the wake shedding process in UVLM [12].

1.3.4. Methodology for External Coupling

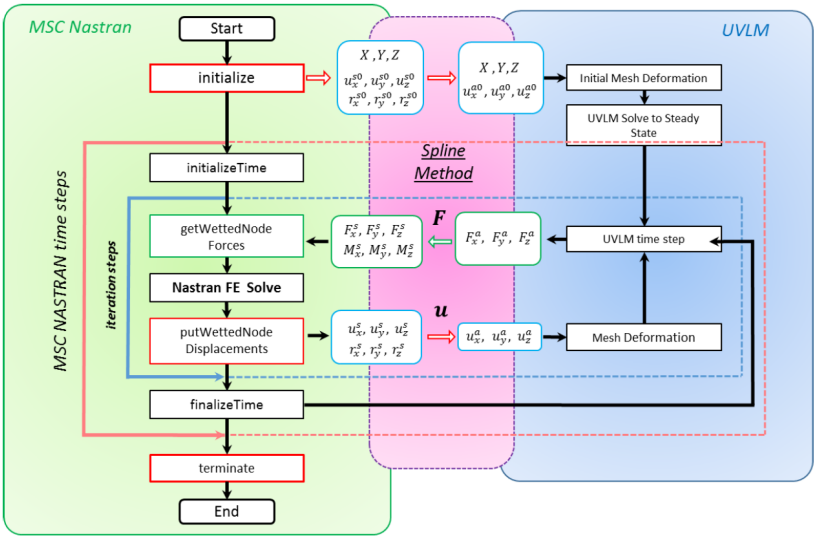

(a) Guide to Numerical modelling [13]

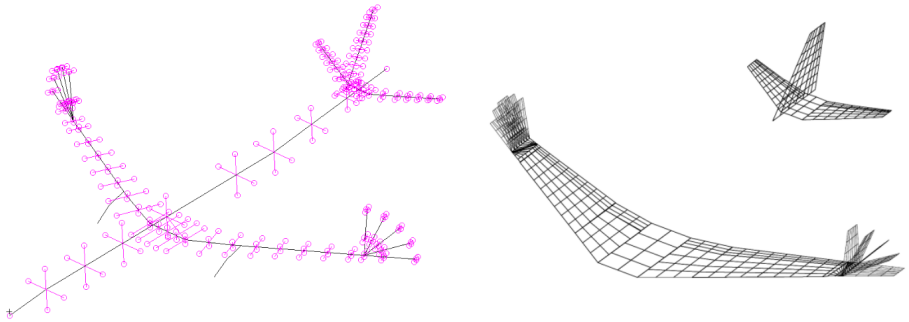

(b) Numerical models of structure (beams) and aerodynamics (UVLM panels)[14]

Figure 1.10: Prescribed computational modelling approach for aeroelasticity [13, 14].

In order to overcome the aforementioned limitations of standard solvers, recent trends in research is towards external aeroelastic coupling. The objective is to use Nastran and/or other commercial packages as main structural solvers due to their exceptional capabilities of linear and nonlinear structural modelling. For the aeroelastic coupling, these solvers

are externally linked to aerodynamic solvers with wake modelling capabilities. The focus of this literature is towards panel codes and will be dealt with in more detail. Essentially, similar frameworks can also be employed for more advanced CFD codes that are based on Navier-Stokes equations. Figure 1.10a shows the idea behind external coupling algorithms prescribed in state-of-the-art [13]. MSC Nastran is externally linked to panel aerodynamics via coupling algorithms like OpenFSI that are licensed under MSC software Inc. For a static simulation, aeroelastic trim is the main objective. First aerodynamic loads are to be evaluated for an undeflected configuration from the aero solver. These are then applied onto the structural nodes which results in it's deformation. This is iteratively performed between the two solvers until trim is achieved. Next, for a dynamic simulation, time stepping is an additional iteration. For a given time step, convergence is to be first achieved between the structure and aerodynamics.

Partitioned Fluid Structure Coupling

MSC Nastran employs Thin Plate Splines (TPS) and Infinite Plate Splines (IPS) for the spatial coupling of aerodynamic and structural domains, as briefly discussed in the previous section [48]. This is to ensure consistency between the two fields. Splines fall into the general category of Radial Basis Functions (RBFs) which are commonly preferred algorithms for coupling of aeroelastic phenomenon [54]. Usually, RBFs are employed with a specific support radius, that defines the influence region of the kernel function and hence work, exceptionally well, for scattered and unstructured data. However, a major disadvantage of this support radius is the additional dependency introduced in terms of sensitivity. Thus, the user, often, has to perform a search for the optimum values. In addition to the RBFs, time marching of the coupled solution is commonly achieved using Conventional Serial Staggered (CSS) scheme [54].

A Multi-Language Programming Approach

The most crucial aspect of the numerical modelling is the computational efficiency of a solver. It is well known that lower the level coding language, higher is the computational power. And therefore, languages like C and Fortran are among the fastest and most efficient of all. However, it is also found that most engineers and scientists prefer to use high level languages like Python and Matlab due to the ease of use, in-spite of their low efficiency. In order to resolve this problem of computational efficiency versus ease of usability, recent trend [49, 55] is towards the concept of multi-language programming. The idea behind this is to extradite the complex, memory intensive computations to faster low level languages like C and Fortran, which are then wrapped around with high level Python scripts which are easy and straight forward to use. This is also seen in the recently published open-source software "*SHARPy*" [56] which is a nonlinear, time domain aeroelastic solver that couples geometrically exact beam models to UVLM. The source codes for structural modules are written in Fortran while those for the aerodynamic modules are written in C++. These kernel solvers then consist of simple Python wrappers. *"PyFly"* is another example of such an open source multi-language approach [57] for flapping flight simulation. Cristina Riso *et al* [58] formalised a nonlinear coupling of Nastran SOL 400 for static trim simulation of X-HALE. This was a coupling of a structural beam mode in Nastran with external VLM that was written in Fortran. Thus no wake information was needed for this simulation.

The state-of-the-art for achieving the best computational efficiency is through conjugation of Python and Fortran codes for individual domains linked together with open source packages and/or self written scripts as this combines the fast, easy-to-use Python coding with extensive computational capabilities of Fortran based codes [57]. The proposed method is analysed for computational savings and is traded off against the accuracy of computation by the calculation of the L2 norm error. Since MSC Nastran is a Fortran based package, the techniques involved in this work will be evaluated for inspiration for modelling aspects in this thesis. Table 1.2 below, presents a breakdown of common numerical approaches in aeroelastic modelling. It can be observed that the key shift in trend is towards overcoming the limitations of commercial packages with external and cross platform, efficient algorithms.

Year	Author	Title	Software/Programming Language used	Structural Model	Aerodynamics Model
2005	[43] Thiemo R kier	Comparison of Unsteady Aerodynamic Modelling Methodologies with respect to Flight Loads Analysis	VarLoads (matlab/simulink)	FEM with separate mass estimation route	QS-VLM, Strip theory with IFM and DLM with RFA.
2006	[44] David J. Willis et al	A combined pFFT-multipole tree code, unsteady panel method with vortex particle wakes	FastAero (Python*)	FEM	Panel Method with pFFT-multipole algorithm
2006	[45]Hu Yu et al	The analysis of cyclogyro using unsteady vortex lattice method	N/A	N/A	UVLM
2011	[46]Harmin, M. Y. Cooper, J. E.	Aeroelastic behaviour of a wing including geometric nonlinearities	NASTRAN and ZAERO	FEM with geometric nonlinearities	Unsteady DLM on ZAERO
2011	[47]Benjamin P. Hallissy, Carlos E.S. Cesnik	High-fidelity Aeroelastic Analysis of Very Flexible Aircraft	HiFi-VFA(coupled solver)	Quasi 3D FEM based solver	CFD
2012	[49]Joseba Murua et al	Applications of the unsteady vortex-lattice method in aircraft aeroelasticity and flight dynamics	N/A	N/A	UVLM
2015	[50]Noud P.M. Werter et al	Continuous-time state-space unsteady aerodynamic modelling for efficient aeroelastic load analysis	N/A	N/A	UVLM
2017	[51]Francesco Saltari et al	Finite-Element-Based Modeling for Flight Dynamics and Aeroelasticity of Flexible Aircraft	NASTRAN	FEM	DLM
2018	[52]Y Yao et al	A Numerical Study on Free Hovering Fruit-Fly with Flexible Wings	Vega (Open Source FEA)	FEM	CFD
2018	[53]Alessandro Pontillo et al	Flexible High Aspect Ratio Wing: Low Cost Experimental Model and Computational Framework	BEARDS (optimization and manufacturing)	Reduced order model	Modified Strip Theory
2018	[57]Mehdi Ghommem et al	A Fast, Portable Computational Framework for Aerodynamic Simulations	Nastran, Python and Fortran	FEM	UVLM
2018	[58]Cristina Riso et al	Nonlinear Aeroelastic Trim of Very Flexible Aircraft Described by Detailed Models	Nastran, Fortran, DLR Toolbox (Matlab)	Nonlinear FEM	VLM (No wake)
2019	[56] del Carre et al	SHARPy: A dynamic aeroelastic simulation toolbox for very flexible aircraft and wind turbines	Python, C++ and Fortran	Nonlinear FEM	UVLM

Table 1.2: Breakdown of Numerical techniques in Literature that illustrates the shift towards multi-language programming

This section presents a review of the evolution/trends in the computational aspects of aeroelastic simulations. In particular, the focus is driven towards the development of low to medium fidelity modelling techniques for efficient numerical implementations. The limitations of commercial software packages are discussed in brief. The recent trend has been towards the development of cross-platform/multi language coding and external coupling of these commercial software with open source or self written codes/scripts on Python/C++/Fortran. In particular, the shift is towards object oriented programming (OOP) techniques that provide logical groupings of functions called methods within classes that are then instantiated as objects. The focus is towards bridging the gap between complex coding sequences that scientists and engineers often avoid by use of high-level languages like Python and Matlab, whilst maintaining code efficiency by implementing core kernels in low level languages. The major limitation in the aeroelastic analysis in commercial packages like Nastran is the absence of wake effects that affect the accuracy of simulations significantly. To circumvent this problem, ways of external coupling of Nastran to unsteady panel codes and CFD have gained popularity. The work by Imperial College London (*SHARPy*) [56] and Cristina Riso [58] are the most recent and up-to-date work in terms of nonlinear static and dynamic simulations. *PyFly* [57] is among the latest codes that are built on object oriented programming.

1.4. ALBATROSSONE - A SEMI-AEROELASTIC HINGE MECHANISM

This section presents work done specifically by Airbus UK on folding wingtips on the project AlbatrossONE. Section 1.4.1 introduces the concept of flared hinge folding wingtips by Airbus. Section 1.4.2 discusses some of the preliminary studies conducted on folding wingtips. Next, section 1.4.3 shows some of the techniques in which numerical models are developed and validated against wind tunnel data. Sections 1.4.3 and 1.4.3 discusses the work published related to nonlinear hinge setup, flight dynamics effect and landing characteristics respectively. Finally section 1.4.4 presents some results from successful flight test campaigns conducted at Bristol, UK.

1.4.1. THE CONCEPT OF FOLDING WING TIPS

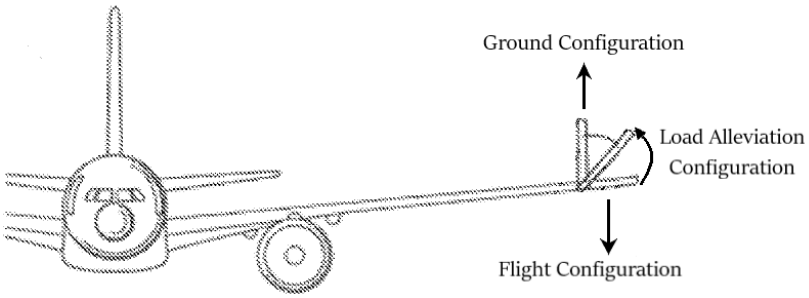

Figure 1.11: Patented folding wing tip mechanism - Wilson *et al* [15]

(a) Description of angles involved in the concept -(i) the hinge flare angle "γ" , (ii) the fold angle "θ"

(b) Conceptual description of the difference in folding mechanism (i) Without flare angle "γ", (ii) With flare angle "γ".

Figure 1.12: Hinge line concepts for loads alleviation - Airbus UK [13].

The concept of flared hinges for the folding mechanism prescribed by Wilson *et al* [14, 15] is illustrated in figure 1.12. Particularly, the difference in folding mechanism is evident in 1.12b. With the incorporation of a positive flare angle in the hinge, a nose down pitching of the wingtip is observed as the fold occurs. This is similar to a washout effect at the wingtip which causes the center of pressure on the wing to move towards the root (inboard). This results in reduction of the Wing Root Bending Moment (WRBM) due to a lower offset loading and thus alleviation can be achieved. This "semi-aeroelastic hinge" mechanism is patented by Wilson *et al* [15].

1.4.2. Preliminary Studies on Aeroelastic Effects

Literature published specifically by Airbus related to the Albatross one project reveals the main focus areas of the research. Vijayakumari *et al* [14, 59] have the hinge angle, fold angle and hinge stiffness as the main design parameters. Load alleviation was observed to be achievable only for positive hinge angle for both fixed and flexible hinges, the latter of which possess higher load alleviation capability. The tests performed were mainly static aeroelastic trim, flutter analysis and discrete “1-cos” gust. Low wing tip mass coupled with low stiffness of the hinge is beneficial for flutter [59]. However it was seen that the stream wise hinge performed better for flutter while no load alleviation was observed. The trend there-off was conflicting for the two and thus a trade-off must be attained. It is evident from relevant literature [59], that load alleviation is achievable using flared hinge wing tips. However, alleviation capability reduces with increase in wing tip mass and hinge stiffness [14]. Conversely, a reduction in the hinge stiffness makes the wing prone to flutter, which can be stabilised via wing tip masses, hinge flare angle and spanwise hinge location [60]. Reduction in roll damping alleviation introduced by the earlier use of fixed wing tips is also achieved by increasing the aileron effectiveness, which is also validated with flight test data of a 1:14 scaled prototype [61]. These are discussed in the subsequent subsections.

1.4.3. Numerical Modelling Techniques and Validation Tests

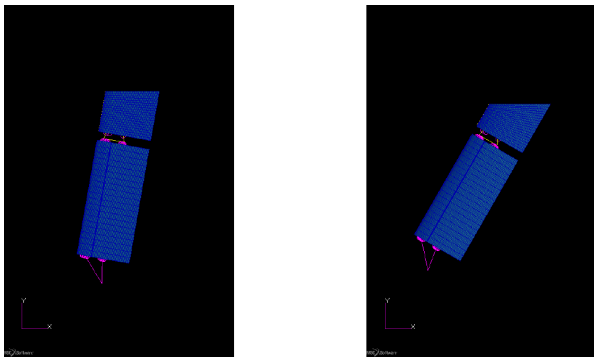

(a) Nastran model showing how sweep angle causes flaring of hinge angle. From 10^o (left) to 30^o (right) [13].

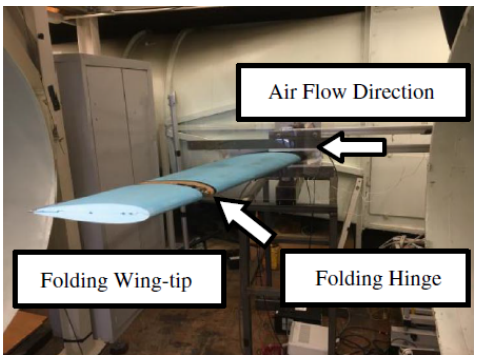

(b) Wind tunnel test setup for flare angle research [62].

The preliminary numerical tests discussed in the previous section were carried out on MSC Nastran (SOL144,145 and 146 which comprises the aeroelastic module). The structural model used were stick models and the wing tip hinge was modelled using RJOINT elements. Later, a high fidelity model of XRF1 Airbus research aircraft was also used to study the CSM-CFD coupling for accuracy of results [22]. Apart from MSC Nastran, Airbus also uses Siemens Virtual Labs Motion (Siemens VLM) for it's aeroelastic studies [63]. A wind tunnel experimentation was conducted [62] as shown in figure 1.13b, which provided accurate validation of the obtained Nastran predictions from the model showed in figure 1.13a. Differences between the predicted and actual load alleviation capabilities were observed for larger angles of deflection. Analyses of both linear and non-linear structural models produced little to no change in the predicted results [13]. Thus, geometric nonlinearity does not cause the above discrepancy. It can then be hypothesized that better aerodynamic modelling (especially at the wing tips) can lead to a more accurate prediction.

Nonlinear Wing Tip Actuation Mechanisms

The trend of interest in structural non-linearity is also evident here with the design of non-linear springs that get "activated" only during gust encounter. These designs involve the mechanisms of piecewise linearity of springs having high static low, dynamic (HSLD) stiffness [63] and "negative stiffness" characteristics with a snapping system based on bifurcation diagrams [64]. This is also inspired from the bistable winglets design as proposed by Gatto *et al*[**?**]. The "negative-stiffness" winglets have the obvious disadvantage that there exists only two states at which it operates and the unstable region during bifurcation cannot be utilised for intermediate angles. Although nonlinear actuation of hinge mechanism is proven here, the *AlbatrossOne* scaled model does not possess this capability yet.

Flight Dynamics and Landing Characteristics

With the introduction of free floating wingtips, the low frequency wingtip mode can potentially combine structural flexibility effects with flight dynamics. This is, in general, true for any high aspect ratio flexible aircraft and highly detrimental. For this purpose, Castrachini *et al* [65] developed a nonlinear reduced order beam model with wingtips. Tests on

aerodynamic derivatives, dynamic manoeuvres using aileron, rudder, elevator and wingtip deflections indicate that handling qualities of the aircraft are not affected. A free-floating hinge will maintain the zero-moment condition at the hinge at all times.

Another very important investigation is on the dynamic landing characteristics. With the hinge freely floating, a likely scenario is the wingtip-ground contact during hard landing. Raul et al [66] constructed a mathematical model, around an FE model, for dynamic landing with wing-tips. The archived hard-landing data of Airbus A321 was used with three different descent rates (maximum being 15ft/s). Two loading scenarios (with and without aircraft bounce loads) were simulated. Bounce loads were applied by time-shifting the load by a few seconds. To simulate a rolling whilst landing, similar time-shifting of loads on either landing gears were performed. This causes antisymmetric deflection of the wing tip on either side. Along with these, tests were also conducted to evaluate the effect of length of the wing tips during landing and a maximum of 7m wingtips (from earlier 4.5m ones). Vertical wingtip-ground clearances from these analyses prove that no contact will occur during hard landings.

1.4.4. Scaled Model Flight Testing

(a) Van-Test used as makeshift wind tunnel [16].

(b) Tether-Test for handling characteristics [16].

(c) Coasting angle of free-floating wing-tips during flight manoeuvre [16]

Figure 1.14: AlbatrossONE - "Semi-Aeroelastic" hinge demonstration by Airbus UK [16].

The AlbatrossONE, for the first time, took to skies in February 2019 (figure 1.14c), demonstrating the "semi-aeroelastic", free-floating hinge mechanism. The 1:14 scaled demonstrator was built using a combination of CFRP, GFRP , Plywood and some additively manufactured plastic parts (AMP) and weighed about 19 kilograms. Five variants, one with a 2.6m wing span (baseline w/o wing-tips), two with 3.2m wing spans (with wing-tips) and two more with 3.7m wing spans were used for the test. The fuselage, HTP and VTP were based on the Airbus A321 [61]. Prior to the flight testing, a wind tunnel test was performed to ensure that wing-tip flapping and wing bending frequencies do not coalesce. This would lead to flutter. At this point, it is evident that for a full-sized aircraft, as the wing gets more flexible, the probability of occurrence of this coalescence is high and must be mitigated. It is suspected that the hinge flare angle could be used to advantage here. During the flight tests, the wing tips were stable (both statically and dynamically) and responded to gust maintaining a zero moment condition at the hinge. The handling characteristics with free floating tips were satisfactory.

Flight Test Phase II was carried out on July 2nd, 2020 (figures 1.14a,1.14b) which portrayed a 75 percent increase in wing-span as compared to the baseline. Several additional tests were carried out to accurately specify the model. A van test was conducted to validate the wing-tip deployment, actuation, locking mechanisms and other aerodynamic evaluations. A tether test, where the demonstrator was hung upside-down using strings to perform flight manoeuvres, was performed to evaluate handling characteristics. A swing test for qualifying the mass distribution was also demonstrated. Currently, only flight test videos have been published.

1.4.5. Conclusions

Thus, from the preliminary investigations carried out at Airbus as summarised above, future work requires accurate numerical modelling of the hinged wing tip concepts in order to match the level of load alleviation achieved in wind tunnel tests. Conclusive evidence has been presented related to the under-prediction of the load alleviation achievable by the hinged wing tip concept. Due to this, it is imperative to build a numerical model that accurately captures the geometric nonlinear effects of the structure, the complete aerodynamic effects including the wake. Also, it is observed that the wind tunnel and the flight test demo were performed with rigid aircraft models and no tests have been performed using aeroelastically scaled models. The research gaps in each sub-field of the current thesis have been identified and presented in the concluding statements of the respective chapters in this document. These gaps, in conjunction with the latest developments at Airbus Innovations UK, suggest the way forward for the current work. The following section presents the formulation of the research questions for this thesis.

1.5. Research Objectives and Goals

The objectives and goals of this thesis are arrived at based on the literature review presented in the previous sections. Section 1.5.1 poses the research questions for the current work and the main objective is presented in section 1.5.2.

1.5.1. Research Question(s)

The main research question of the current work is,

"How can a computational framework be set up that accurately predicts the geometrically nonlinear aeroelastic behaviour of a realistic airliner with free hinged folding wing tips in free flight?"

The main goals of the current work is presented below in terms of Research Questions:

1. How to build the computational framework of the concept?
   (a) How to build the structural model with hinged wing tips on MSC Nastran? How to alter the SOL400 module (Implicit Nonlinear Analysis) to model nonlinear actuation of hinged wingtips for loads alleviation?
   (b) How to build the 3D UVLM panel code for aerodynamics of the hinged wing tip design using open source UVLM modules? How to accurately model the wing tips with flared hinges using the aerodynamic panels?
   (c) How to link the structural and aerodynamic solvers using MATLAB/ Python scripts? i.e How to best couple the fluid and structural domain that are analysed in time domain ?
2. What are the analyses to be performed numerically?
   (a) What is the aeroelastic performance i.e static and dynamic responses of the aircraft with wing tip compared to those of the baseline aircraft without the tips?
3. How can the proposed work be verified and validated?
   (a) How does the Numerical model proposed perform in comparison to the existing codes or theories?
   (b) How do the obtained numerical results fare in comparison with flight test / experimental data?

1.5.2. Research Objective

The objective of this thesis work is:

"To develop a computational geometrically nonlinear aeroelastic framework using commercial analysis software and open source programming languages, that captures the unsteady and nonlinear responses of hinged wingtips, which are dynamically actuated for loads alleviation during flight."

2

Mathematical Description of the Aeroelastic Phenomenon

MSC Nastran for the structural domain and Unsteady Vortex Lattice Method (UVLM) for aerodynamics have been employed in this work. While MSC Nastran is an industry standard aeroelastic toolbox, the choice of UVLM was based on the requirement of a time domain solver while maintaining acceptable accuracy and lower computational resources. Panel codes are medium fidelity aerodynamic solvers based on potential flow theory. This brings in an approximation as viscosity is not considered. However, for most subsonic speeds, these methods prove to be beneficial. In these techniques, a given singularity is distributed across the wing geometry that are used to calculate the lift generated by solving for their strengths. These codes are classified based on the type of singularities that are used in simulation - i.e a lattice of doublet distribution (DLM), a lattice of vortex ring distribution (VLM).

In order to incorporate unsteady effects, wake influence must be computed for each time-step. The technique is then termed as Unsteady Vortex Lattice Method (UVLM). Section 2.1 discusses in detail, the mathematical equations and laws that govern potential flow aerodynamics. Section 2.2 discusses in brief, the structural dynamics and direct time integration techniques. Finally 2.3 discusses in detail the methods of fluid structure coupling.

2.1. Fluid Dynamics and The Potential Flow Theory

The fluid domain is governed by the well known Navier Stokes Equations, consisting of three parts. These are conservation of mass, momentum and energy, and are respectively given by:

$$\nabla \cdot (\rho u) = 0 \tag{2.1}$$

$$(\rho u)t + \nabla \cdot \rho u \otimes u = -\nabla p + \nabla \cdot \tau + \rho f \tag{2.2}$$

$$(\rho e)t + \nabla \cdot (\rho e + p)u = \nabla \cdot (\tau \cdot u) + \rho f u + \nabla \cdot \dot{q} + r \tag{2.3}$$

Assuming the fluid flow to be irrotational and incompressible, the NS continuity equation reduces to Laplace equation and is given by,

$$\nabla^2 \phi = 0 \tag{2.4}$$

Laplace equation is a solution to the continuity equation of flow around an airfoil at low speeds (Mach Numbers). The partial differential equations that results is solved by distributing singularity solutions on the problem boundary where the velocity potential is determined through a pair of boundary conditions namely,

(i) Flow tangency (No penetration) boundary condition:

$$(\nabla \phi + \mathbf{v}).\mathbf{n} = 0 \tag{2.5}$$

where $\mathbf{v}$ is the tangential velocity of the fluid at the surface.

(ii) Kelvin Theorem (Zero circulation) theorem

The velocity disturbance due to the body motion must vanish in the far field. This is an infinity boundary condition and is given mathematically as,

$$\lim_{|r| \to \infty} \nabla \phi = 0 \tag{2.6}$$

Figure 2.1 shows the most commonly used singularities in aerodynamics that satisfy the Laplace equation.

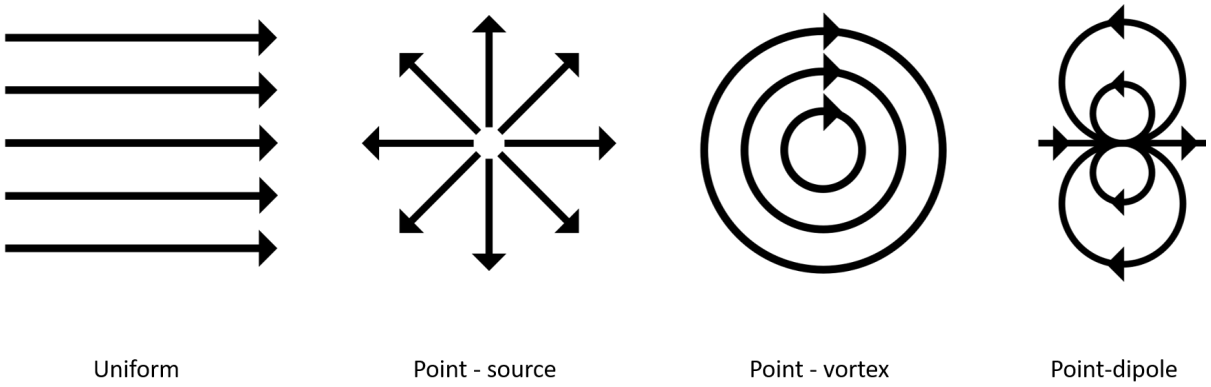

Figure 2.1: Examples of singularities in potential flow theory [17].

According to the Kutta-Jukowski's theorem, lift is directly proportional to the strength of vorticity present in the fluid domain. Therefore to numerically model a lifting surface, vorticity must be included in the solution. While commercial packages like MSC Nastran employ the Doublet Lattice Method (DLM) for its ease in frequency domain representations, Vortex Lattice Method (VLM) is the preferred solver for time domain computations where wake effects are to be modelled. Both the former and the latter are singularity elements that satisfy the Laplace equation. Ideally, unsteady aerodynamics and it's effects can be easily captured using the latter due to its capability to model the time domain wake evolution.

2.1.1. SINGULARITY ELEMENTS - THE VORTEX FILAMENT AND VORTEX RING

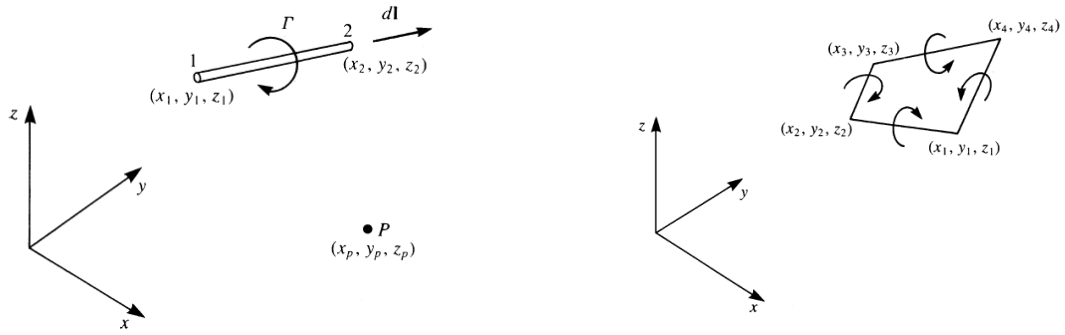

(a) vortex line element

(b) Vortex ring element.

Figure 2.2: Constituent aerodynamic singularity element representation [7]

Figure 2.2 shows the forms of vortex singularity elements used in aerodynamic computations. The vorticity induced by the vortex element is given by Biot-Savart law, which is mathematically represented as:

$$\mathbf{q}_{kl} = \oint \frac{d\mathbf{s} \times \mathbf{r}_{kl}}{4\pi |\mathbf{r}_{kl}|^3} \tag{2.7}$$

where $d\mathbf{s}$ is the vortex segment under consideration, $\mathbf{r}_{kl}$ is the distance vector.

Once the induced velocity is determined, the influence coefficient is computed as,

$$(\mathbf{A}_b)_{kl} = \mathbf{q}_{kl}.\mathbf{n}_k \qquad k,l = 1,2...,M*N, \tag{2.8}$$

A matrix is assembled using the definition of Biot-Savart's law which governs the induced velocity at a given location **k** by a vortex element **l**, and M*N is the total number of panels. Finally , the RHS vector for the given time i.e. the downwash at the collocation point is calculated,

$$\mathbf{w}^t = W_b(\dot{\chi}_b^t + \mathbf{v}_d^t) \tag{2.9}$$

where $\dot{\chi}_b^t$ is the grid velocity and $\mathbf{v}_d^t$ is the atmospheric disturbances. This is to account for elastic deformation and rigid motion [12]. Figure 1.9 illustrates the time-stepping algorithm of UVLM codes in literature.

The time-domain solution for this problem is to apply the no-penetration boundary condition at each control point of the surface panels at a given time t,

$$\mathbf{A}_b\Gamma_b^t + \mathbf{A}_w\Gamma_w^t - \mathbf{w}^t = 0, \tag{2.10}$$

where the subscripts b and w are for bound and wake panels respectively, **A** is the Influence matrix and **w** is the downwash vector.

2.1.2. Types of Wake Modelling

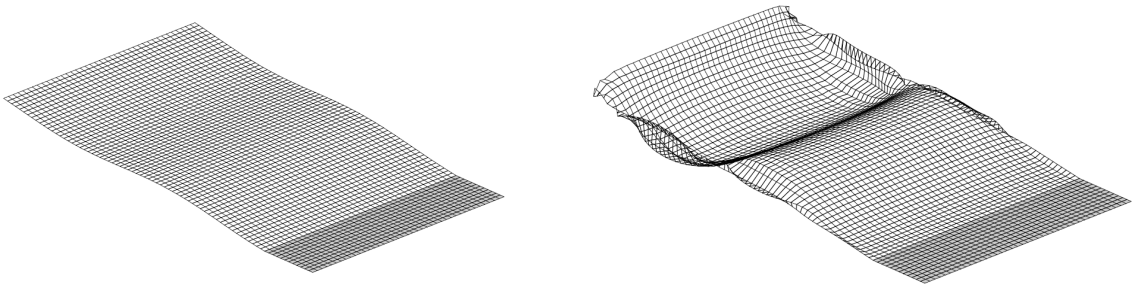

(a) Fixed prescribed wake without convection

(b) Force free wake with roll up and convection

Figure 2.3: General types of wake modelling strategies employed in literature [12]

At the core of UVLM is the wake modelling technique. To include the effect of the wake on the lift generated on a given lifting surface, three common modelling strategies are often employed. First, is a horse-shoe wake where the downwash induced by the complete wake is modelled using a single chord-wise wake panel that extends to infinity. Numerically, a wake length of about 20 chords behind the trailing edge has shown to converge. Next, is a prescribed fixed-wake representation, where a fixed number of chordwise wake panels are placed behind the trailing edge and the effects of individual wake vortex rings on each lifting bound vortex ring is computed. Lastly and the most completely defined wake, is the force-free wake that is convected downstream with the local velocity at every timestep of the simulation.In order to simulate wake roll-up, the effect of wake and bound vortices on every shed wake vortex must be added in the routine and is computationally quite expensive. Figure 2.3 shows these general classification of types of wake models in UVLM implementations in the current solver.

2.1.3. Helmholtz Theorem

Helmholtz Theorem can be summarized as follows:

1. The vortex filament strength remains constant along the length.

2. The modelled vortex must always form a closed loop and cannot start or end in the fluid domain.

3. The properties of fluid elements (such as vorticity and irrotationality) continue to remain in their initial state until acted upon by a force that causes a change.

2.1.4. KELVIN'S CIRCULATION THEOREM

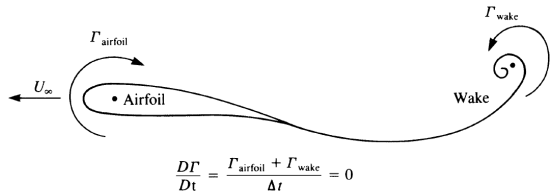

Figure 2.4: Kelvin's Circulation Theorem [7]

Kelvin's Circulation Theorem states that the total circulation in any closed domain is a constant. This translates to the interpretation that perturbation caused by a solid body in a fluid having a relative motion diminishes far field (at infinity). Thus, in the formulation of the Unsteady Vortex Lattice Method that models the wake evolution in time, the vorticity is classified into two types - Bound and Wake Vortices which have opposite sign, maintaining Kelvin's condition at any instant of time. This is illustrated in 2.4

2.1.5. KUTTA JOUKOWSKI THEOREM

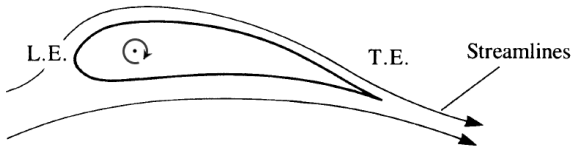

(a) 2D illustration of circulation around an airfoil modelled using vortex elements [7]

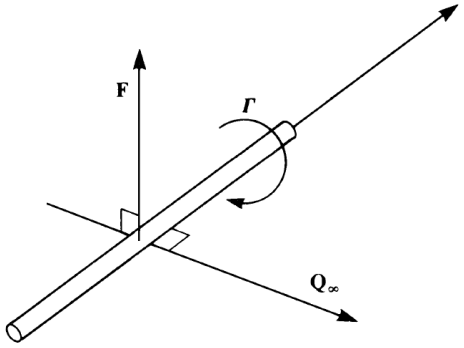

(b) Sign Convention for K-J Theorem [7]

Figure 2.5: Kutta Joukowski Theorem[7]

Kutta-Joukowski Theorem states that the lift generated in body having relative motion in a fluid is directly proportional to the circulation around the body. Figure 2.5 shows the mathematical modelling of a lifting airfoil and the sign convention (Right hand rule) prescribed by Kutta and Joukowski. The equation is given by,

$$L' = \rho_\infty V_\infty \Gamma L' = \rho_\infty V_\infty \Gamma \tag{2.11}$$

2.1.6. Bernoulli's steady and unsteady Force Equations

The total lift in transient simulations includes the instantaneous rate of change of vorticity. The lift expression for each panel is derived from the unsteady version of the Bernoulli's equation and is given by [67]:

$$\Delta L_{i,j} = \rho \left[\mathbf{V}_\infty (\Gamma_{i,j} - \Gamma_{i-1,j}) \Delta y_{i,j} + \Delta x_{i,j} \Delta y_{i,j} \frac{\partial}{\partial t} \left(\frac{\Gamma_{i,j} + \Gamma_{i-1,j}}{2} \right) \right] cos(\alpha_{i,j}) \tag{2.12}$$

where $\alpha_{i,j}$ is the local angle of attack of the panel, $\Delta x_{i,j}$ and $\Delta y_{i,j}$ are the panel widths in the chord and span directions respectively. The first term is the steady lift and is computed from the chordwise difference in the panel vortex strength. The second term is the unsteady part of the lift whose maximum effect is in the initial period of the simulation where maximum difference exists between the strengths of the shed vortices. Subsequently, this unsteadiness diminishes with time.

2.2. Structural Dynamics and The Finite Element Procedure

This section presents in brief, the major theories that make up the field of structural dynamics. Beginning with the Lagrangian Mechanics in 2.2.1 using which, governing equations are arrived at. Next, Ritz method is introduced in section 2.2.2 which forms the basis of Finite Element approaches. Following which, governing equations of structural dynamics and it's time integration schemes are described in sections 2.2.3 and 2.2.4 respectively. Finally the concept of structural nonlinearity is introduced in 2.2.5.

2.2.1. Lagrangian Mechanics

In contrast to the Newtonian Mechanics which is defined in terms of vectorial forces , Lagrangian Mechanics is defined in terms of energies which are scalar. Lagrangian Mechanics deals with the minimization of the *action* of a given system in a configuration space. Mathematically,

$$\delta \int_{t1}^{t2} L dt = 0$$

where $L = T - \Pi = T - (U + V)$ is the Lagrangian of the system. T is the Kinetic Energy and Π is the Total Potential Energy of the system. U is the internal Strain Energy and V is the External Work. The theorem can also be stated as follows:

"Among all motions that will carry a conservative system from one configuration time t_1 to another configuration time t_2, that which actually occurs provides a stationary value of the integral"

The Lagrange equation of motion can be arrived at by employing variational principle to the individual terms in the above definition and is given by,

$$\frac{d}{dt}\left(\frac{\partial T}{\partial \dot{u}_j}\right) - \frac{\partial T}{\partial u_j} + \frac{\partial (U+V)}{\partial u_j} - Q_j = 0$$

Where T,U and V carry the same definition as before and Q_j is the external generalised force acting on the system.

2.2.2. Ritz Method

In this method, the complete displacement field of a continuous structure is assumed to be a linear combination of weighted basis functions. Mathematically,

$$u(x,y,z,t) = \sum_{n=1}^{N} a_i(t)\phi_i(x,y,z)$$

where a_i is the generalised coordinates that are time dependent and ϕ_i are spatial trial functions. In essence, this is a variable separable approach. This definition of the displacement field is then used in the expressions of the system energy relations.

2.2.3. Governing Equation of Motion

In the dynamic analysis of continuous system (distributed systems), two additional factors are considered when compared to a static case. i.e The inertial effects and the temporal variation of all quantities. The equation of motion can be derived by substituting the analytical expressions for kinetic and potential energy in the Lagrange Equation. Mathematically, the equation of motion in generalised coordinates is given as,

$$[M_s]\ddot{x} + [C_s]\dot{x} + [K_s]x = F_a(t)$$

Where $[M_s], [C_s], [K_s]$ are the generalised mass, damping and stiffness matrices of the structure. In Finite Element Method, a given continuous system is discretised into finite elements. Ritz method is applied to individual elements using locally defined shape functions to obtain elemental matrices. These elemental matrices are then assembled into global matrices depending on the element connectivity.

Due to the flexibility of the lifting surfaces of an aircraft, wing structures can exhibit large deformation and small strain behaviour and hence it is imperative to include the geometric non-linearity of these structures in the order to numerically predict the physical behaviour of these real structures. In cases of large strains, material nonlinearity must also be considered. In general, the equation of motion including nonlinearities will be of the form

$$M_s\ddot{x} + h(x,\dot{x}) = F_a(t)$$

where h is a nonlinear function that varies with displacement/velocity.

Neglecting damping, it can be seen that often in a linear case, we end up with constant mass and stiffness matrices as a result of the spatial discretisation of the system that is a function of space and time. Thus, once discretized in space, we have a differential equation in time

for which numerical time integration techniques are employed. Modal analysis techniques are generally employed in linear structural dynamics of relatively simple formulations. As complexities in models are introduced, direct numerical time integration techniques are employed like Newmark β method or Generalised α methods. Nonlinearities can be easily incorporated into the Newmark schemes with the addition of a Newton-Ralphson iteration whereby a residual is evaluated by assembling a tangent stiffness matrix (Jacobian) which is now a function of displacement.

2.2.4. Direct Time Integration Equations - Newmark Beta Method.

Considering the above given equation of motion in structural dynamics, it is our aim to perform a temporal discretization process and find the values of the structural states at discrete time intervals.
Applying mean value theorem to the first and second time derivatives, the discretised equations for the velocity and displacement can be given as,

$$v_{n+1} = v_n + \Delta t\left[(1-\gamma)a_n + \gamma a_{n+1}\right] \quad \text{where} \quad 0 \leq \gamma \leq 1$$

$$x_{n+1} = x_n + (\Delta t)v_n + \frac{\Delta t^2}{2}\left[(1-2\beta)a_n + 2\beta a_{n+1}\right] \quad \text{where} \quad 0 \leq 2\beta \leq 1 \tag{2.13}$$

In the discrete form, the equation of motion to be solved can be written as,

$$Ma_{n+1} + Cv_{n+1} + Kx_{n+1} = f_{n+1} \tag{2.14}$$

Plugging in the definition of discretised displacements and velocities in eq. 2.13 into eq. 2.14 and rearranging, we get the final form as,

$$(M + \gamma\Delta tC + \beta\Delta t^2 K)a_{n+1} = f_{n+1} - C\left\{v_n + \Delta t(1-\gamma)a_n\right\} - K\left\{x_n + \Delta t v_n + \frac{\Delta t^2}{2}(1-2\beta)a_n\right\}$$

Initial Conditions (ICs) are prescribed for displacement and velocity as,

$$x_0 = x(0) \quad v_0 = \dot{x}(0)$$

through which the initial acceleration can be found. Now the state $\{x_n, v_n, a_n\}$ is completely known. Using a predictor-corrector approach, the state at next timestep $\{x_{n+1}, y_{n+1}, z_{n+1}\}$ can be found. In the final equation given above, the terms on the RHS are the predictors for displacement and velocity as they are evaluated using the known values from previous timestep. Equation 2.13 is then used to correct the predicted values.
The above procedure can also be followed for problems including structural nonlinearity. In which case, the governing equation is of the form,

$$Ma_{n+1} + h(x_{n+1}, v_{n+1}) = f_{n+1}$$

The procedure for timestepping from t_n to t_{n+1} involves an additional intermediate Newton-Raphson iteration as shown below [obtained from TUD SASII course material 2019].

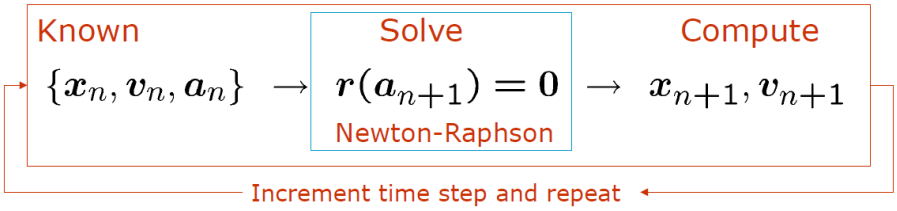

2.2.5. GEOMETRIC NONLINEARITY USING IMPLICIT ITERATIVE PROCEDURES

In problems that involve the geometric nonlinearity of the structure, the load displacement curve is no longer linear. This is indicative of a change in stiffness of the structure due to its deformation. Implicit iterative procedures such as Newton-Raphson are commonly used for such scenarios. Figure 2.6 illustrates this scheme.

Any iterative scheme follows a general procedure. The prediction of the total displacement is adapted in an incremental manner until convergence is obtained. The standard Newton-Raphson method is often modified to include multiple iterations for a given step until convergence is obtained. The stiffness matrix is updated only at the end of the step. Quasi Newton Techniques employ the information from the previous step and prove to be computationally more efficient.

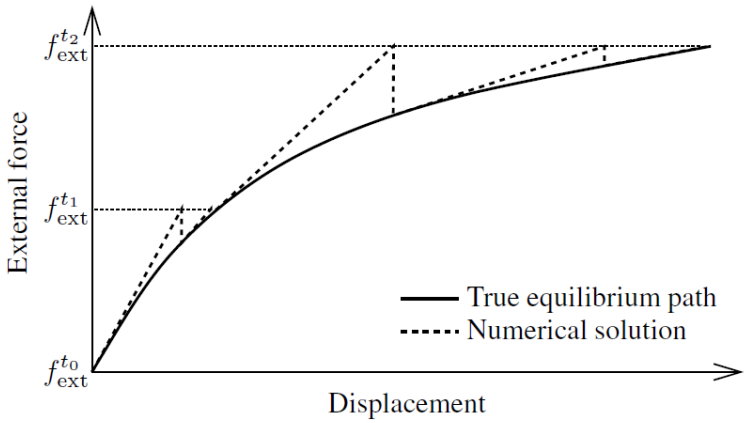

Figure 2.6: Standard Newton-Raphson iteration scheme for nonlinear phenomenon [18].

2.3. FLUID-STRUCTURE INTERACTION - COUPLING STRATEGIES

Following the description of the individual physical domains that make up the field of aeroelasticity, a third and the most important consideration is the coupling of the independent domains within the realm of numerical considerations. As discussed previously, the numerical discretization schemes applied to each domain can vary significantly which results in non matching meshes. This section presents theory of coupling such domains. Section 2.3.1 presents the most commonly employed technique, namely the conventional serial staggered scheme for iterative and temporal coupling. The next two sections 2.3.2 and 2.3.3 present the mathematical formulations of Radial Basis Functions (RBF) and Nearest Neigh-

bour (NN) method respectively.

2.3.1. SERIAL-STAGGERED APPROACH

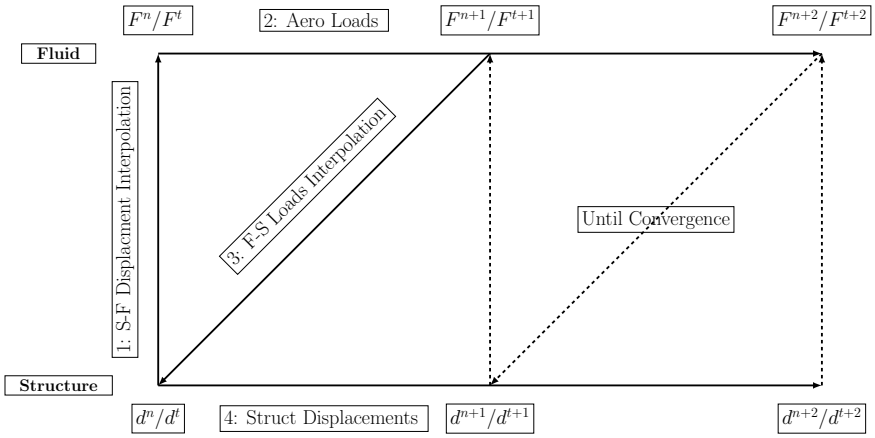

Figure 2.7: Conventional Serial Staggered (CSS) scheme for partitioned nonlinear coupling

Figure 2.7 shows the schematic flow of information according to the conventional staggered scheme. For an incremental approach to nonlinear static simulation such as the one in the current thesis, the procedure is similar for static and dynamic simulations as shown. For an iterative aeroelastic static solution, we first obtain the aerodynamic loads in the undeformed configuration, which is transferred to the structure which results in its deformation. This deformation information is then transferred back to the aero domain to obtain new loads in the deformed configuration. This process is continued until convergence of displacements or loads are obtained. As shown, this information transfer is identical in dynamic simulations, where the only difference is the introduction of a temporal marching.

2.3.2. RADIAL BASIS FUNCTIONS - MATHEMATICAL FORMULATIONS

This interpolation procedure prescribed by Ahrem et al [54] is followed and briefly summarised here:

The deformation is known at structural nodes $X = \{x_1, ..x_n \in \mathbb{R}^3\}$ and this is to be transferred to the fluid nodes $Y = \{y_1, ..y_m \in \mathbb{R}^3\}$. Radial Basis Function Interpolation technique relies on representing this known (structural X) displacement field using a continuous function. Thus, the unknown displacements of the domain Y are obtained by evaluating this function at the fluid nodes. A generic radial basis function is of the form:

$$s(x) = \sum_{j=1}^{N} \alpha_j \phi(||x - x_j||_2) + p(x) \tag{2.15}$$

where, ϕ is a positive definite function of order m,
$p(x)$ is a polynomial of at most m-1 terms ($\in \mathbb{R}^3$)

The compact support radial basis function prescribed by Wendland [54] is defined by,

$$\phi(\|x\|) = (1 - \|x\|)_+^4 (4\|x\| + 1) \tag{2.16}$$

Coefficient vectors α and β are determined by the interpolation conditions given by,

$$s(x_j) = v_j; 1 \leq j \leq N, \tag{2.17}$$

$$\sum_{j=1}^{N} \alpha_j q(x_j) = 0; \forall q \in \Pi_{m-1}(R^3) \tag{2.18}$$

The resulting coupling matrix can be set up in the following way.

Let, $p = \{p_1, ...p_q \in \mathbb{R}^3\}$ form a set of basis for polynomials.
By defining $A = \phi(\|x_j - x_k\|_2) \in \mathbb{R}^{NxN}$ and $P = (p_j(x_i) \in \mathbb{R}^{NxQ})$.

The coefficient vectors α and β (which is now $\sum_k \beta_k p_k$) can then be determined by,

$$\begin{bmatrix} a_{11} & a_{12} & \dots & a_{1n} \\ a_{21} & a_{22} & \dots & a_{2n} \\ \dots & \dots & \dots & \dots \\ a_{m1} & a_{m2} & \dots & a_{mn} \end{bmatrix} \begin{bmatrix} \Gamma_1 \\ \Gamma_2 \\ \dots \\ \Gamma_m \end{bmatrix} = \begin{bmatrix} B_1 \\ B_2 \\ \vdots \\ B_m \end{bmatrix} \tag{2.19}$$

$$\begin{pmatrix} A & P \\ P^T & 0 \end{pmatrix} \begin{pmatrix} \alpha \\ \beta \end{pmatrix} = \begin{pmatrix} d \\ 0 \end{pmatrix} \tag{2.20}$$

Now, in order to map to the fluid domain, we define $\tilde{A} = \phi(\|y_i - x_j\|_2) \in \mathbb{R}^{MxN}$ and $P = (p_j(y_i) \in \mathbb{R}^{MxQ}$.Then, the fluid domain deformation is given by,

$$s(y_i) = \begin{pmatrix} \tilde{A} & \tilde{P} \end{pmatrix} \begin{pmatrix} A & P \\ P^T & 0 \end{pmatrix}^{-1} \begin{pmatrix} d \\ 0 \end{pmatrix} = \mathbf{C} \begin{pmatrix} d \\ 0 \end{pmatrix} \tag{2.21}$$

For a conservative approach, the transpose of the coupling matrix C_T is to be employed. However in practical applications, using the transpose of the radial basis coupling matrix leads to oscillations in the interpolated pressure loads. This is attributed to the fact that the row-sum of the transpose matrix is not unity. In such cases, it is apt to use the consistent approach by defining two separate matrices for force and displacement interpolations as implemented in the proposed solver here.

2.3.3. Nearest Neighbour Interpolation

This is the simplest form of data transfer between two domains. The technique relies on transferring information completely to the nearest data point in the required domain. Therefore, the interpolating matrix H_{fs} of dimensions n_s x n_f is a boolean matrix. The row-sum of such matrix is unity and the method is thus, inherently consistent. Figure 2.8 illustrates an example of the nearest neighbour search in the proposed solver. The structural points (green) nearest to the aerodynamic collocation points (red) are obtained and a one-on-one mapping from red to green is carried out.

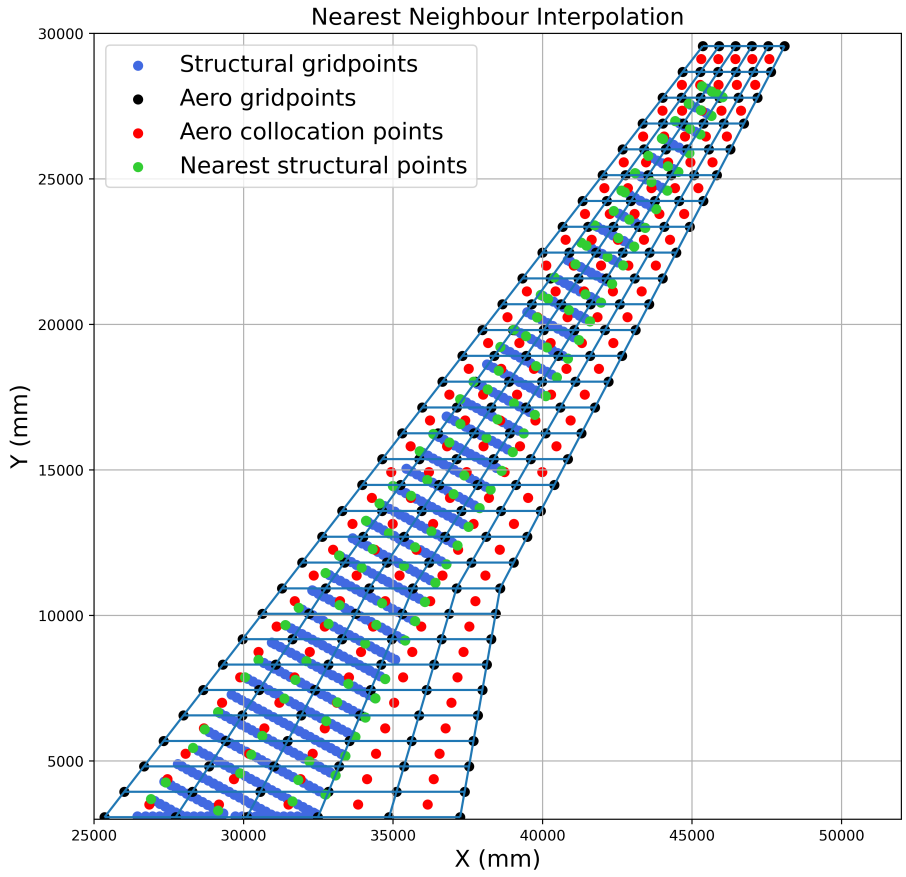

Figure 2.8: Fluid-to-Structure force interpolation using nearest neighbours algorithm.

NOTE: The disadvantage of using Nearest Neighbour Interpolation for displacement is that it can result in staggered (step-like) representation of a continuous displacement field and hence erroneous. Such errors can however be reduced by maintaining similar meshes in the two domains. But it is recommended that other higher order techniques be employed for displacement interpolation.

3

Partitioned Nonlinear Aeroelastic Solver Description

This chapter includes the description of the solver developed along with the flowcharts, explanations and capabilities. Section 3.1 describes the object oriented setup of the UVLM solver. Next, the solvers of MSC Nastran used in the framework are discussed in section 3.2. Detail description of implemented procedures such as Advanced Restart for static and dynamic aeroelastic coupling are presented. Finally, section 3.3 presents the manner in which all the developed solvers come together into a complete nonlinear aeroelastic toolbox that is proposed in this thesis.

3.1. PyUVLM Solver

The UVLM solution procedure is implemented using an Object Oriented Programming (OOP) approach in Python. Figure 3.1 illustrates the main functions of the solver and flow of the information. The function are named in an intuitive manner for convenience and readability. The solver method has been developed using theory from Katz and Plotkin [7], and object oriented methodologies prescribed by Garcia et al [57] and del Carre et al [56].

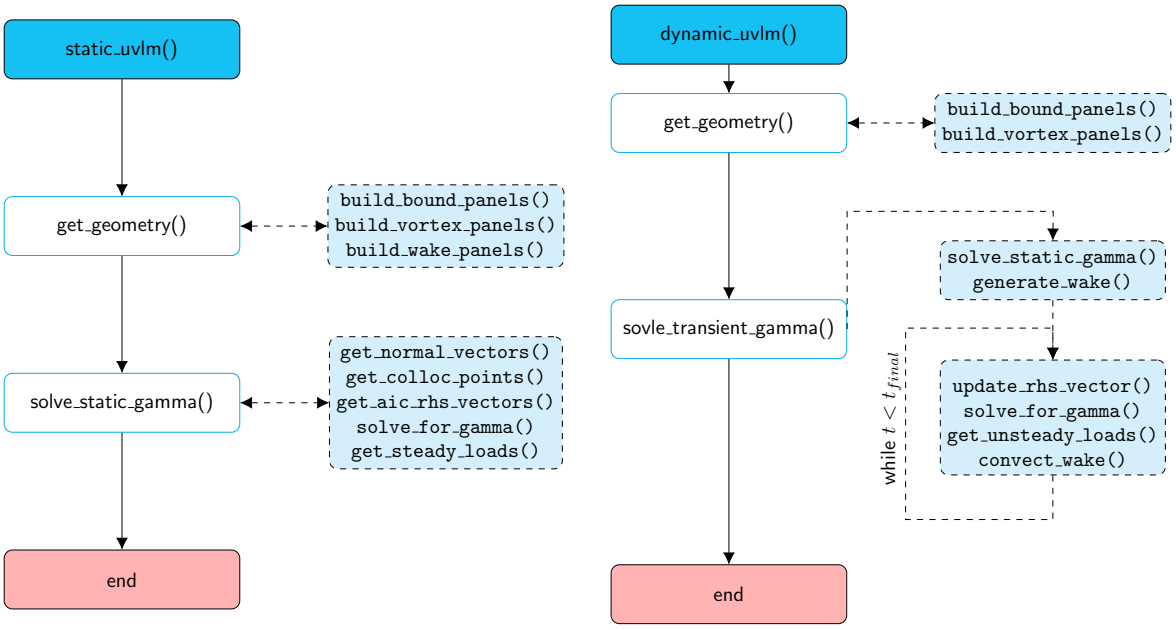

(a) Static aerodynamic solution sequence

(b) Dynamic solution sequence.

Figure 3.1: Object oriented setup of the PyUVLM static and dynamic solvers.

Figures 3.1a and 3.1b sequentially show the functions used to evaluate steady and transient aerodynamic loads, respectively. It can be broadly described in three steps. First is to build the geometry of the wing panels. Next, using the defined geometry, derive other parameters that depend on the geometry, such as collocation points and panel normals. Finally, solve the linear system of equations by defining the Aerodynamic Influence Coefficients (AIC) using Biot-Savart's Law. The procedure for transient case differs from the static case in two major aspects. Namely, the inclusion of a time-stepping loop and a wake convection procedure within it. The RHS vector will change with time due to the influence of the evolving wake. Also, unsteady aerodynamic loads are computed for each time-step taking into account the rate of change in vorticity. The mathematical theory and equations that are used in these solution procedures are discussed in detail in chapter 2.

3.2. MSC Nastran Solver Modules

This section begins with the description of the MSC Nastran aeroelasticity modules in 3.2.1. Following this, the manner in which nonlinear solution sequence employed in external coupling is described in sections 3.2.2 and 3.2.3. The methods of static and dynamic solution sequences employed in the coupled solver are then described in sections 3.2.4 and 3.2.5.

3.2.1. Standard Solution Sequences for Aeroelasticity

The aeroelastic toolbox in MSC Nastran employs the standard finite element procedures for the structural modelling and panel methods for aerodynamics, in particular, Doublet Lattice Method (DLM) for subsonic and ZONA51 for supersonic aerodynamics. SOL 144 is a static aeroelasticity solution sequence where the input is the flight parameters and the output is

the trim and control variables. SOL 145 studies the eigen modes and flutter. SOL 146 solves the equations for dynamic aeroelastic response [18]. These outputs are illustrated in figure 3.3.

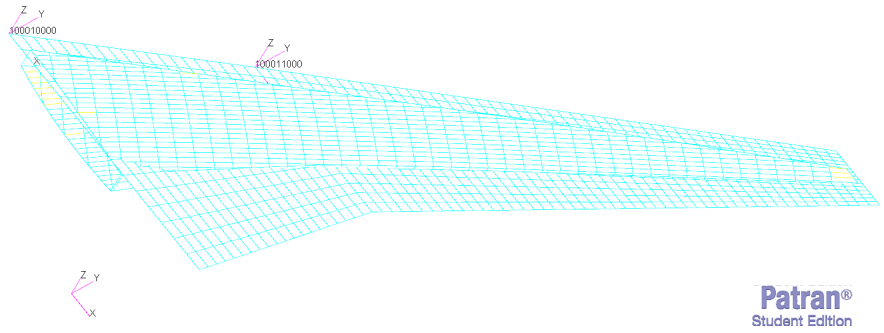

Figure 3.2: Model description in MSC Nastran for Aeroelastic Analysis- Nasa CRM wingbox splined to DLM panels for load/displacement interpolation.

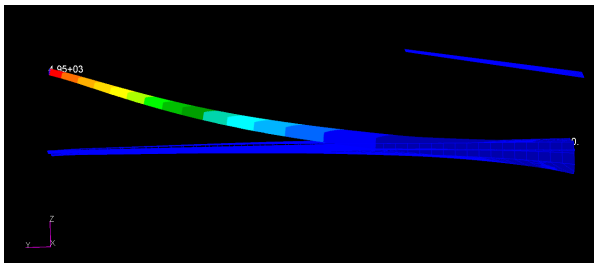

(a) Static aeroelastic deflection of NASA CRM - SOL144

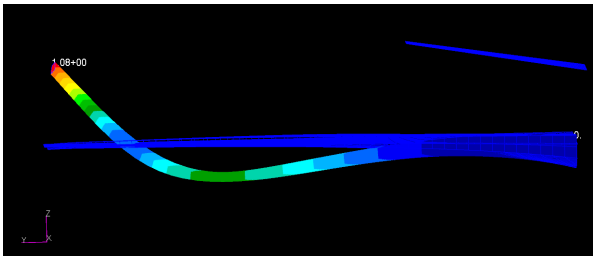

(b) Second bending mode of NASA CRM - SOL145

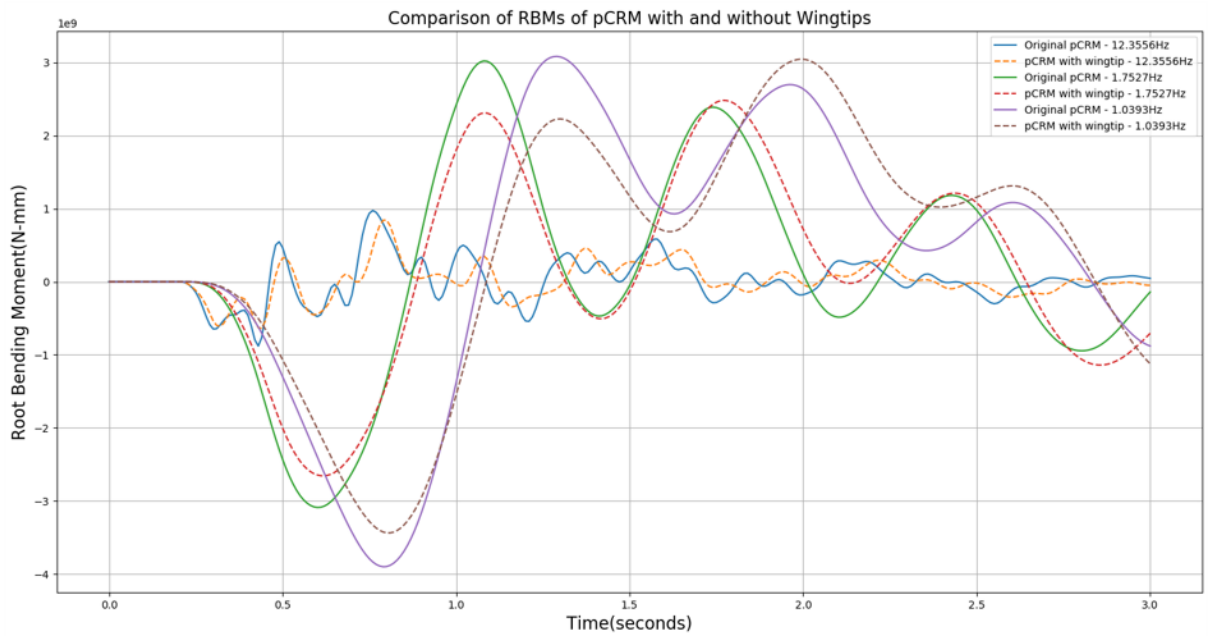

(c) Comparison of Root Bending Moment (RBM) on baseline and hinged wingtips - SOL146.

Figure 3.3: Nastran Aeroelastic Toolbox

While the aeroelastic module of MSC Nastran offers external aerodynamic data input on to predefined grids within the solvers, limitations arise in terms of analysing with transient aerodynamic loads. This is due to the frequency domain representation within Nastran. Thus, the aeroelastic toolbox cannot be utilised as is, to couple with external aerodynamic solvers that provide time domain solutions such as UVLM. While techniques for CSM-CFD coupling using OpenFSI platforms are available in literature [68], these are not open sourced methods and hence are not preferred. Thus, the current thesis attempts to accomplish the external coupling of MSC Nastran to time domain UVLM aerodynamics using partitioned coupling techniques. The aerodynamic solver developed was exhaustively discussed in the previous section. The following subsections discuss the solution sequences of MSC Nastran employed as structural modules in the coupling algorithm.

3.2.2. SOL 400 - A POWERFUL TOOL FOR IMPLICIT NONLINEAR SIMULATIONS

SOL 400 is a wrapper to almost all the solution sequences within MSC Nastran and is the main solver for nonlinear simulations. The linear aeroelastic module (i.e. SOL144 SOL145 and SOL146) is not compatible with and hence cannot be invoked using SOL 400. The ANALYSIS command in "Case Control Section" activates specific solution sequences within MSC Nastran. For example "ANALYSIS=NLSTAT" activates SOL106 (Nonlinear Static) and "ANALYSIS=NLTRAN" activates SOL129 (Nonlinear Transient Dynamics) [69]. Following this the appropriate settings for nonlinear simulations can be provided as input using NLPARM,NLSTEP and TSTEPNL data cards in the bulk data section.

3.2.3. ADVANCED RESTART ANALYSIS

One of the key features of MSC Nastran is the Restart option. A *"Restart Analysis"* allows to continue a simulation from a previously converged "check-point". This is applicable for both static and dynamic simulations and is especially useful for analyses that require external load control. For static aeroelastic cases, this means that iterative external loading of nonlinear structures for static equilibrium and trim are achievable. For transient aeroelastic simulations, this enables external loading of a structure at specific timesteps that are controlled by the numerical integration scheme. However care must be taken in evaluating the continuity of loads defined in such a manner as large timesteps would mean kinks/discontinuities in the loads and hence will lead to erroneous results.

Figure 3.4 shows a generic restart input file format for both static and dynamic cases on MSC Nastran. The key difference between the two formats is in the definition of the *NLRESTART* command in the case control section and in the specification of the NLPARM for static / TSTEPNL for dynamic. It is to be noted here that the geometry and boundary conditions cannot be changed in a restart run.

```
$ Generic SOL400 - Static restart format
$---------------------------------------
$ File Management Section
$---------------------------------------
RESTART VERSION k+1, KEEP
ASSIGN MASTER = 'static_coldstart.master'
$---------------------------------------
$ Executive Section
$---------------------------------------
SOL400
CEND
$---------------------------------------
$ Case Control Section
$---------------------------------------
DISP = ALL
STRESS = ALL
SPC = 1          $ Global definition BCs
$ Restart command
NLRESTART SUBCASE 1, STEP k
SUBCASE 1
        STEP 1  $ Coldstart
                ANAYSIS = NLSTAT
                LOAD = 1
                NLPARM = 1
        STEP 2  $ Restart 1
                LOAD = 2
                NLPARM = 1
        .
        .
        .
        STEP k-1
                LOAD = k-1
                NLPARM = 1
        STEP k
                LOAD = k
                NLPARM = 1
$-------------------------------------
$ Bulk Data Section
$-------------------------------------
BEGIN BULK
$ Include the loads for current step
INCLUDE 'loads_restart_k.dat'
ENDDATA
```

(a) Nonlinear static restart input format

```
$ Generic SOL400 - Dynamic restart format
$---------------------------------------
$ File Management Section
$---------------------------------------
RESTART VERSION k+1, KEEP
ASSIGN MASTER = 'static_coldstart.master'
$---------------------------------------
$ Executive Section
$---------------------------------------
SOL400
CEND
$---------------------------------------
$ Case Control Section
$---------------------------------------
DISP = ALL
STRESS = ALL
SPC = 1          $ Global definition BCs
$ Restart command
NLRESTART SUBCASE 1, STEP k, TIME n
SUBCASE 1
        STEP 1  $ Coldstart
                ANAYSIS = NLTRAN
                DLOAD = 1
                TSTEPNL = 1
        STEP 2  $ Restart 1
                DLOAD = 2
                TSTEPNL = 1
        .
        .
        .
        STEP k-1
                DLOAD = k-1
                TSTEPNL = 1
        STEP k
                DLOAD = k
                TSTEPNL = 1
$-------------------------------------
$ Bulk Data Section
$-------------------------------------
BEGIN BULK
$ Include the loads for current step
INCLUDE 'loads_restart_k.dat'
ENDDATA
```

(b) Nonlinear dynamic restart input format

Figure 3.4: Input file format for a generic restart at k^{th} iteration using MSC Nastran SOL400 solver

Using such a straightforward procedure can be highly beneficial in switching to a dynamic solution using static results as initial conditions. Specifically, dynamic simulations can be controlled with external changing loads at specific time-steps. Figure 3.5 shows two examples of such an external control. Restart analyses employ convolution theorem and hence take into account the loading and response histories. A step response to an aerodynamic external load (shown in figure 3.5a) or a response to arbitrary loading (figure 3.5b) can be obtained using restarts. It is imperative to pay attention to the SIDs of static and dynamic load entries (FORCEi and TLOADi) in such attempts of load restarts. As, load histories are taken into account, at every new load introduction, separate SIDs must be defined. It is also important to maintain the discontinuities in load introduction to a minimum as this would lead to erroneous results.

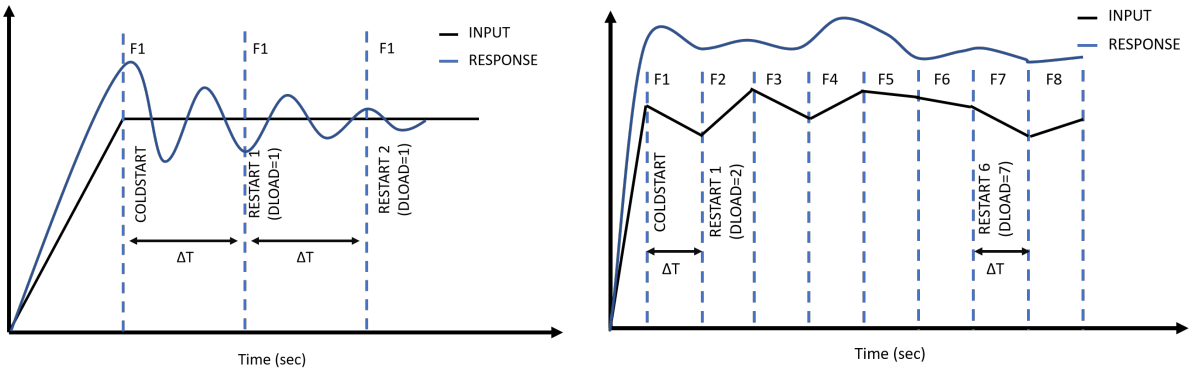

(a) Response to step input

(b) Response to arbitrary input

Figure 3.5: Schematic illustration of dynamic response analysis using Restart Analysis for various input loading curves

3.2.4. Static Solution Sequences using advanced restart SOL400

As discussed in the previous section, SOL 144 in MSC Nastran solves equations for static equilibrium of aeroelastic phenomenon, i.e. trim equations. In an iterative approach, the aerodynamic loads result in deformation of the structure, which in turn changes the aerodynamic loads. These aerodynamic loads are obtained using the UVLM solver are interpolated onto the structure, due to which the structure deforms. SOL 101 is the main linear, static structural solver in MSC Nastran. With the current trend of increasing interest towards HALE aircraft, slender wings with large deformations introduce geometric nonlinearity for which SOL 106 (Nonlinear Statics) is a suitable solver. Also, as the aeroelastic trim is obtained iteratively, the displacements and loads must attain convergence. This calls for the capability of a solver to update both the loads and displacements and thus nonlinear solvers are preferred. The main requirements for static solutions are static description of loads using FORCEi or PLOADi entries, boundary conditions using the SPCi entries. For nonlinearities, NLSTEP or NLPARM are defined. [69].

3.2.5. Dynamic Solution Sequences using advanced restart SOL400

The transient dynamic simulations can be carried out using both frequency and time domains. The frequency domain method involves the transformation of time domain loads into frequency domain using FFT and the simultaneous modal decomposition of the structure. Direct time integration techniques are employed for time domain solutions. In MSC Nastran, SOL 109 and SOL 129 are linear and nonlinear transient dynamic solvers that employ direct time integration techniques. Two main aspects of these dynamic solvers are spatial and temporal description of loading information. The spatial description refers to the static load definition using FORCEi, PLOADi or DAREA entries on specific GRID points. Dynamic description refers to the temporal dependence of these loads using TLOADi entries. An important step is to link these spatial and temporal descriptions using LSEQ (static load sequence) entries that have the same EXCITEDs as the TLOADi entries. This requirement can also be bypassed by having the static FORCEi cards having the same EXCITEIDs as the TLOADi entries. TSTEPNL sets the nonlinear solution procedure [69].

Transient dynamic simulations of structures are most commonly carried out using direct time integration techniques. The popular methods employed are the Newmark β and Generalised α methods, whose mathematical formulations are discussed in section 2.2.4. MSC Nastran allows the use of both these methods for linear and nonlinear solutions. Dynamic simulations are sensitive to time-steps, initial and boundary conditions.

Since the solver is coupled externally to the UVLM for every time-step, it is imperative to reduce any computational complexity that may arise due to nonlinearities, time-steps and other inaccuracies (such as phase and artificial damping). In the current implementation of the proposed solver, Newmark β method with constant time-steps is utilised. The choice of this method is justified due to it's unconditional stability, no numerical damping. The dynamic solution on MSC Nastran is controlled by the use of NLSTEP and TSTEPNL where the time integration options are set [48].

3.2.6. MSC NASTRAN - PYTHON INTERFACE - INPUT AND OUTPUT

HDF5 is a file format that stores big data into files and folders,enabling easy data extraction, efficient I/O functionalities and cross platform data exchange capabilities. In MSC Nastran, implementing a HDF5 request involves using the command MDLPRM,HDF5,0 statement just after the BEGIN BULK statement to request for output files with ".h5" extension.

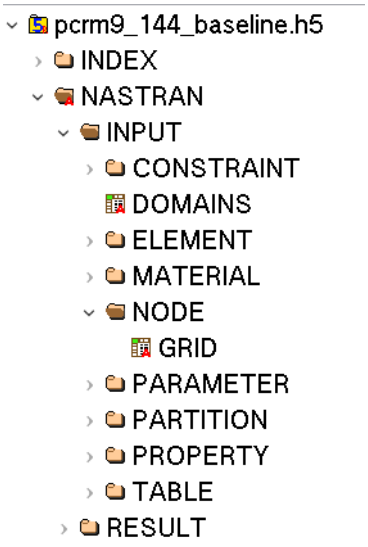

(a) HDF5 file format - data stored in files and folders.

```python
import numpy as np
import h5py

def get_geom(h5file):

    #undelfected postion
    file = h5py.File(h5file,'r')
    data = file.get('NASTRAN/INPUT/NODE/GRID')
    data = np.asarray([data])
    geom = data[('X')]
    file.close()

return geom

geom = get_geom('pcrm9_144_baseline.h5')
```

(b) Example Python script for data extraction from hdf5 file

Figure 3.6: Python - HDF5 Interfacing for data extraction from MSC Nastran output.

3.3. SOL400-PyUVLM - A Geometrically Nonlinear Aeroelastic Solver

The previous sections described in detail the manner in which the two individual solvers are built. This section provides a closure to description of the complete nonlinear aeroelastic solver built. The mathematical formulations of fluid-structure coupling was discussed in section 2.3 of the previous chapter, which enables information transfer between the two independent and modular solvers. The following subsections illustrate and describe the coupling methodology, the flow of information and hence the complete picture of the developed partitioned nonlinear aeroelastic framework.

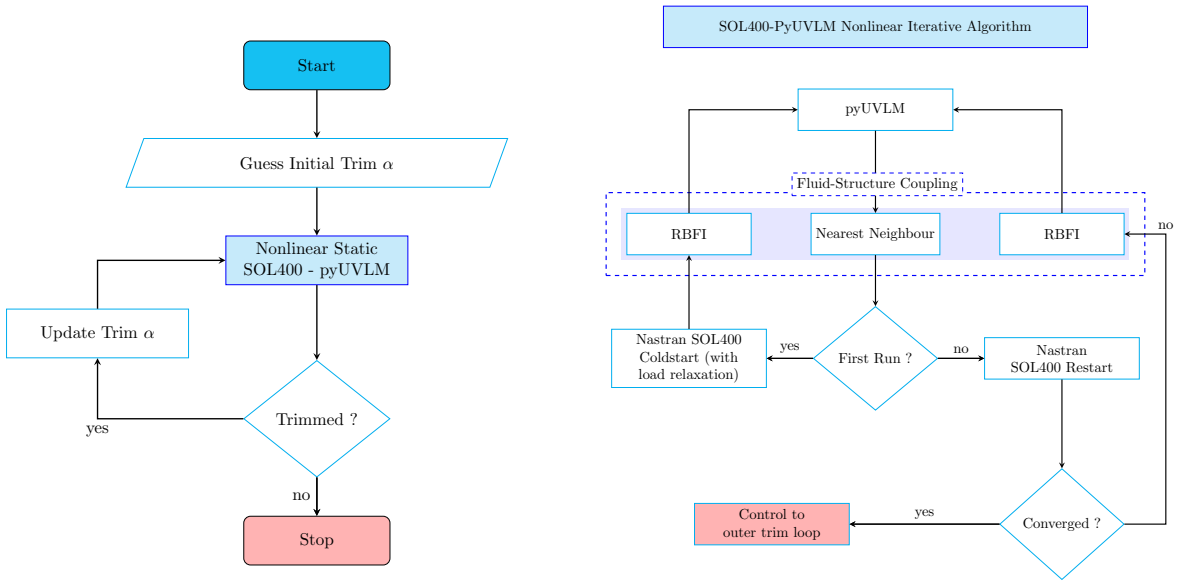

(a) Nonlinear Static Aeroelastic Trim Algorithm

(b) External Coupling of MSC Nastran for Static Aeroelastic Equilibrium with Nonlinear capabilities

Figure 3.7: Algorithms for external coupling of MSC Nastran for static and dynamic aeroelastic simulations

Figure 3.7 shows the flow of information in a nonlinear aeroelastic trim analysis using the proposed solver. The methodology described by Cristina Riso et al [58] is followed here. In addition, an external coupling module (using RBF and NN) has been implemented that is capable of accurate scattered data interpolation. The two equations namely, trim and static aeroelastic equilibrium are solved in a nested manner. The outer loop evaluates the trim condition, while the inner loop solves for the latter, with the inclusion of geometric nonlinearities. The solution begins by determining the aerodynamic loads on the undeformed configuration of a lifting surface represented by flat panels using Vortex Lattice Method (VLM). The input to the VLM solver is a set of parameters that fix the dynamic pressure (i.e. air density ρ based on altitude and Mach Number,M), and an initial guess of the angle of attack. The output of pyVLM, a load vector, is then interpolated onto the structure using a *Nearest Neighbour* approach with appropriate moment balance. The structure is then allowed to deform in a nonlinear manner. Here, the advanced restart algorithms (described in section 3.2.3) are employed to solve the equations in an iterative manner. Once convergence

of the static equilibrium is achieved, the outer trim loop is evaluated. The initial guess of α (angle of attack) is then updated until trim is achieved.

For externally coupled dynamic simulations, the procedure of coupling is similar to the static case. The serial staggered coupling (explained in section 2.3.1) now includes the time-marching problem of the two modular domains. In UVLM, time marching is performed using a backward difference (BDF) algorithm. A row of wake panels are shed from the trailing edge at each timestep whose effect are included in the interpolated load vector F_t. The time integration of the structural domain is done using Newmark Beta schemes. The interpolated displacements d_t at any timestep includes the response of structure at that timestep under the influence of the load history upto that timestep.

Figure 3.8 presents the workflow of information during a typical aeroelastic simulation using the proposed solver. The simulation settings are provided as input to the solver. A given simulation begins with the loading of aerodynamic and structural data in the undeformed configuration. Once the required data is loaded, depending on the type of simulation, either static or dynamic solver modules are imported. Figure also illustrates the presence of a temporal loop in the dynamic simulations in addition to the inner FSI loop. Once the simulations are complete, the output is a data object with structured and segregated data. i.e. *self.aero* contains all the aerodynamic information from the UVLM and *self.structure* contains all the structural information from Nastran. Stand-alone utility modules for input and output operations such as, reading and writing bdf files for Nastran, extracting data from Nastran hdf5 files are also developed.

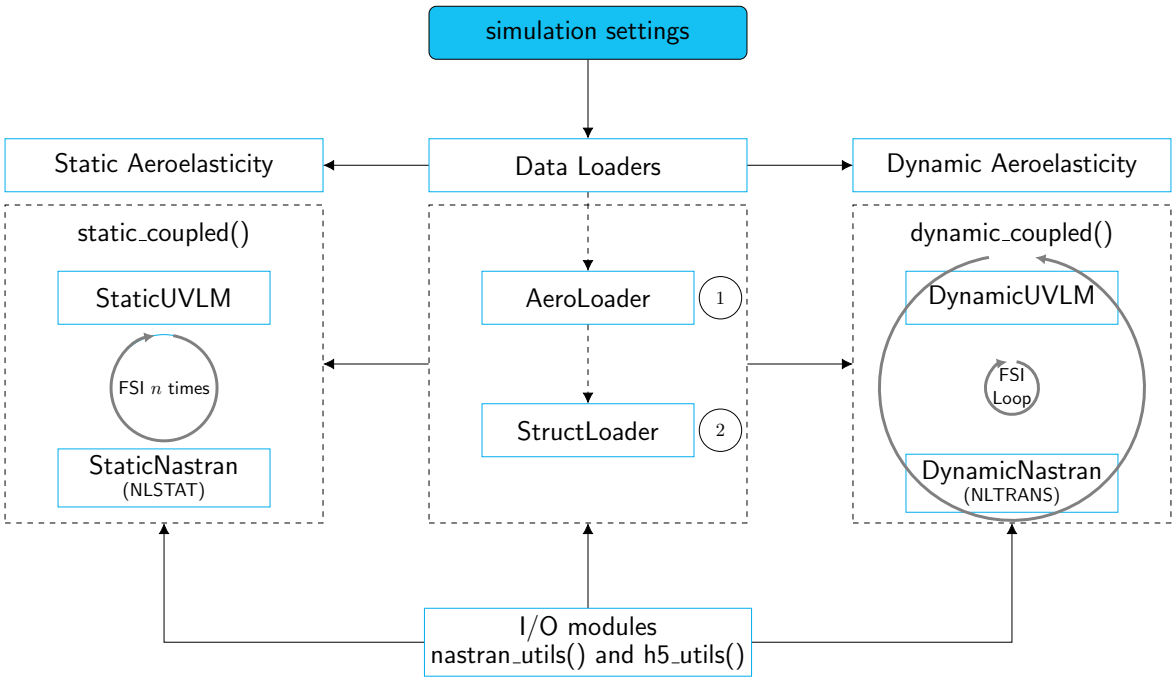

Figure 3.8: Illustration of the complete partitioned aeroelastic framework

4

Framework Verification and Validation

This chapter includes the verification and validation of the solvers developed in this thesis. The theory behind the UVLM solver was discussed in section 2.1 and the functionalities of the same were discussed in detail in section 3.1. Here, section 4.1 presents the static and transient simulation results using the developed UVLM solver. Following the validation of the PyUVLM solver, section 4.2 presents the verification and validation of the complete nonlinear aeroelastic solver for two test cases. Both standard solution sequences and experimental data are used.

4.1. Rigid Aerodynamic Analyses using PyUVLM

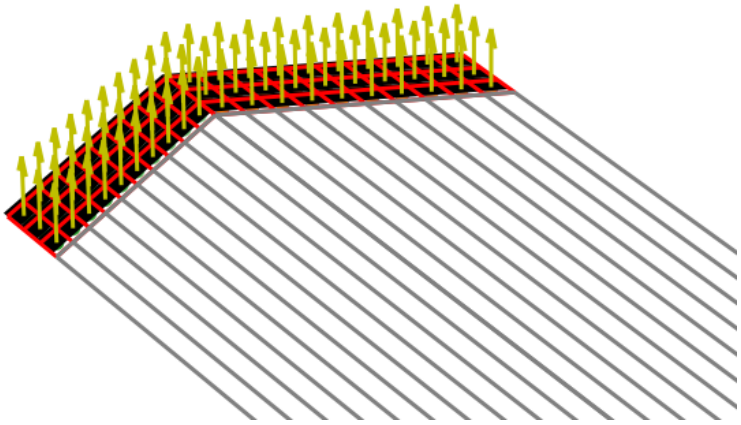

Figure 4.1: Illustration of numerical modelling strategy for static simulations showing panel discretization (swept wing), panel normals and horse-shoe wake extending to infinity.

Figure 4.1 illustrates a swept rectangular wing used for static simulations. The bound vortex panels (in red) are offset by 25% behind the leading edge to define the collocation points

at three quarter chord where the flow tangency boundary condition is matched. The panel normals (in yellow) are also defined at the collocation points. A horseshoe wake is employed for static cases which extend to infinity behind the TE (in grey).
In this section, First static validation results are discussed in section 4.1.1 and section 4.1.2 presents the transient simulation of a rectangular flat plate.

4.1.1. Static Simulations

It is imperative to perform a mesh convergence study as a first step towards validating a given solution technique. Figure 4.2 shows the convergence studies for number of bound panels. It can be seen that the spanwise discretization (in fig 4.2a) is more sensitive than the chordwise discretization (in fig 4.2b). Atleast 20-30 spanwise panels must be employed for a converged solution. This is due to the increase in number of horse-shoe wake panels with spanwise panels.

Figure 4.2c show the effect of wake length (represented in terms of number of chords) in generation of lift over the surface. The influence of the wake converges beyond 20 chords behind the trailing edge. This result is consistent with the ideal wake length prescribed in literature [7].

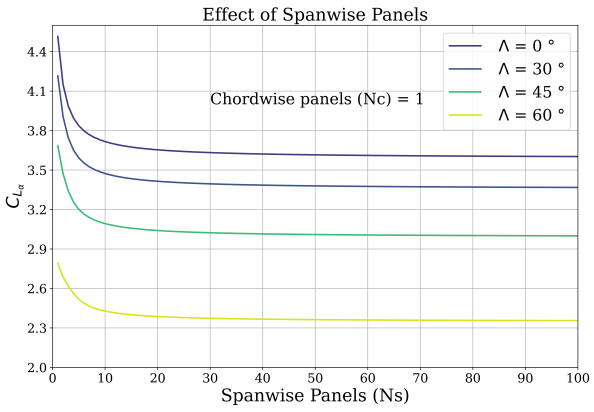

(a) Effect of spanwise discretisation on C_{l_α}

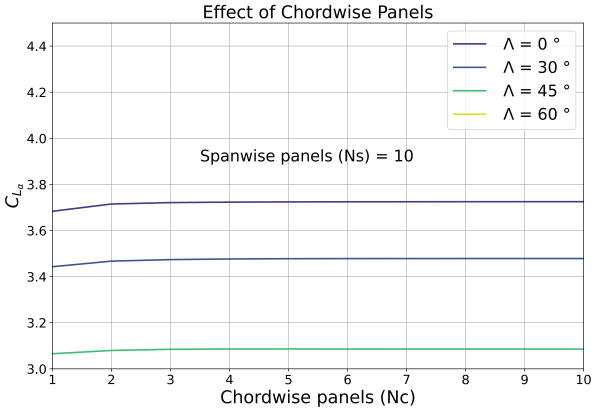

(b) Effect of chord-wise discretisation on C_{l_α}

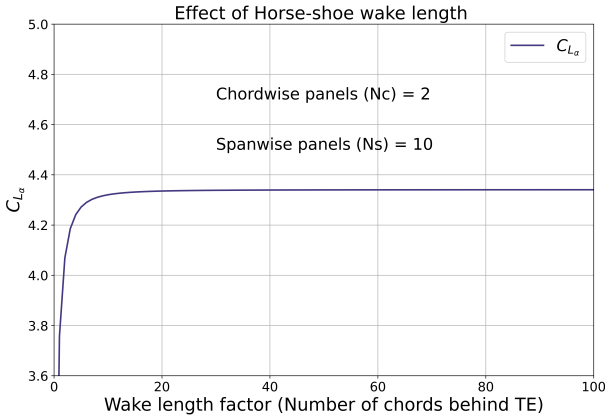

(c) Effect of length of horseshoe wake panels on the generated lift

Figure 4.2: Convergence studies on discretization of panels and horse shoe wake length effect.

Figure 4.3a presents the variation in lift coefficient with aspect ratio of uncambered, rectangular wings for different sweep angles. The experimental values given in [7] are found to be consistent with these predictions as shown. Excellent agreement is obtained with experimental results even for extreme configurations such as a very low aspect ratios, and high sweep angles (upto 60^o).

Finally, Figure 4.3b shows the effect of sweep on the spanwise distribution on the wing. Normalised values are plotted for three sweep angles, $-45^o, 0^o, 45^o$. It is observed that an aft swept wing moves the center of pressure outwards and there by increasing the root bending moment. This is also the reason why forward swept wings are good for aeroelastic phenomenon as they reduce the root bending moment due the shift in peak load towards the root.

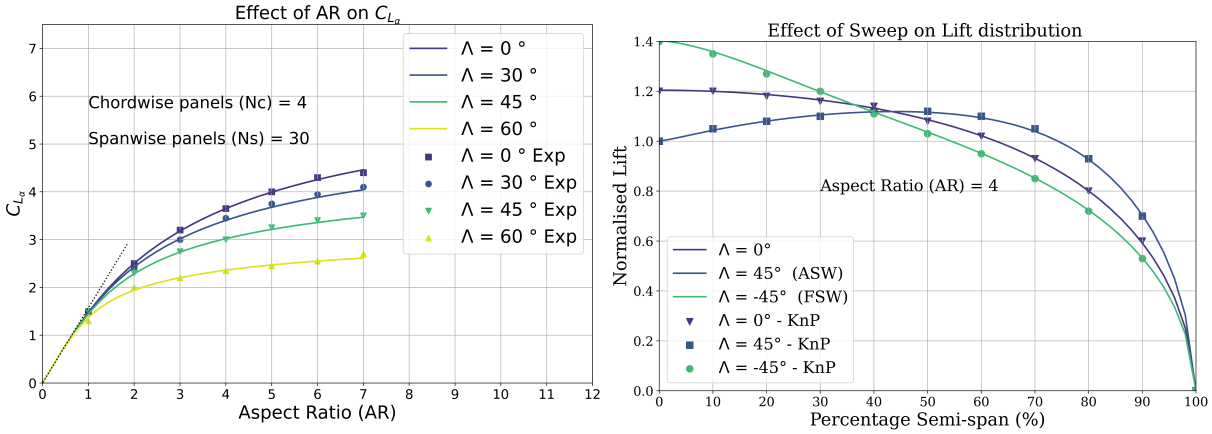

(a) Variation of lift coefficient Cl_α with Aspect Ratio for varying sweep angles.

(b) Variation in spanwise lift distribution with sweep angles.

Figure 4.3: Validation of static UVLM results

4.1.2. TRANSIENT SIMULATIONS

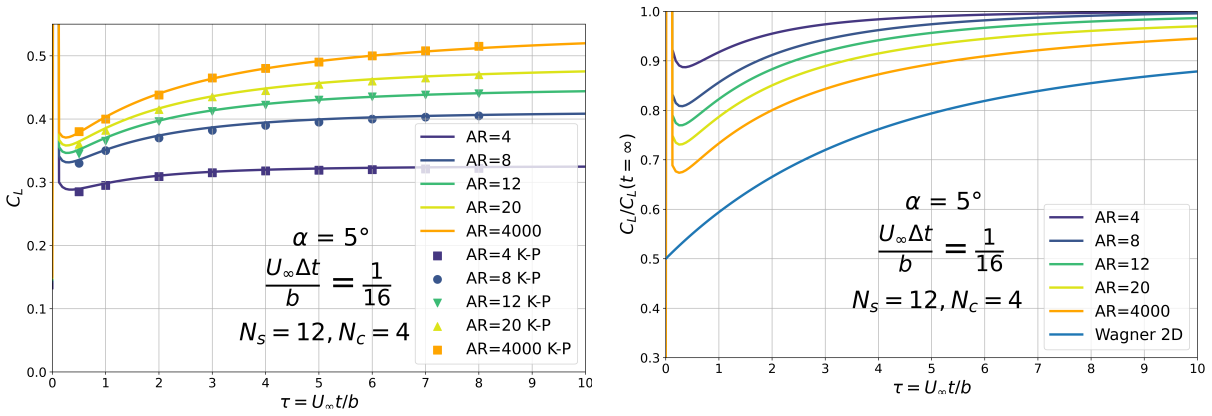

(a) unsteady transient lift buildup on a rectangular flat plate.

(b) Normalised C_L for comparison with Wagner function for 2D airfoils

Figure 4.4: A rectangular panel subjected to a sudden constant acceleration at $\alpha = 5^o$

Figure 4.4 shows the time response of a rigid wing (with varying aspect ratios) set into a sudden motion at a given angle of attack. For a 2D wing, this time dependent lift built up on an airfoil is given by Wagner function. Conventionally, a 2D airfoil is considered to be a 3D wing with infinite span. Therefore, it is expected that as the aspect ratio is increased, the response will approach that of a 2D airfoil as shown in figure 4.4b. This can be explained using the downwash induced by the wake. Higher the span of the wing, higher is the induced downwash, which asymptotes for high aspect ratio wings. Comparing the initial transient region for varying aspect ratios, maximum transient nature is also observed for higher aspect ratio wings. The wing with aspect ratio 4 has little transient behaviour in lift buildup. Simulation results are compared against those from Katz and Plotkin [7] and excellent agreement is obtained for both the unsteady transient region (initial period upto $\tau = 2-3$ chords) and the subsequent steady region. It is to be noted that panel discretization is maintained similar to literature for direct comparison. In principle, one would attain closer match to Wagner function in figure 4.4b with increased chordwise discretization.

Figure 4.5 shows additional capability of the current solver in terms wake modelling where by wake roll up is included. This is brought about by including the influence of each bound panel and each wake panel on each wake panel that is governed by Biot-Savart Law. It was found that including the roll up doesn't change the results significantly from those obtained by only convection along freestream direction. This is because the effect of distance between wake panels is far greater than the orientation of the panels. In addition, including a rollup sequence is computationally expensive and is not recommended.

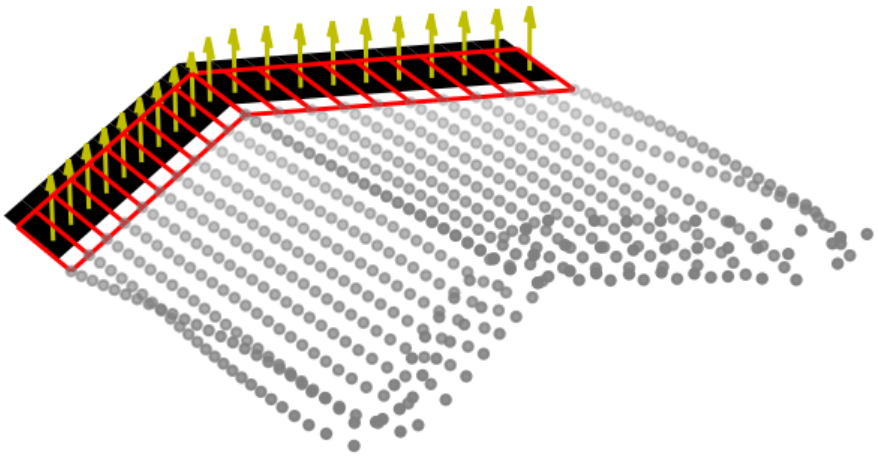

Figure 4.5: Wake roll up

4.1.3. Convention for Motion Prescription

The intended objective behind the development of this solver is to have external aerodynamic computations that interact with the existing structural solvers such as MSC Nastran in a partitioned manner. To this end, the dynamic behaviour is constrained in such a way to

allow ease of information transfer between the two domains.

The wing panels are modelled to be stationary with 0 incidence angle in the global coordinate system. The wake panels are then shed along the positive x direction behind the trailing edge of the wing at freestream velocity including rollup effects. The angle of attack variations are brought about by prescribing the components of the freestream velocity at a given timestep. Therefore, the wake is shed at an angle as illustrated in figure 4.6.

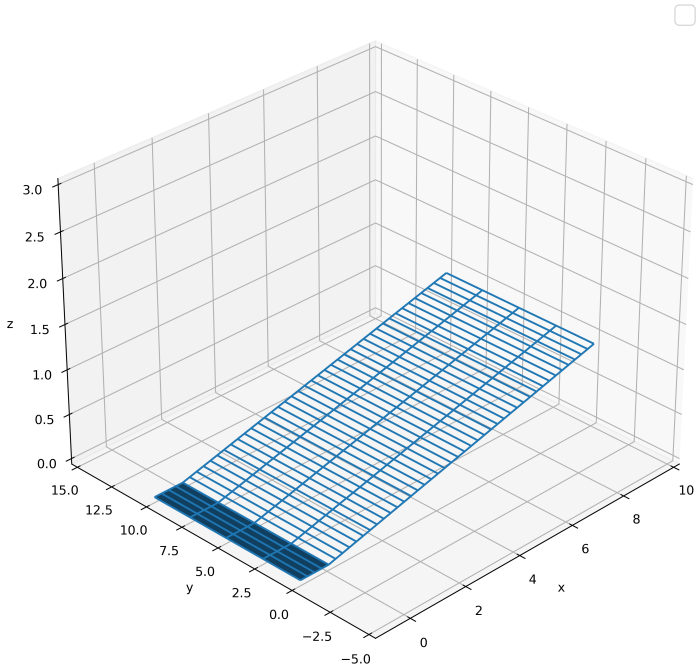

Figure 4.6: Illustration of panel orientation, wake convection direction in UVLM solver for ease of coupling with fixed structure in MSC Nastran.

4.2. Aeroelastic Test Cases using SOL400-PyUVLM solver

With the validation of the UVLM solver presented in sec 4.1, the performance of the proposed aeroelastic solver is evaluated in this section. To this end, two aeroelastic wings are chosen as test cases. Sub-section 4.2.1 presents the static simulations of the baseline CRM wing-box with an Aspect-Ratio 9. Sub-section 4.2.2 presents the static simulations of Pazy wing, a nonlinear wing developed at Technion.

4.2.1. NASA CRM WING - BASELINE

This section begins with the description of the numerical models employed. High fidelity structural model of the NASA CRM wingbox is coupled to the medium fidelity aerodynamic vortex panels in PyUVLM. The results are then verified against standard Nastran aeroelastic solution sequence, namely, SOL144.

MODEL DESCRIPTION

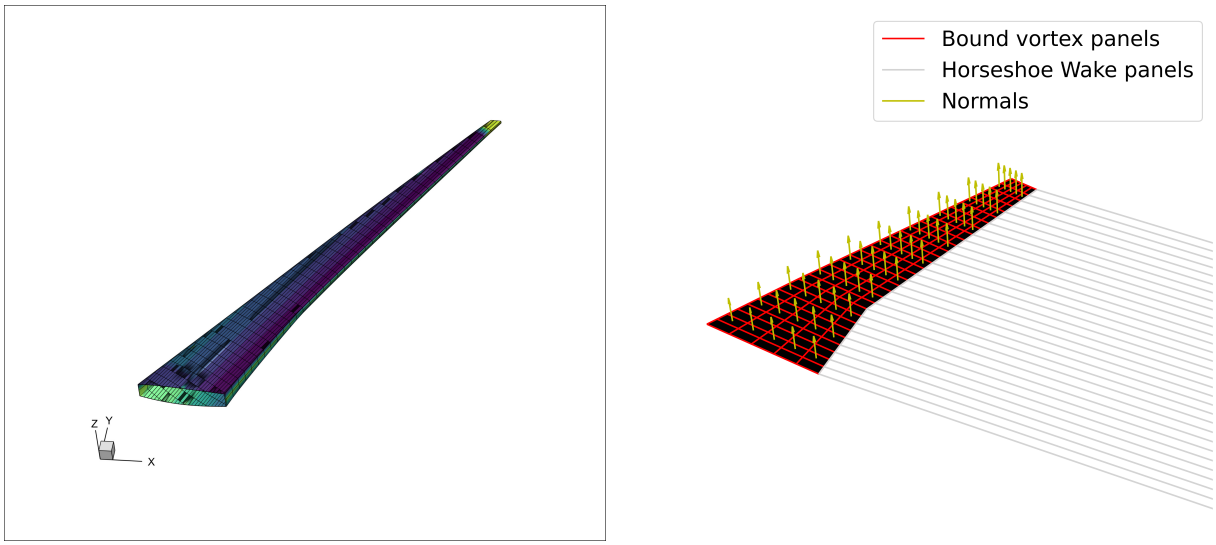

(a) Structural Finite Element Model - MSC Nastran

(b) Aerodynamic Vortex Panels (flat panels) - UVLM

Figure 4.7: Description of the computational domains used for aeroelastic analyses of NASA CRM baseline model.

Figure 4.7 shows the numerical models used for validation of the proposed partitioned non-linear aeroelastic solver. The structural model (figure 4.7a) used is the NASA CRM wingbox with an aspect ratio 9 developed by Brooks et al [70] and adapted to it's current form by Lancelot et al [to be published soon]. The aerodynamic model is a flat surface, with vortex panels (arranged as shown in figure 4.7b) modelled using Vortex Lattice Method, that represents the planform of the complete wing.

The structural FE model (MSC Nastran) consists of 1422 nodes (8532 dofs), with 1365 CQUAD4 and 152 CTRIA3 elements that make up the complete the structure. Mass is modelled using distributing CONM2 entries along the span at front, rear spars and wingbox centerlines. Total modelled weight is equal to half the MTOW weight (134 Tonnes).

The vortex lattice model used for aerodynamic evaluation is discretised into 30 spanwise and 5 chordwise panels that distributed on the planform. These numbers were chosen based on the convergence studies carried out in section 4.1.1 of the previous chapter.

The figure 4.8 shows the simulation configuration of the analysis. The two independent models, in addition to having non-matching meshes, also possess different geometries. This

complicates the information transfer across domains. For this coupling, radial basis functions are employed for displacement transfer and nearest neighbours are used for load mapping.

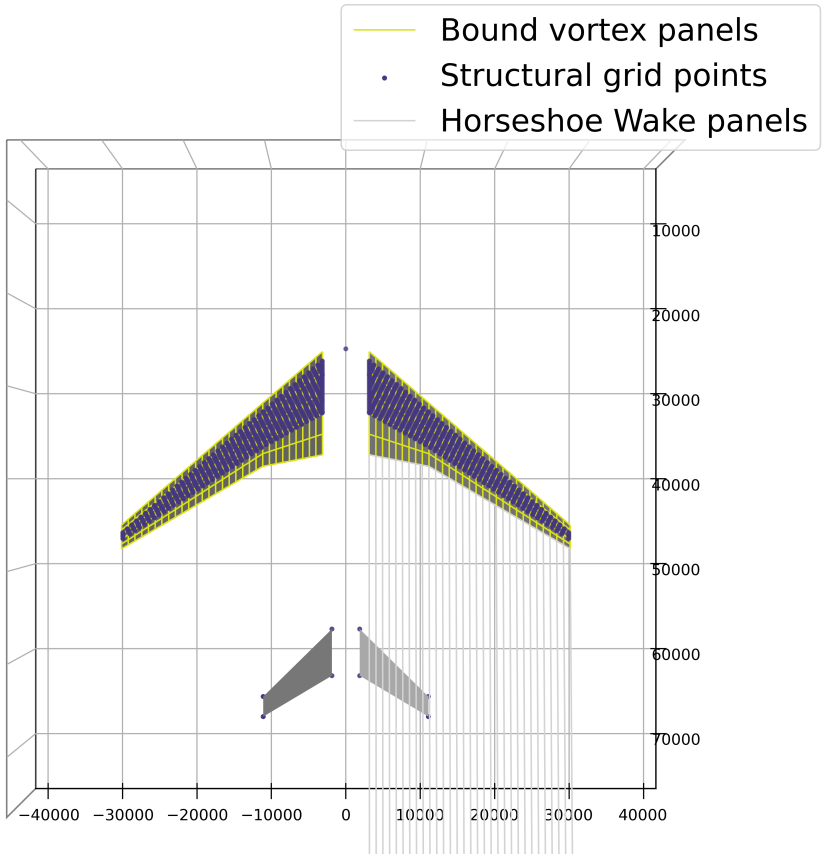

Figure 4.8: Illustration of the aeroelastic simulations of CRM Baseline Model using the coupled solver.

Static Aeroelastic Trim

Aeroelastic trim is a state at which the aircraft is said to achieve the trim condition (i.e. L=W) when in static equilibrium with the aerodynamic loads acting on it. Figure 4.9 shows the aircraft configuration at two load factors n=1 and n=2.5 respectively. For convenience, the spanwise wingbox centers of the structure are plotted. The results obtained for the two configurations using the proposed partitioned nonlinear solver are verified against those obtained from standard commercial package, MSC Nastran SOL144. For static simulations, the Unsteady Vortex Lattice Method (UVLM) with horse-shoe wake reduces to a steady VLM whose equivalence with the Doublet Lattice Method (DLM) is also verified here.

It can be observed from table 4.1 that, the trim angle predicted by the externally coupled algorithm matches the Nastran SOL144 results with a maximum error of 1.5 percent. This slight difference is expected as the current solver achieves a linear solution in an iterative manner. Nastran SOL144 employes a monolithic approach to calculate trim angles. It is to be noted here that the Prandtl-Glauert correction for compressibility is not taken into account in UVLM. The DLM in Nastran SOL 144 inherently applies this correction. Therefore,

Nastran results are generated by running simulations at Mach 0.0. It is also seen that linear and nonlinear simulations converge to the similar trim results in terms of deflections as expected.

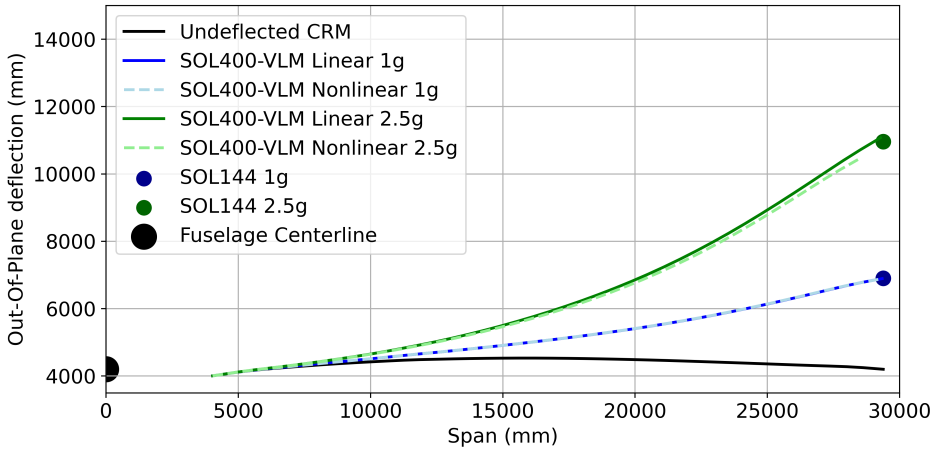

Figure 4.9: Out of plane deflections of the baseline CRM model for two trim configurations (n=1 and n=2.5).

Trim Condition Load factor (n)	**Nastran (SOL144)**	**SOL400-VLM**		Δ_{error}(%)
		Linear	**Nonlinear**	
1	11.308	11.253	11.253	0.486
2.5	28.271	28.700	28.699	1.5

Table 4.1: Trim angles of attack (in degrees) for aeroelastic simulation of the baseline CRM model at two load factors.

NOTE: Fully clamped boundary conditions are used in the above comparison plots. In Nastran SOL144, the usual procedures for trim evaluation include a SUPORT card for the pitching dof while the remaining 5 dofs are constrained. This mimics the unconstrained flight configuration while using UDDR3 for load factor input. For obtaining the fully clamped root static response, Nastran SOL144 analysis is carried out in two steps. First, the trim angle is obtained using the usual trim procedure using SPC on 5 dofs and SUPORT on the pitching dof. Next, the static response is obtained by feeding this trim angle back as input to the analysis without SUPORT and using SPC on all 6 dofs. The deflections of the clamped wing will be higher than that of the unconstrained free flying wing and hence deemed conservative.

4.2.2. PAZY WING

This section begins with the description of the numerical models employed. High fidelity structural model of the Pazy wing (without skin) is coupled to aerodynamic vortex panels in PyUVLM. The results are then verified and validated against numerical and test data form literature.

Model Description

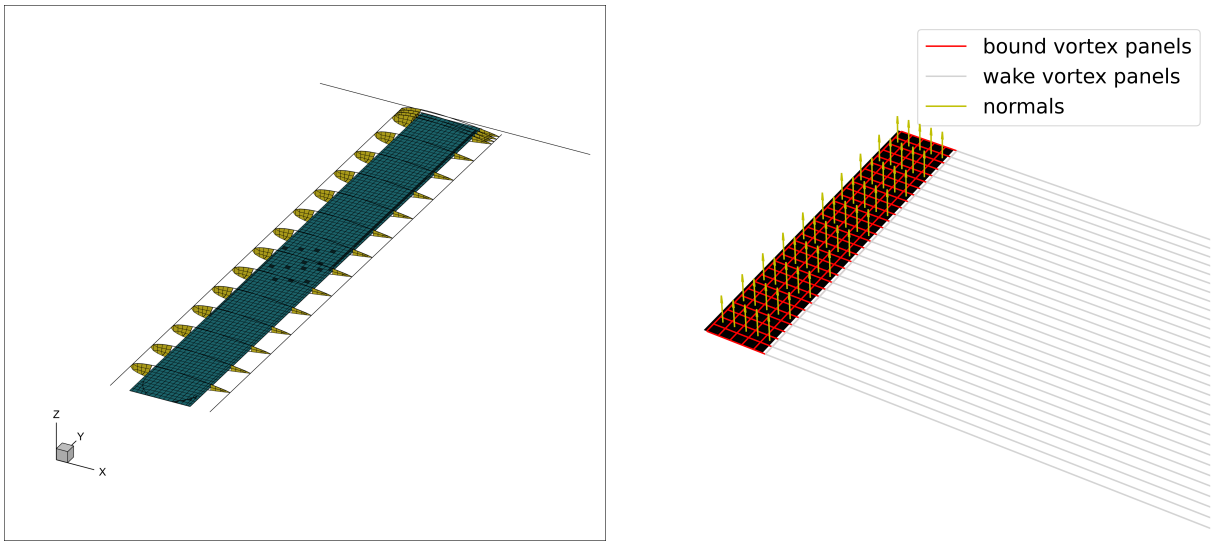

(a) Pazy wing (without skin) Nastran FE model used for the current analysis

(b) Vortex panels used for Aerodynamic Simulation of Pazy wing.

Figure 4.10: Model description of Pazy wing from Technion [19].

The structural model used in this analysis is the no-skin wing FEM (Nastran) model from Avin et al [19]. This is a high fidelity model consisting of a wingbox in the form of an aluminium plate, ribs, leading and trailing edge beam elements and a torsion bar at the wingtip to introduce torsional loads as shown in figure 4.10a

The aerodynamic model used is a flat plate discretized into 30 spanwise and 5 chordwise vortex ring elements. The convergence study for this discretization was made in the previous chapter for the rigid aerodynamic analysis and the same results hold true for the current study. The wake is represented by horse-shoe vortices that extend upto a distance of 20 chords behind the trailing edge. These aero panels are illustrated in figure 4.10b

The aeroelastic simulation begin with the aerodynamic loads evaluation of the undeflected Pazy wing at a given angle of attack and flight speed. The loads obtained at the collocation points of the panels are interpolated onto the aluminium wingbox (blue region in figure 4.10a) as distributed static loads. Following this, the structure is allowed to deform under the obtained loads. Radial Basis Functions are used for displacement interpolation and Nearest Neighbour algorithm for mapping the loads. This is continued until convergence is obtained in terms of deformation residual of the structure.

Static Aeroelastic Trim

Figure 4.11 shows the static aeroelastic deformations of the Pazy wing obtained using the current solver for 4 specific aerodynamic configurations. These are (1) $\alpha = 5°, U_\infty = 30 m/s$ (2) $\alpha = 5°, U_\infty = 50 m/s$ (3) $\alpha = 10°, U_\infty = 40 m/s$ (4)$\alpha = 10°, U_\infty = 50 m/s$. The reasons for the choice of these test conditions are twofold. Primarily, these flight configurations exhibit a transition from small (linear) to very large (nonlinear) deformations of the wing respectively.

Secondly, results from numerical and wind tunnel tests conducted at Technion [19] provide a direct correlation for validation of the proposed solver.

The linear results obtained using the current solver is compared against the ZAERO static aeroelastic analysis conducted at Technion [19] and the nonlinear results are compared against the Nonlinear Modal Rotation Method (MRM) by [71]. Finally, the obtained results are compared to the wind tunnel data from Technion. Table 4.2 shows these validation and verification results. The specific case of $5°, U_\infty = 50 m/s$ is also validated against the results obtained for the reduced model of the pazy wing with the UM/NAST results [72].

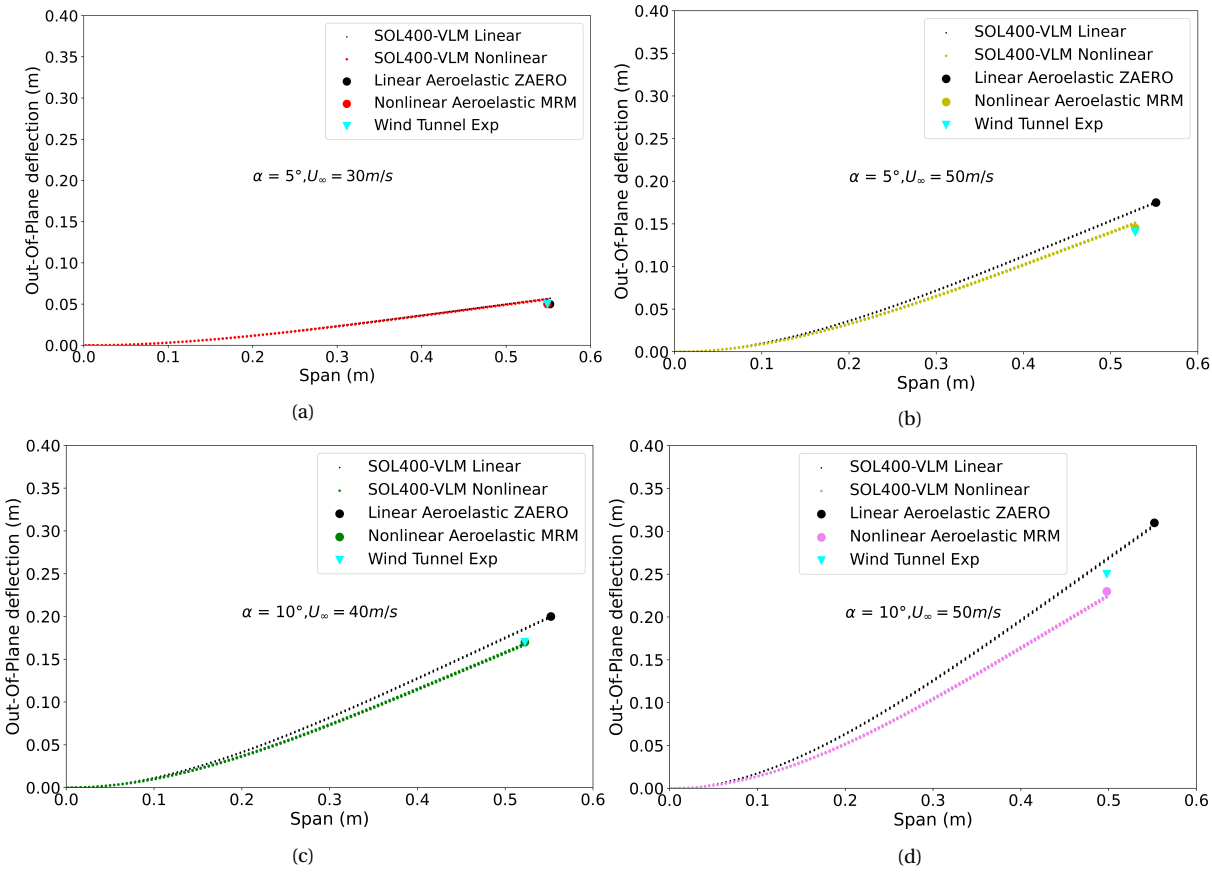

Figure 4.11: Static aeroelastic deflections of Pazy wing at four flight configurations showing the transition to geometric nonlinearity.

The table 4.2 illustrates the expected transition from linear to nonlinear deformations by comparing the two numerical methods with the test data from Technion. Table 4.3 further shows the percentage difference in results obtained between a linear and nonlinear analysis of the Pazy wing. It can be seen that the difference between linear and nonlinear results increase and the nonlinear FEM results match closely with the wind tunnel data with a maximum difference of 4 percent for the highly nonlinear case. These differences are attributed to the variation in the structural models. The wind tunnel tests were conducted on the Pazy wing with skin on and the numerical model used is that without the skin.

Test Cases	**Linear SOL400-VLM**	**Linear Aeroelastic (ZAERO)**	**Nonlinear SOL400-VLM**	**Nonlinear MRM**	**Wind Tunnel Data**
$\alpha = 5°$, $U_\infty = 30m/s$	0.057 (10%)	0.05	0.055 (10%)	0.05	0.05 (9%)
$\alpha = 5°$, $U_\infty = 50m/s$	0.176 (32 %)	0.17	0.151 (27.5%)	0.15	0.14 (25%)
$\alpha = 10°$, $U_\infty = 40m/s$	0.200 (36%)	0.20	0.168 (30.5%)	0.17	0.17 (31%)
$\alpha = 10°$, $U_\infty = 50m/s$	0.310 (56%)	0.31	0.225 (41%)	0.24	0.25 (45%)

Table 4.2: Static aeroelastic tip deflections (in meters and % semi-span) of Pazy wing at four flight configurations.

$\Delta_{Linear-NonlinearFEM}(\%)$	$\Delta_{NonlinearFEM-WTD}(\%)$
0.0	1.0
4.5	2.5
5.5	0.0
15	4.0

Table 4.3: Comparison of deviation in results obtained using linear, nonlinear and wind tunnel tests.

5

STATIC AEROELASTIC EVALUATION OF ALBATROSSONE CONCEPT

This chapter presents numerical analyses of the hinged wingtips concept proposed and developed by Airbus UK in the project AlbatrossONE. The aim here to use the developed aeroelastic solver in this thesis to evaluate loads alleviation capabilities of such wingtip designs. To this end, a baseline model CRM was chosen and a hinge was incorporated to study the effects. Section 5.1 presents the modelling of hinge and the associated sign convention followed for the hinge axis and hinge flare. Section 5.2 then discusses the Maneuver Load Alleviation capabilities of hinged wingtips using the proposed SOL400-PyUVLM solver.

5.1. NUMERICAL MODEL DESCRIPTION

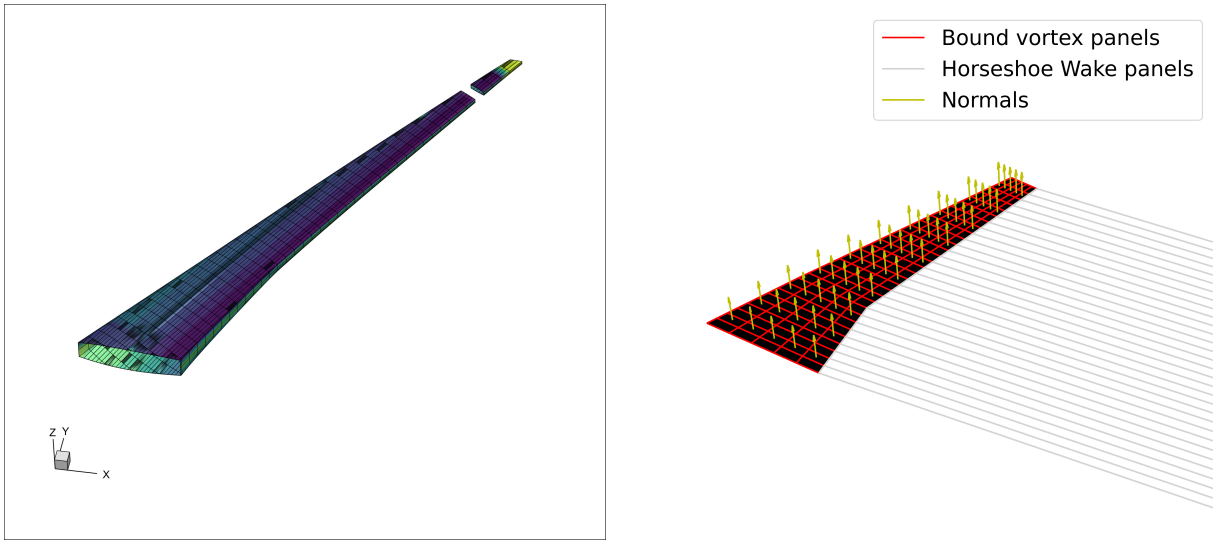

(a) Structural Finite Element Model - MSC Nastran

(b) UVLM vortex flat plate model comparable to Nastran

Figure 5.1: Model description of baseline NASA CRM wing used for the analysis.

For the evaluation of the hinged winglet concept, the baseline CRM model was chosen and the hinge was incorporated into the wing. The structural and aero models used for the cur-

rent analysis are shown in figure 5.1 and are similar to the ones used for the baseline CRM in section 4.2.1, the only difference being the incorporation of the hinge in the structural model. The hinge mechanism is modelled by introducing a CELAS1 element between 2 coincidental nodes, having a stiffness parameter in one DOF (i.e. rotation about X_L). This makes the CELAS1 element behave as a torsional spring with a stiffness parameter. This is shown in the figure 5.2.

It is to be noted here that the hinge coordinate system i.e (X_L, Y_L, Z_L) is allowed to have a relative angle with respect to the global coordinate system (X_G, Y_G, Z_G)). The sign convention for this relative angle is represented in the figure, where a positive hinge angle causes a wash-in effect of the wingtips.

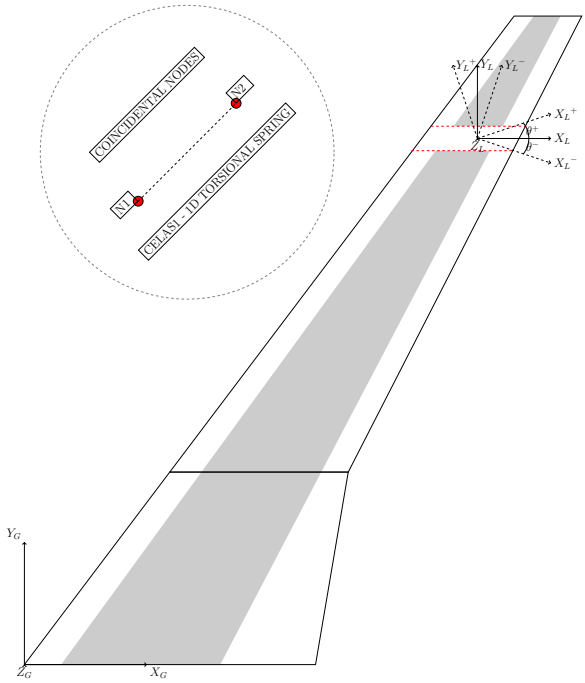

Figure 5.2: Hinge modelling and sign convention used for hinged wingtips.

According to the represented sign convention,the following variations in the wingtip configurations are chosen for the current study:

1. Three Spring stiffness values that differ by an order of magnitude, i.e $k_{\theta_1} = 2.0E+7$ N-mm/rad, $k_{\theta_2} = 2.0E+8$ N-mm/rad, $k_{\theta_3} = 2.0E+9$ N-mm/rad

2. Three hinge angle orientations, -15^o,$+0^o$, $+15^o$

5.2. Maneuver Load Alleviation using Folding Wing Tips

In presence of the hinge at the winglet root, a large tip rotation (depending on the hinge stiffness) is expected. Thus, small angle approximations are no longer valid due to the presence of such geometric nonlinearities. The following sections discuss the effects of hinge

stiffness and hinge angle on the aeroelastic performance of the wing. All the static results are plotted for trimmed configurations of the wing at maneuver load factors.

5.2.1. Hinge Stiffness Variation

Figure 5.3 shows the effect of hinge stiffness on accuracy of displacement predicted using linear and nonlinear analyses. Two trim configurations (i.e load factor n=1 and n=2.5) are analysed for 3 different hinge stiffness values ranging from 2.0E+7 to 2.0E+9 Nmm/rad. The results obtained for these analyses with the proposed solver (nonlinear) are compared with the Nastran SOL144 (linear) results.

It is quickly recognised that a linear analysis will lead to unrealistic values of the wingtip deflections for lower hinge stiffness range (i.e. 2.0E+7 Nmm/rad 2.5g case). Another important phenomenon observable is that a linear analysis consistently predicts higher coasting angles of the wingtip. Thus, a linear analysis will predict higher load alleviation capability of a given configuration.

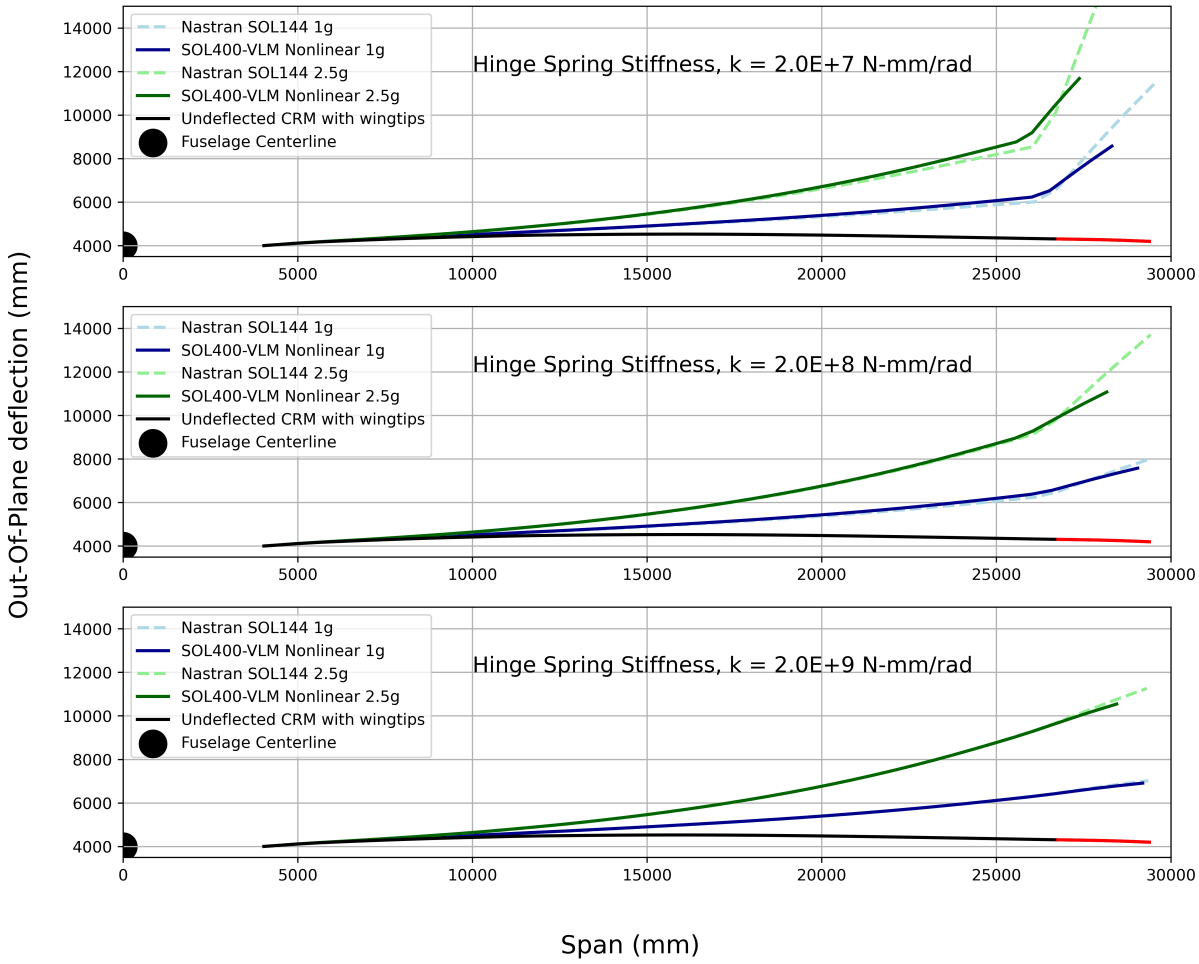

Figure 5.3: Static trimming of CRM with wingtips at 1g and 2.5g load factors.

It is interesting to note that, with the reduction in hinge stiffness while maintaining the hinge angle at 0^o , no significant load redistribution occurs on the main wing. The spanwise lift profile in figure 5.4 shows a local redistribution on the wingtips and the outboard sections of the main wing. The peak load that occurs at about 30 percent span has minimal effect due to the hinge actuation. This is evident from the bending moment distribution along the span plotted in the figure. Thus, illustrating that a 0^o hinge does not possess load alleviation capabilities.

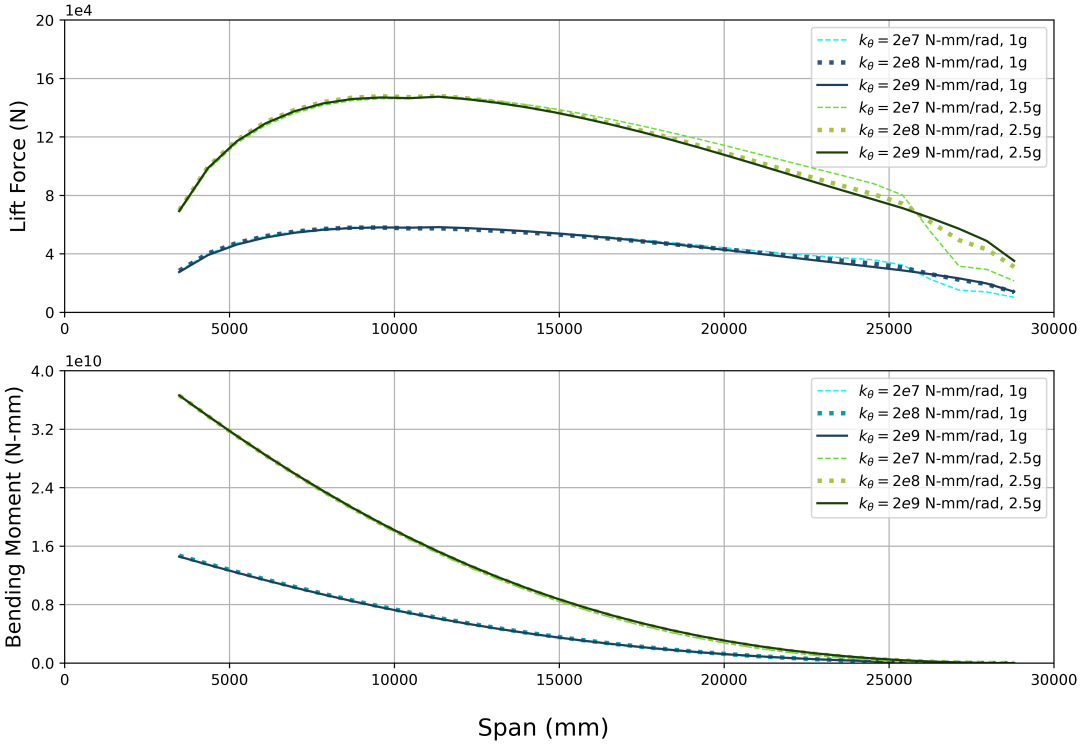

Figure 5.4: Effect of hinge stiffness on the load redistribution and bending moment distribution.

The trim angles obtained using hinge stiffness analysis are shown in table 5.1. The general trend in linear and nonlinear simulations is a reduction in trim angle with lower hinge stiffness values.

Trim	**H1 – 2.0E+7 Nmm/rad**		**H2 – 2.0E+8 Nmm/rad**		**H3 – 2.0E+9 Nmm/rad**	
	SOL400-VLM	**SOL144**	**SOL400-VLM**	**SOL144**	**SOL400-VLM**	**SOL144**
1g	10.590	10.581	8.840	11.132	11.110	11.289
2.5g	27.937	26.453	27.788	27.831	28.212	28.222

Table 5.1: Angle of attack (in degrees) obtained for varying hinge stiffness values.

5.2.2. Hinge Angle Variation

Figure 5.5 illustrates the effect of introducing an angle to the wingtip hinge according to the sign convention shown in figure 5.2. Based on the hinge stiffness analysis, a stiffness value of

$k_\theta = 1.0E+8 Nmm/rad$ was chosen to have a nominal and distinguishable wingtip deflection that aids in the study of load alleviation. The chosen flight condition is 1g trim at 0.85 Mach at an altitude of 37000ft. The figure shows the spanwise profile of the distributed lift load, followed by the Bending Moment Diagram (BMD) considering the wing as a cantilever beam fully clamped at the root. Finally, the deflection of the wing under the developed loads are plotted. It can be observed that a negative hinge angle leads to a redistributed load that moves the peak lift load towards the root, thereby reducing the bending moment at the root (lower eccentric loading). This also leads to a lower out board deflection of the wing as seen in the figure.

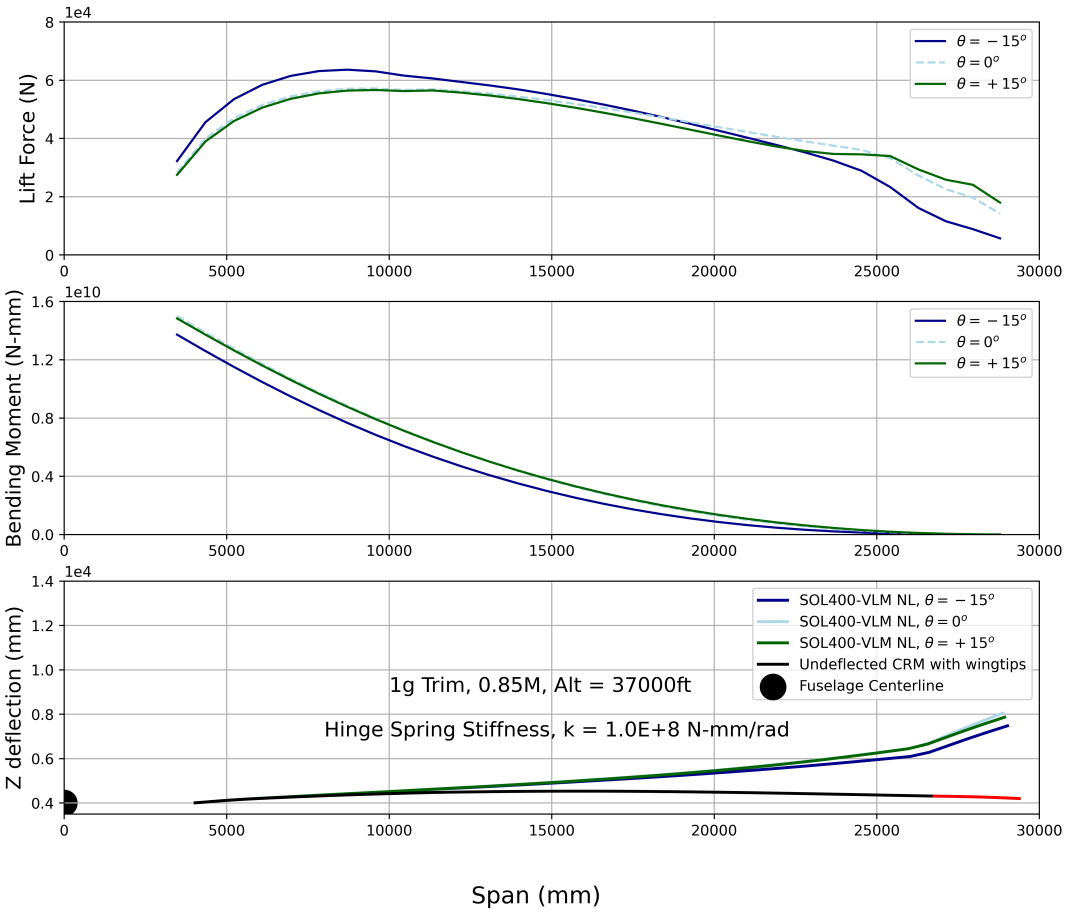

Figure 5.5: Redistribution of loads over lifting surface with change in hinge flare angle.

The effect of hinge angle can also be observed in the trim angle of attack where in an increase in the hinge angle from -15 to +15 directly translates to an increase in trim angle as shown in table 5.2. This suggests that with a negative hinge angle, the lift curve slope translates in +y direction, thereby achieving a higher CL_{max}

-15^o	0^o	15^o
5.0191	9.5455	10.2330

Table 5.2: Angle of attack (in degrees) obtained for varying hinge angle values

6

CONCLUSIONS AND RECOMMENDATIONS

6.1. CONCLUSIONS

The major conclusions to the research questions of this thesis are:

"How can a computational framework be set up that accurately predicts the aeroelastic behaviour of a realistic airliner with free hinged folding wing tips in free flight?"

As a part of this master's thesis, a computational framework was developed that externally couples MSC Nastran's nonlinear solution sequences to a medium fidelity aerodynamics solver, namely, the Unsteady Vortex Lattice Method (UVLM). The fluid structure interaction is thus carried out in a partitioned fashion. The solver follows a Serial Staggered Coupling (SSC) approach using Radial Basis Functions (RBF) and Nearest Neighbours (NN) interpolation techniques for information transfer across the modular domains. The solver is validated with test cases that involve geometric nonlinearities. Specifically, for the case of hinged wingtips, the solver is capable of accurately capturing the nonlinearity and unsteadiness introduced due to large deflections of the wingtips.

1. **How to build the computational framework of the concept?**

   (a) **How to build the structural model with hinged wing tips on MSC Nastran? How to alter the SOL400 module (Implicit Nonlinear Analysis) to model nonlinear actuation of hinged wingtips for loads alleviation**?

   The hinge is modelled using CELAS1, a 1D scalar spring element with a specific stiffness value for the rotational dof. The hinge actuation is then realised by introducing this CELAS1 element between two coincidental nodes. The hinge axis is then determined using a local coordinate system that has a local flare angle when compared to the global reference coordinate system.

   (b) **How to build the 3D UVLM panel code for aerodynamics of the hinged wing tip design using open source UVLM modules? How to accurately model the wing tips with flared hinges using the aerodynamic panels**?

   A complete Unsteady Vortex Lattice Method (UVLM) solver was built by the author with the help of available literature. No open sourced UVLM modules were

available that was suitable for the current application. This, combined with the author's curiosity to understand the computational modelling techniques better lead to this complete build up.

(c) **How to link the structural and aerodynamic solvers using MATLAB/ Python scripts ? i.e How to best couple the fluid and structural domain that are analysed in time domain** ?

The fluid structure interaction of the partitioned solver is realised using the conventional serial staggered (CSS) approach. Radial Basis Functions are used for displacement interpolation from the structure to the fluid domain and Nearest Neighbour scheme is used for the fluid to structure force interpolation. RBFs perform well on scattered data set and hence require very little input. In general, Nearest Neighbour interpolation leads to staggered (step-like) interpolated values for displacement interpolation and hence is not recommended.

2. **What are the analyses to be performed numerically?**

(a) **What is the aeroelastic performance i.e static and dynamic responses of the aircraft with wing tip compared to those of the baseline aircraft without the tips**?

The aeroelastic responses that can be analysed using the developed solver are static equilibrium and static trim, dynamic step response and dynamic gust response. The linear responses obtained using the proposed solver are compared against standard commercial packages like Nastran SOL144 and SOL146. The nonlinear responses are then evaluated by incorporating geometric nonlinearities.

3. **How can the proposed work be verified and validated?**

(a) **How does the Numerical model proposed perform in comparison to the existing codes or theories**?

The two major test cases used in this thesis are NASA CRM wing (AR 9.0) and Pazy wing from Technion (Israel). The results for these test cases from the proposed solver are verified against standard solution results from commercial packages and existing literature.

(b) **How do the obtained numerical results fare in comparison with flight test / experimental data?**

Due to the manner in which the solver is built, a one on one comparison can be made with the wind tunnel results. Excellent agreement is obtained in the predicted nonlinear aeroelastic behaviour of the Pazy wing, with a maximum error of 4 percent in the predicted highly nonlinear deflection. This is attributed to the differences in physical model and numerical truncation errors.

6.2. FUTURE RECOMMENDATIONS

In it's current version the solver provides accurate predictions to extreme nonlinear behaviour of structures and also predicts the unsteady nature of fluid flow. This thesis evaluates extensively the static aeroelastic capabilities of the solver. The dynamic solver is also functional without errors. However some more work remains in it's validation.

While the developed solver is capable of producing reasonably accurate predictions to linear and nonlinear phenomenon, there is wide scope for it's improvement. The following points indicate the domains for further advancement of this solver.

1. **Validation plots of the externally coupled dynamic aeroelastic solver**

   The externally coupled dynamic aeroelastic solver is functional as presented in the Appendix. The solver is able to capture the dynamic structural response under the influence of temporally varying aerodynamic loads. It is the author's view to complete some more validation cases before final gust load alleviation plots can be achieved. For gust analysis, the initial transient response of the structure needs to die out before a gust input can be given to the simulation. Applying a 4 percent damping to the first bending mode of the structure at 0.8Hz, it was found that the structure reaches steady state after 4 seconds. Ideally, a gust input should occur after this. With the smallest timestep of 0.01 seconds, this simulation is computationally very expensive using the solver in it's current version.

2. **Reduce the structural degrees of freedom to geometrically nonlinear beam or stick models**

   The current thesis has employed only high fidelity structural models in all of the generated results. This is however not recommended for such computationally expensive tasks. Reducing the structure to beam models as used in *"SHARPy"* and *"UMNAST"* can exponentially reduce the dofs and hence the computational time. This procedure of reducing the dofs can be done using inverse optimization techniques such as the *"Fermat"* configuration from DLR.

3. **Use of multi-language coding approach: Use of low level languages such as C++ and Fortran**

   The state-of-the-art for achieving the best computational efficiency is through conjugation of Python and Fortran codes for individual domains linked together with open source packages and/or self written scripts as this combines the fast, easy-to-use Python coding with extensive computational capabilities of Fortran based codes such as *PyFly* [57] and "*SHARPy*" [56]. In it's current version, due the author's limited knowledge in efficient code build up, scope for performance improvement is plenty. Although minor instances of fast codes are implemented such as numba and cython, more can be done.

4. **Use of high fidelity aerodynamics to achieve full field CSM-CFD coupling**

Although UVLM provides reasonable results in the subsonic regime, such potential flow based solvers do not capture the accurate flow physics due to the absence of viscosity. This thesis has proven a UVLM-CSM coupling and techniques used here can be extrapolated to fully coupled CFD-CSM solvers that are open sourced and of academic value.

5. **Use wake truncation if number of timesteps are high.**

   In it's current form, UVLM solver used here does not include wake truncation techniques. Truncation can prove to be extremely beneficial as for each timestep, a row of trailing edge vortices are shed, making the number of wake panels grow exponentially. A convergence study can be performed to evaluate the wake length saturation limit.

6. **Use implicit coupling with UVLM.**

   MSC Nastran SOL400 module is implicit i.e consists of load relaxations for a given load vector F. However coupling with aerodynamic solver is explicit. With one coupling step per iteration. This leads to convergence issues, especially with folding wingtips having low hinge stiffness. Thus, it is best to have subiterations to introduce the aerodynamic load with user-specified relaxations.

BIBLIOGRAPHY

[1] E. E. Agency, *"european aviation environmental report 2019",* (2019).

[2] R. L. Bisplinghoff, H. Ashley, and R. L. Halfman, *Aeroelasticity* (Courier Corporation, 2013).

[3] G. Gratton, *Initial airworthiness: Determining the acceptability of new airborne systems* (Springer, 2018).

[4] R. Cook, C. Wales, A. Gaitonde, D. Jones, and J. Cooper, *Uncertainty quantification in gust loads analysis of a highly flexible aircraft wing,* (2017).

[5] T. Klimmek, *Parametric set-up of a structural model for fermat configuration aeroelastic and loads analysis,* Journal of Aeroelasticity and Structural Dynamics **3** (2014).

[6] T. R. Brooks, G. K. Kenway, and J. Martins, *Undeflected common research model (ucrm): an aerostructural model for the study of high aspect ratio transport aircraft wings,* in *35th AIAA Applied Aerodynamics Conference* (2017) p. 4456.

[7] J. Katz and A. Plotkin, *Low-speed aerodynamics*, Vol. 13 (Cambridge university press, 2001).

[8] J. Vassberg, M. Dehaan, M. Rivers, and R. Wahls, *Development of a common research model for applied cfd validation studies,* in *26th AIAA Applied Aerodynamics Conference* (2008) p. 6919.

[9] S. Guo, J. De Los Monteros, and Y. Liu, *Gust alleviation of a large aircraft with a passive twist wingtip,* Aerospace **2**, 135 (2015).

[10] R. De Breuker, S. Binder, and A. Wildschek, *Combined active and passive loads alleviation through aeroelastic tailoring and control surface/control system optimization,* in *2018 AIAA Aerospace Sciences Meeting* (2018) p. 0764.

[11] W. Krüger, J. Dillinger, R. De Breuker, and K. Haydn, *Investigations of passive wing technologies for load reduction,* CEAS Aeronautical Journal **10**, 977 (2019).

[12] H. Hesse, *Consistent aeroelastic linearisation and reduced-order modelling in the dynamics of manoeuvring flexible aircraft,* (2013), phD Dissertation.

[13] R. C. Cheung, C. Wales, D. Rezgui, J. E. Cooper, and T. Wilson, *Modelling of folding wing-tip devices for gust loads alleviation,* in *2018 AIAA/ASCE/AHS/ASC Structures, Structural Dynamics, and Materials Conference* (2018) p. 0462.

[14] V. Hodigere Siddaramaiah, D. Calderon, J. Cooper, and T. Wilson, *Preliminary studies in the use of folding wing tips for loads alleviation,* in *Royal Aeronautical Society Applied Aerodynamics Conference* (2014).

[15] T. Wilson, M. Herring, J. Pattinson, J. Cooper, A. Castrichini, A. Rafic, and H. Dhoru, *An aircraft wing with a moveable wing tip device for load alleviation,* (2019), uS Patent App. 16/067,221.

[16] Airbus, *AlbatrossONE* (accessed 2021), https://www.airbus.com/innovation/future-concepts/biomimicry/albatrossone.html.

[17] *Potential flow* (accessed 2021), https://potentialflow.com/.

[18] E. Field, D. Herting, and M. Morgan, *Nastran user's guide (level 17.5),* (1979).

[19] O. Avin, A. Drachinsky, Y. Ben-Shmuel, and D. Raveh, *Design of an experimental benchmark of a highly flexible wing,* in *60th Israel Annual Conference on Aerospace Sciences* (2020) pp. 1–18.

[20] J. Cooper, *From blue skies to green skies: how structural dynamics and uncertainty quantification can benefit future aircraft designs,* in *Proceedings of the International Conference on Noise and Vibration Engineering ISMA* (2014) pp. 1–15.

[21] I. P. Release, *"IATA forecast predicts 8.2 billion air travellers in 2037",* (24 October 2018).

[22] J. Pattinson, T. Wilson, and M. Herring, *High fidelity simulation of the folding wing tip for loads alleviaton,* .

[23] NationalGeographic, *Albatrosses* (accessed 2020), https://www.nationalgeographic.com/animals/birds/group/albatrosses/.

[24] D. J. Inman, *Engineering vibration*, Vol. 3.

[25] T. Hughes, *The Finite Element Method: Linear Static and Dynamic Finite Element Analysis*, Dover Civil and Mechanical Engineering (Dover Publications, 2003).

[26] L. Barba and O. Mesnard, *Aero python: classical aerodynamics of potential flow using python,* Journal of Open Source Education **2**, 45 (2019).

[27] A. de Boer, A. H. van Zuijlen, and H. Bijl, *Review of coupling methods for non-matching meshes,* Computer methods in applied mechanics and engineering **196**, 1515 (2007).

[28] Z. Wu, Y. Cao, and M. Ismail, *Gust loads on aircraft,* The Aeronautical Journal **123**, 1216 (2019).

[29] B. K. Stanford, C. V. Jutte, and K. C. Wu, *Aeroelastic benefits of tow steering for composite plates,* Composite Structures **118**, 416 (2014).

[30] Y. Bi, C. Xie, C. An, and C. Yang, *Gust load alleviation wind tunnel tests of a large-aspect-ratio flexible wing with piezoelectric control,* Chinese Journal of Aeronautics **30**, 292 (2017).

[31] Y. Zhao, C. Yue, and H. Hu, *Gust load alleviation on a large transport airplane,* Journal of Aircraft **53**, 1932 (2016).

[32] J. Bussemaker, *Wing optimization with active load control: Integrating maneuver load control and gust load alleviation in wing structural optimization of large transport aircraft,* (2018).

[33] C. An, C. Xie, Y. Meng, and C. Yang, *Wind tunnel test and gust load alleviation of flexible wing including geometric nonlinearities with servo control,* in *2018 AIAA/ASCE/AHS/ASC Structures, Structural Dynamics, and Materials Conference* (2018) p. 0192.

[34] N. T. Nguyen, K. E. Hashemi, and M. C. Drew, *Multi-objective adaptive control for load alleviation and drag minimization of flexible aircraft,* in *2018 AIAA Guidance, Navigation, and Control Conference* (2018) p. 0622.

[35] V. Handojo, P. Lancelot, and R. De Breuker, *Implementation of active and passive load alleviation methods on a generic mid-range aircraft configuration,* in *2018 Multidisciplinary Analysis and Optimization Conference* (2018) p. 3573.

[36] L. O. Bernhammer, J. Sodja, M. Karpel, and R. De Breuker, *Design of an autonomous flap for load alleviation,* .

[37] D. Rajpal and R. De Breuker, *Preliminary aeroelastic design framework for composite wings subjected to gust loads,* in *International Forum on Aeroelasticity and Structural Dynamics (IFASD), Jun. 25-28, 2017, Como, Italy* (2017).

[38] S. J. Lee, K. E. Hashemi, M. C. Drew, N. T. Nguyen, and H. J. Kim, *Robust gust load alleviation control using disturbance observer for generic flexible wing aircraft in cruising condition,* in *2018 Annual American Control Conference (ACC)* (IEEE, 2018) pp. 2257–2263.

[39] F. Fonte, F. Toffol, and S. Ricci, *Design of a wing tip device for active maneuver and gust load alleviation,* in *2018 AIAA/ASCE/AHS/ASC Structures, Structural Dynamics, and Materials Conference* (2018) p. 1442.

[40] T. d. S. S. Versiani, F. J. Silvestre, A. B. G. Neto, D. A. Rade, R. G. A. da Silva, M. V. Donadon, R. M. Bertolin, and G. C. Silva, *Gust load alleviation in a flexible smart idealized wing,* Aerospace Science and Technology **86**, 762 (2019).

[41] H. Liu and X. Wang, *Aeroservoelastic design of piezo-composite wings for gust load alleviation,* Journal of Fluids and Structures **88**, 83 (2019).

[42] D. M. Bushnell, *Scaling: Wind tunnel to flight,* Annu. Rev. Fluid Mech. **38**, 111 (2006).

[43] T. Kier, *Comparison of unsteady aerodynamic modelling methodologies with respect to flight loads analysis,* in *AIAA Atmospheric Flight Mechanics Conference and Exhibit* (2005) p. 6027.

[44] D. J. Willis, J. Peraire, and J. K. White, *A combined pfft-multipole tree code, unsteady panel method with vortex particle wakes,* International Journal for numerical methods in fluids **53**, 1399 (2007).

[45] Y. Hu, W. Tay, and K. Lim, *The analysis of cyclogyro using unsteady vortex lattice method,* in *Proceedings of 25th Congress of the International Council of the Aeronautical Sciences. Hamburg: Curran Associates* (2006) pp. 930–935.

[46] M. Harmin and J. Cooper, *Aeroelastic behaviour of a wing including geometric nonlinearities,* The Aeronautical Journal **115**, 767 (2011).

[47] B. Hallissy and C. Cesnik, *High-fidelity aeroelastic analysis of very flexible aircraft,* in *52nd AIAA/ASME/ASCE/AHS/ASC Structures, Structural Dynamics and Materials Conference 19th AIAA/ASME/AHS Adaptive Structures Conference 13t* (2011) p. 1914.

[48] W. Rodden and E. Johnson, *Msc/nastran aeroelasticity analysis users guide,* .

[49] J. Murua, R. Palacios, and J. M. R. Graham, *Applications of the unsteady vortex-lattice method in aircraft aeroelasticity and flight dynamics,* Progress in Aerospace Sciences **55**, 46 (2012).

[50] N. P. Werter, R. De Breuker, and M. M. Abdalla, *Continuous-time state-space unsteady aerodynamic modelling for efficient aeroelastic load analysis,* in *International Forum on Aeroelasticity and Structural Dynamics* (2015).

[51] F. Saltari, C. Riso, G. D. Matteis, and F. Mastroddi, *Finite-element-based modeling for flight dynamics and aeroelasticity of flexible aircraft,* Journal of Aircraft **54**, 2350 (2017).

[52] Y. Yao, K. Yeo, and T. Nguyen, *A numerical study on free hovering fruit-fly with flexible wings,* in *IUTAM Symposium on Recent Advances in Moving Boundary Problems in Mechanics* (Springer, 2019) pp. 15–25.

[53] A. Pontillo, D. Hayes, G. X. Dussart, G. E. Lopez Matos, M. A. Carrizales, S. Y. Yusuf, and M. M. Lone, *Flexible high aspect ratio wing: Low cost experimental model and computational framework,* in *2018 AIAA Atmospheric Flight Mechanics Conference* (2018) p. 1014.

[54] R. Ahrem, A. Beckert, and H. Wendland, *A new multivariate interpolation method for large-scale spatial coupling problems in aeroelasticity,* in *Conference Proceedings to the Int. Forum on Aeroelasticity and Structural Dynamics (IFASD), DGLR-Bericht,* Vol. 4 (2005).

[55] J. Murua, *Flexible aircraft dynamics with a geometrically-nonlinear description of the unsteady aerodynamics,* (2012), phD Dissertation.

[56] A. del Carre, A. Muñoz-Simón, N. Goizueta, and R. Palacios, *SHARPy: A dynamic aeroelastic simulation toolbox for very flexible aircraft and wind turbines,* Journal of Open Source Software **4**, 1885 (2019).

[57] D. Garcia, M. Ghommem, N. Collier, B. Varga, and V. M. Calo, *Pyfly: A fast, portable aerodynamics simulator,* Journal of Computational and Applied Mathematics **344**, 875 (2018).

[58] C. Riso, F. G. Di Vincenzo, M. Ritter, C. E. Cesnik, and F. Mastroddi, *Nonlinear aeroelastic trim of very flexible aircraft described by detailed models,* Journal of Aircraft **55**, 2338 (2018).

[59] A. Castrichini, V. H. Siddaramaiah, D. Calderon, J. Cooper, T. Wilson, and Y. Lemmens, *Preliminary investigation of use of flexible folding wing tips for static and dynamic load alleviation,* The Aeronautical Journal **121**, 73 (2017).

[60] T. Wilson, A. Azabal, A. Castrichini, J. Cooper, R. Ajaj, and M. Herring, *Aeroelastic behaviour of hinged wing tips,* (2016).

[61] K. J. H. J. C. A. Wilson, Thomas, *Small scale flying demonstration of semi aeroelastic hinged wing tips,* IFASD (2019).

[62] R. C. Cheung, D. Rezgui, J. E. Cooper, and T. Wilson, *Testing of a hinged wingtip device for gust loads alleviation,* Journal of Aircraft **55**, 2050 (2018).

[63] A. Castrichini, V. Hodigere Siddaramaiah, D. Calderon, J. E. Cooper, T. Wilson, and Y. Lemmens, *Nonlinear folding wing tips for gust loads alleviation,* Journal of Aircraft **53**, 1391 (2016).

[64] A. Castrichini, J. E. Cooper, T. Wilson, A. Carrella, and Y. Lemmens, *Nonlinear negative stiffness wing-tip spring device for gust loads alleviation,* in *15th Dynamics Specialists Conference* (2016) p. 1574.

[65] S. F. V. N. W. T. C. J. M. F. Castrichini, Andrea, *Aeroelastic flight dynamics coupling effects of the semi aeroelastic hinge device,* IFASD (2019).

[66] T. Wilson, A. Castrichini, J. Paterson, and R. Arribas, *Non-linear aeroelastic behaviour of hinged wing tips,* .

[67] B. K. Stanford and P. S. Beran, *Analytical sensitivity analysis of an unsteady vortex-lattice method for flapping-wing optimization,* Journal of Aircraft **47**, 647 (2010).

[68] C. Wales, C. Valente, R. Cook, A. Gaitonde, D. Jones, and J. E. Cooper, *The future of nonlinear modelling of aeroelastic gust interaction,* in *2018 Applied Aerodynamics Conference* (2018) p. 3632.

[69] M. Nastran, *Release guide,* MSC Software Corporation (2004).

[70] T. R. Brooks, G. K. Kenway, and J. R. Martins, *Benchmark aerostructural models for the study of transonic aircraft wings,* AIAA Journal **56**, 2840 (2018).

[71] A. Drachinsky and D. E. Raveh, *Nonlinear aeroelastic analysis of very flexible wings using the modal rotation method,* in *AIAA Scitech 2021 Forum* (2021) p. 1710.

[72] C. Riso and C. E. Cesnik, *Correlations between um/nast nonlinear aeroelastic simulations and the pre-pazy wing experiment,* in *AIAA Scitech 2021 Forum* (2021) p. 1712.

A

TRANSIENT DYNAMIC RESULTS

This chapter presents some of the dynamic simulation results obtained using the solver in it's current implementation. Although dynamic simulations using the proposed solver runs to completion, it is the author's view to perform some more validation before claiming to be fully functional. Hence, these intermediate simulations are attached here for a sense of completion in work. The validation is also proposed as future work of the current thesis.

A.1. DYNAMIC SIMULATIONS OF BASELINE CRM

For dynamic simulations in a partitioned manner, it is imperative to perform temporal marching in both solvers in a dependent manner. i.e If the UVLM solver is time integrated first, the forces from t_{n+1} are then applied to the structure at time t_n. This lag in timesteps is an inherent error in such simulations and is accepted as long as the timesteps are small enough. Accepting this, with advanced restart capabilities in MSC Nastran coupled to a temporally controlled UVLM module, it is possible to perform various types of dynamic analysis like impulse, step and arbitrary loading.

A.1.1. STEP INPUT

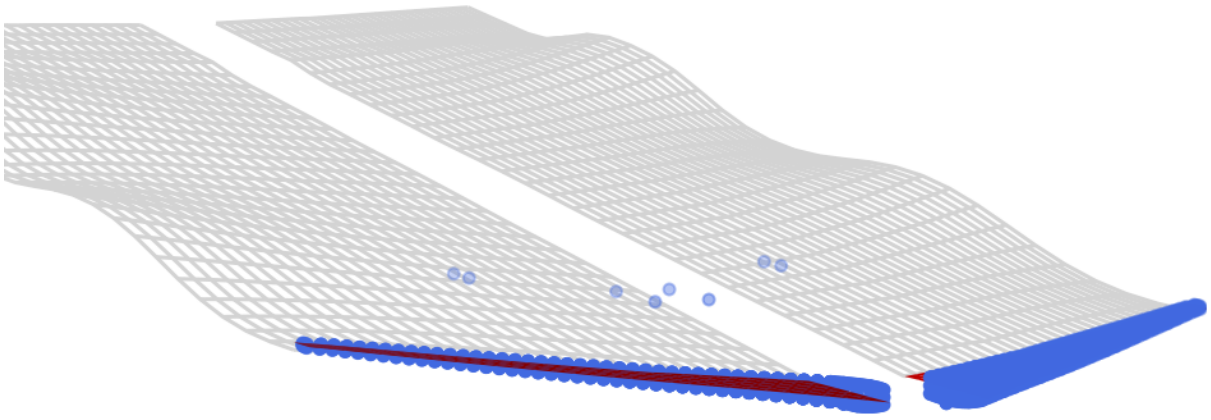

Figure A.1: Dynamic coupled simulation of baseline CRM model for a step input of 1g trim UVLM load

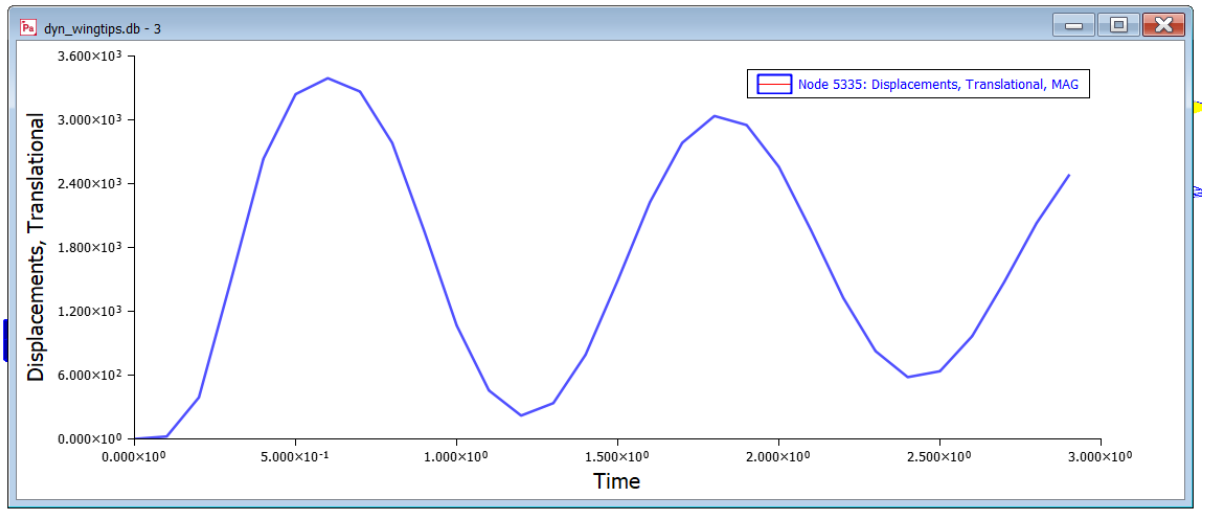

Figure A.2: Tip displacement of CRM baseline for step input of 1g trim UVLM load

The snapshot of simulation in figure A.1 shows the consistent smooth matching of the the UVLM module with the deflection of the structure. The position of the UVLM panels are updated at the start of every timestep after which a row of panels is shed from the trailing edge. Since this is a step response analysis, loads do not change with position. Every dynamic run of the structure uses the load of the first time step. The response of the structure is convoluted by accounting the same load from previous time step. The tip displacement of the structure is plotted in figure A.2. It can be seen that the initial transient period matches the expected damped response whose maximum deflection is always less than the dynamic magnification factor 2.

A.1.2. Arbitrary Input

The arbitrary response is similar to the step response but the structure is now subjected to a time varying load that depends on the deformation of the wing. Thus at every timestep, the structure will be subjected to a new load vector until convergence. A 1g trim load can also be arrive at using the arbitrary response. But the solution may take longer to converge due to oscillating nature of the load due to an oscillating structure in the transient phase. This is illustrated in the figure A.3 and the corresponding tip deflection of the wing is shown in A.4.

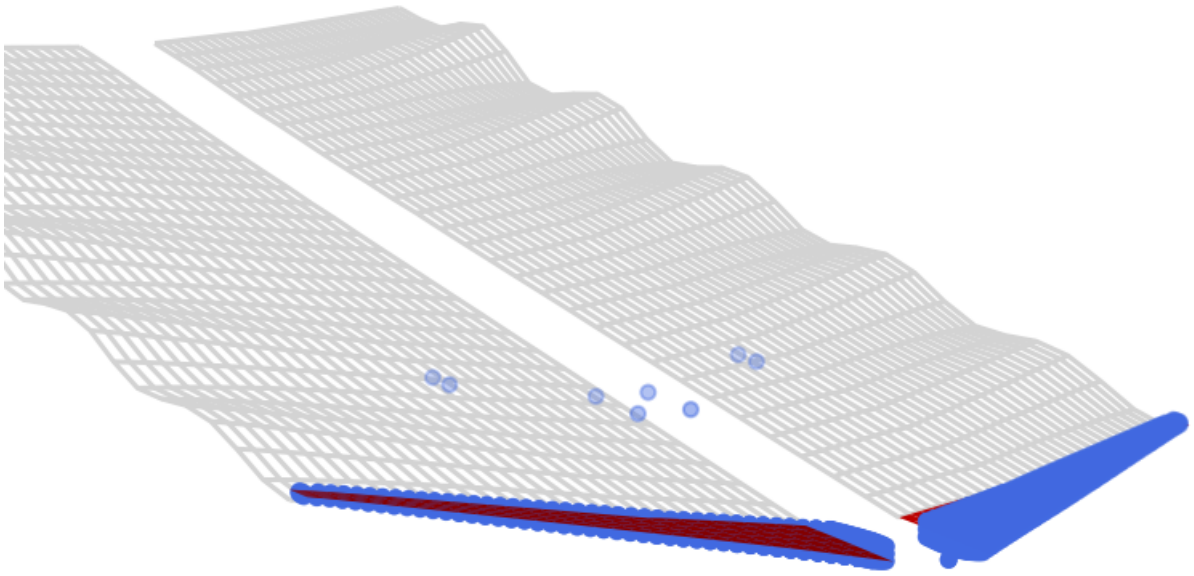

Figure A.3: Dynamic coupled response of CRM baseline for arbitrary input of 1g trim UVLM load

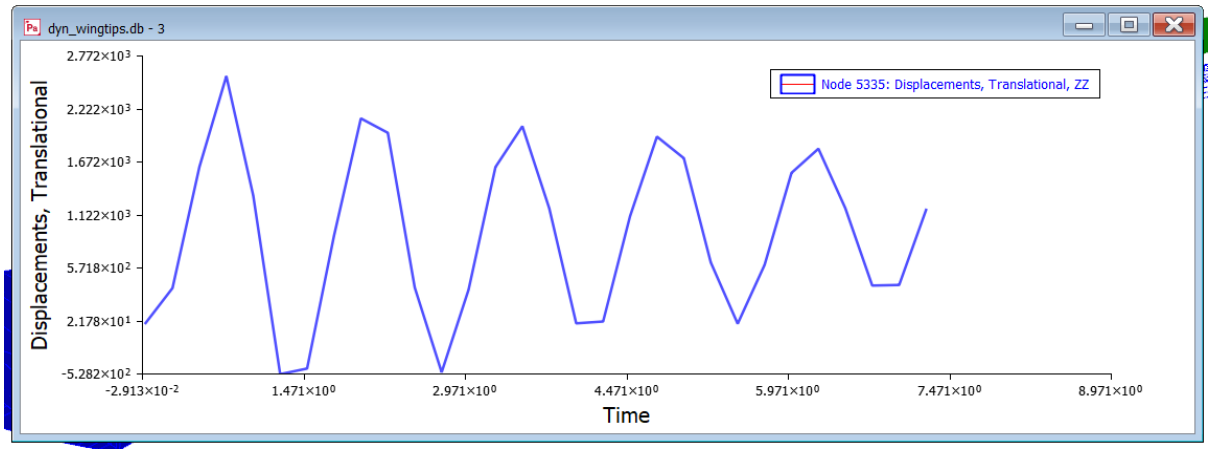

Figure A.4: Tip displacement of CRM baseline for arbitrary input of 1g trim UVLM load

A.2. Dynamic Simulations of Hinged Wingtips

Figure A.5 presents some of the dynamic coupled simulations with hinged wingtips. Again, it is observed that the simulations with damping show the expected behaviour of the solver reaching steady state at the trim configurations after the initial transient oscillations. Some plots also show large deflections in wingtips in consecutive timesteps which causes higher fluctuations in loads and a further investigation must be carried out regarding timesteps and possible implicit coupling with UVLM for a more refined load introduction.

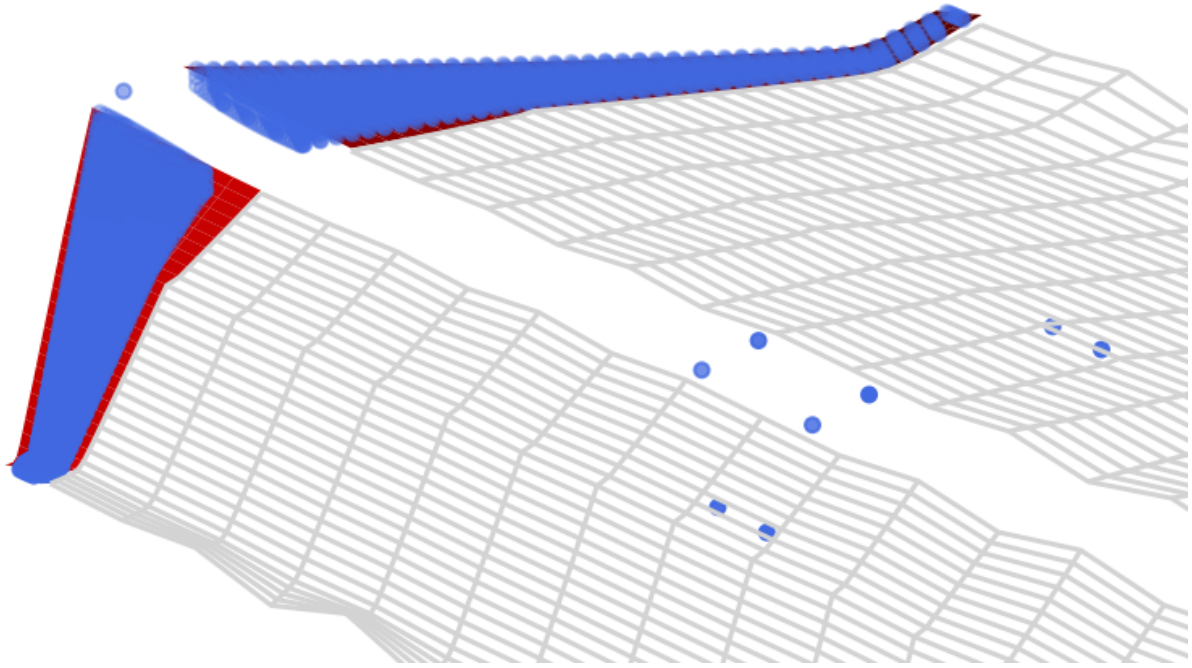

(a) Dynamic simulation of CRM model with hinged wingtips for step input of 1g trim load

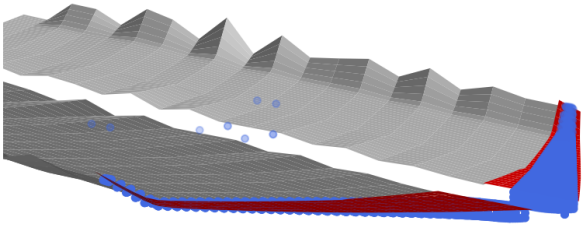

(b) Arbitrary loading trials for hinged wingtips

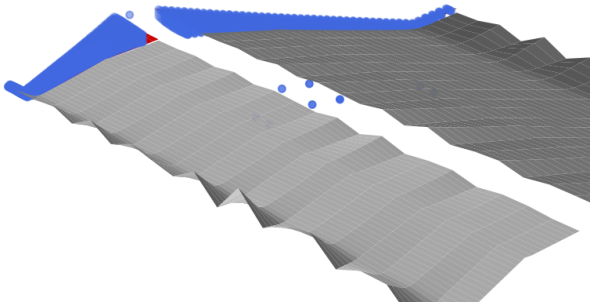

(c) Step loading trials with damping provided to wingtip mode

Figure A.5: Trial dynamic response of CRM model with hinged wingtips undergoing step and arbitrary inputs.